Acoustics of Two-Phase Pipe Flows

Samenstelling promotiecommissie:

prof. dr. ir. L. van Wijngaarden	Universiteit Twente, voorzitter/secretaris
prof. dr. A. Prosperetti	Universiteit Twente/ The Johns Hopkins University, promotor
prof. dr. ir. H.W.M. Hoeijmakers	Universiteit Twente, promotor
dr. A. Franzen	Shell - SIEP
prof. dr. ir. A. Hirschberg	Universiteit Twente
prof. dr. ir. G. Ooms	Technische Universiteit Delft
dr. ir. S.W. Rienstra	Technische Universiteit Eindhoven
prof. dr. ir. H. Tijdeman	Universiteit Twente

Acoustics of Two-Phase Pipe Flows
P.J. van Dijk

Cover: Lidewij van Rijssen

Printed by Febodruk BV, Enschede/Utrecht

Thesis University of Twente, Enschede - With ref. - With summary in Dutch.
ISBN 90-365-2188-2

ACOUSTICS OF TWO-PHASE PIPE FLOWS

PROEFSCHRIFT

ter verkrijging van
de graad van doctor aan de Universiteit Twente,
op gezag van de rector magnificus,
prof. dr. W.H.M. Zijm,
volgens besluit van het College voor Promoties
in het openbaar te verdedigen
op vrijdag 13 mei 2005 om 15.00 uur

door

Peter Jacco van Dijk

geboren op 30 oktober 1974
te Arnhem

Dit proefschrift is goedgekeurd door de promotoren:

prof. dr. A. Prosperetti,
prof. dr. ir. H.W.M. Hoeijmakers

en de assistent-promotor:

dr. ir. A. Biesheuvel.

TABLE OF CONTENTS

1 INTRODUCTION

1.1 Motivation and objective

In order to optimize oil production many technologies have been developed, which has led to complex networks of wells that produce varying amounts of oil, water and gas from multiple zones (Aspelund and Midttveit, 1996). These complex completions make it possible to increase the maximum recovery of the oil reserves in the field which are at present about $35-50\%$ on average (Kersey, Gysling and Bostick, 1999; Kapteijn, 2003). Managing these 'smart wells', e.g. by adjusting the valves in the pipe network, requires accurate downhole-production monitoring to obtain detailed information on the flow in the pipes and through the reservoir.

Modern fiber-optic-sensor technology provides a means, as reported by Gysling, Vandeweijer and van der Spek (2000), to obtain real-time data of the pressure and the temperature fluctuations at the pipe walls within the networks of oil wells. These sensors can also be employed for downstream-process monitoring. This raises the important question what information about the flow or the well might be extracted from these pressure and temperature recordings.

The signals that have been recorded so far suggest the existence of sound waves which propagate through the flow, typically with frequencies in the range $200-2000\,\mathrm{Hz}$. The origin of these sound waves is unknown. They may be generated by the flow at some particular locations along the pipe due to the presence of entrances, fittings, bends, etc. and subsequently propagate through the multiphase flow in a wave-like manner. Other possible sources of sound are the turbulent fluctuations of the flow or sources outside the pipes.

The flow in the pipes basically consists of oil and water. Due to the high pressure downhole gas is usually dissolved in the liquids, mainly in the oil, but upon flowing downstream the pressure in the flow decreases and as a result the gas may come out of solution in the form of bubbles which coagulate into larger bubbles further downstream. Yet, sometimes the gas and even sand are present downhole. Oil-water flows appear in a rich variety of flow patterns which all have different acoustic properties. Many of them resemble a random medium that modulates pressure waves in a ran-

dom manner. Hence, interpreting the pressure recordings and relating them to flow parameters such as the flow rate or the volume fractions of the phases, or even to the flow configuration, let alone to the origin of the sound, is a hard problem.

At present, information on the volume fractions of homogeneous mixtures of oil and water is obtained by measuring the transit time of the acoustic waves as they propagate along different sensors in the pipe through cross-correlating their recordings (Gysling et al., 2000). The ratios of the well-known distances between the sensors and the corresponding transit times yield estimates of the sound speed of the flow. Given the acoustic properties of the individual phases the volume fractions of the oil and of the water are estimated by Wood's relation (Wood, 1941) with an expected accuracy of $5-10\%$. In this approach the generation and dissipation of sound waves between two sensors is neglected, as well as the possible frequency dependency of the sound speed. A better understanding of the acoustics of mixtures of oil and water will probably lead to an improvement of this technique. In addition, knowledge on the acoustics of other flow configurations may yield an extension to the technique above or, perhaps, even better ways to extract information from the pressure recordings.

This study involves a theoretical analysis of the physical mechanisms that play a role in the propagation of sound through oil-water flows in pipes. The aim is to find characteristic acoustic properties that depend on the flow configuration and on the physical properties of the two phases. These characteristic properties, such as the propagation speed and the attenuation of the sound waves, may be recognized in the recorded signals and provide information on the flow.

1.2 Acoustics of two-phase flows in pipes

Although an extensive literature exists on sound propagation through gas-liquid flows, the number of studies on the acoustics of liquid-liquid flows in pipes is small. Most studies on sound propagation through two-phase systems are focussed on dispersions of gas and liquid. These exhibit significant resonance effects when it is the gas that forms the dispersed phase. Also, damping in these flows is substantial. Compared to gas-liquid systems the contrast in density and in compressibility is much smaller in liquid-liquid dispersions, which implies that resonance effects are smaller and do not dominate the acoustics. Hence, although the physics of the acoustics of oil-water dispersions and for gas-liquid dispersions is essentially the same, different mechanisms dominate. Some studies involve the acoustics of well-separated gas-liquid flows (e.g. Morioka and Matsui, 1975; van Wijngaarden, 1976; Sinai, 1984). In contrast to dispersions these resemble the liquid-liquid variant better, at least mathematically, and provide a good starting point to a part of this study.

The propagation speed of sound waves propagating through the flow configura-

tions as mentioned above and also other flow configurations is often calculated from models that describe the two-phase flow in the pipe. These models consist of a system of one-dimensional convection equations whose actual form depends on the specific flow configuration. The effects of the other spatial dimensions as well as effects like those due to the presence of the wall are included in terms of empirical closure relations. Some of the eigenvalues corresponding to the characteristics of this hyperbolic system of equations are then taken as the sonic velocities (e.g. Lee, Chang and Kyungdoo, 1998). In this manner expressions are found for the sound speed in various flow configurations. Unfortunately, the physical mechanisms that cause attenuation and the frequency dependency of the sound velocity are not clearly uncovered in this approach. An example is the effect of multiple scattering which, as will be shown here, plays an important role in the acoustics of oil-water flows.

The propagation of sound in circular ducts filled with a homogeneous medium has been investigated extensively. Among the pioneers were Lord Rayleigh (1896),von Helmholtz (1863) and Kirchhoff (1868). The acoustics of a wider range of systems including sound waves in pipes are discussed in more recent textbooks by for instance Morse and Ingard (1968), Pierce (1981) and Crighton, Dowling, Ffows Williams, Heckle and Leppington (1992).

One of the aspects that play a role in the acoustics in pipes is the influence of the wall elasticity. Although the wall elasticity is negligible for very stiff steel pipes that are filled with a gas, when the pipes are filled with hardly compressible liquids the flexibility of even steel pipes should not be ignored (Lafleur and Shields, 1995). It means that the pipe walls have a non-zero impedance which may affect both the phase velocity and the attenuation of the sound waves. These effects are probably small in pipes surrounded by a stiff medium like water or rock, as in the wells. The two effects will be ignored throughout this thesis, but can be taken into account by a adding a small correction to the speed of sound of the medium.

The flows through which pressure disturbances propagate have nonuniform velocity distributions over the cross-section of the pipe. Since the sound speeds in oil-water flows are much higher than the flow speeds that occur in practice the influence of the flow velocity is expected to be negligibly small and will be ignored in this study; i.e. the flow is assumed to be in rest.

1.3 Overview of this thesis

In this thesis the acoustics of oil-water flows is analyzed for various flow configurations. In Chapter 2 a brief overview will be given of oil-water flow patterns that occur in pipes. The rich variety of configurations that is observed will be discussed on the basis of several papers on experimental observations illuminated by sketches and photographs.

The distribution of the phases in many of the flow configurations does not vary appreciably with axial position along the pipe, as in dispersed and stratified flows. In Chapter 3 the acoustics of these flows will be analyzed. First the equilibrium speed of sound, being the sound speed for very low frequencies such that non-equilibrium effects become negligibly small, will be derived for well-separated flows in which the phases are able to move freely relatively to each other and for dispersions where this is not the case. Furthermore, the effects of attenuation, e.g. by boundary layers at the pipe wall and by the relative motion between the phases, will be discussed.

The frequency range of interest presumably warrants to restrict attention to purely one-dimensional modes of sound propagation. To what extent the one-dimensional approach is judicious will be inquired in Chapter 4. The modes and the corresponding cutoff frequencies will be calculated for core-annular and stratified configurations as well as the dispersion of the fundamental mode.

When the flow configuration exhibits a phase distribution that varies along the pipe, sound waves are reflected, which complicates the acoustics considerably. In Chapter 5 methods are introduced that provide a means to calculate the propagation of sound in these configurations when the phase distribution varies gradually or abruptly.

The methods introduced in Chapter 5 may be usefully applied to periodic or 'close to periodic' flows. Chapter 6 involves the properties of perfectly periodic flows such as slug flows or stratified flows for which the interface is not plane but wavy. The ideal situation of perfectly periodic flows is not realistic. True slug flows, for instance, are close to periodic but the periods differ in a random way. How these random deviations affect the acoustic properties of perfectly periodic flows will be the content of Chapter 7. When the random deviations become large the periodic structure cannot longer be recognized. These fully random flows resemble stratified configurations where larger oil bubbles flow on top of a layer of water.

OIL-WATER FLOWS IN PIPES

CHAPTER 2

2.1 Introduction

Before turning to the acoustics of oil-water flows in pipes first an overview will be given of what has been observed in experiments with respect to the distribution of the phases. The study of the acoustics in this thesis will be based on the characteristic patterns of the phase distribution that have been observed in the experiments.

The distribution of two immiscible fluids flowing through a pipe shows a rich variety of *flow patterns*, *flow configurations*, or *flow regimes* which depend on the physical properties of the two fluids, like the densities, the viscosities, the interfacial tensions, etcetera, as well as on the properties of the duct and the flow rates of the two fluids.

Gas-liquid flows have been studied and are still being studied intensively. On the other hand detailed information on the flow of oil and water in pipes is lacking. The flow structure in the two systems is quite different. Where gas-liquid systems are characterized by extreme density and viscosity contrasts, liquid-liquid flows have similar densities whereas the viscosity contrast covers a range over several orders of magnitude. Also, the lower free energy at the interface allows the formation of shorter interfacial waves and smaller droplet or bubble sizes of the dispersed phase, (Trallero, Sarica and Brill, 1997). Consequently, the size of the parameter space is larger for liquid-liquid flows and the classification of liquid-liquid flows into basic flow configurations is even more complicated than for gas-liquid systems. Figure 2.1 shows sketches by Brauner and Moalem Maron (1999) of many different flow patterns observed in horizontal oil-water systems. In practice the orientation of the pipes is, of course, not always perfectly horizontal and, depending on the angle of inclination of the pipe, an even richer variety and more complex types of flow configurations can be observed. Obviously, the influence of the pipe inclination is caused by gravity and is therefore negligible when the density of the phases are more or less equal.

Due to the high density contrast and the small viscosity of gases the settling of drops by gravity takes place more rapidly in gas-liquid systems than in liquid-liquid systems. Therefore dispersions are a more common structure in liquid-liquid flow

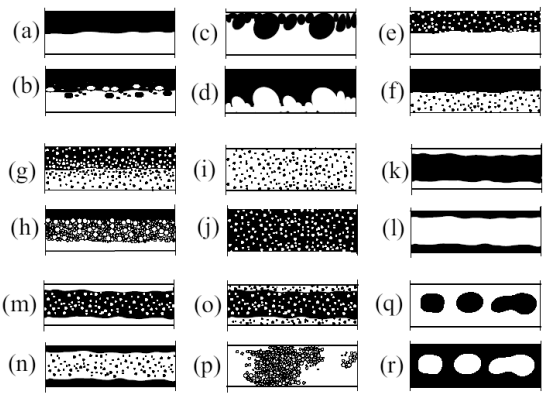

Figure 1 **a/b** Stratified flow of two separated layers (S, possibly with mixing at the interface, SM). **c/d** Stratified layers of a free-liquid and a dispersion of the other liquid (e.g. oil-in-water dispersion above a water layer, Do/w&w). **e/f** Stratified layers of a free liquid and a dispersion in the other liquid (e.g. oil and oil-in-water dispersion, Do/w&o; water and water-in-oil dispersion, Dw/o&w). **g/h** Layers of dispersions (e.g. water-in-oil dispersion above oil in water dispersion Dw/o&o/w, possibly with pure oil at the top and/or water at the bottom). **i/j** Fully dispersion or emulsion of one liquid in the other liquid (e.g. water-in-oil or oil-in-water dispersion or emulsion, Dw/o or Do/w). **k/l** Core-annular flow – a core of one liquid within the other liquid (e.g. a core of viscous oil and water in the annulus, ANw. Oil in the annulus, ANo). **m/n** Annular flow of a liquid with a dispersion in the core (water in the annulus DANw, oil in the annulus DANo). **o** Core-annular flow of two dispersions (CADw or CADo). **p** Intermittent flow (one liquid alternately occupying the pipe as a free liquid or as a dispersion, Io or Iw). **q/r** Large elongated or spherical bubbles of one liquid in the other (SLo,Bo or SLw,Bw).

FIGURE 2.1: *Sketches of various flow patterns (by Brauner and Moalem Maron, 1999).*

configurations. They appear as a stable flow patterns when the motion of the fluids is sufficiently intense; i.e. the dispersive forces by turbulence must overcome the resisting gravity field and surface tension. Dispersions also arise when some mixing device is used and even sustain far downstream as long as coalescence is minimal, e.g. when gravity effects are small (Brauner, 2001). Otherwise, these dispersions are unstable and will develop into a different flow pattern.

2.2 Experimental observations of flow patterns in pipes

Among the first experimental studies on liquid-liquid flows is that of Charles, Govier and Hodgson (1961) who present results of experiments on the flow of oil and water with approximately equal densities of $998\mathrm{kgm}^{-3}$ in a horizontal pipe with a $2.64\mathrm{cm}$ inner diameter and length of $7.3\mathrm{m}$. The viscosities of the oils were $6.29\mathrm{mPas}$, $16.8\mathrm{mPas}$, and $65.0\mathrm{mPas}$. The superficial velocities (the volume flow rate divided by the cross-section of the pipe) varied between $0.012\mathrm{ms}^{-1}$ and $0.073\mathrm{ms}^{-1}$ for the oil and between $0.024\mathrm{ms}^{-1}$ and $0.85\mathrm{ms}^{-1}$ for the water. The flow patterns turned out not to depend much on the oil viscosity. Sketches of what was observed for the oil with a viscosity of $16.8\mathrm{mPas}$ are shown in figures 2.2 and 2.3 (left), taken from the original paper. In each of the three sets the water flow rate is fixed and the oil flow rate decreases from top to bottom. In the words of the authors, as the oil flow rate is decreased for a fixed water flow rate the flow pattern changes from a dispersion of water in oil, through concentric oil in water, oil slugs in water, oil bubbles in water, to oil drops in water. As the total volume flow rate of the two fluids increases the interface between the fluids seems to become less 'smooth': there is more mixing and more variation in the drop sizes, and parts of the interface have a wavy appearance. Note that in all cases, except the water drops in oil configuration, it is the water that wets the pipe wall.

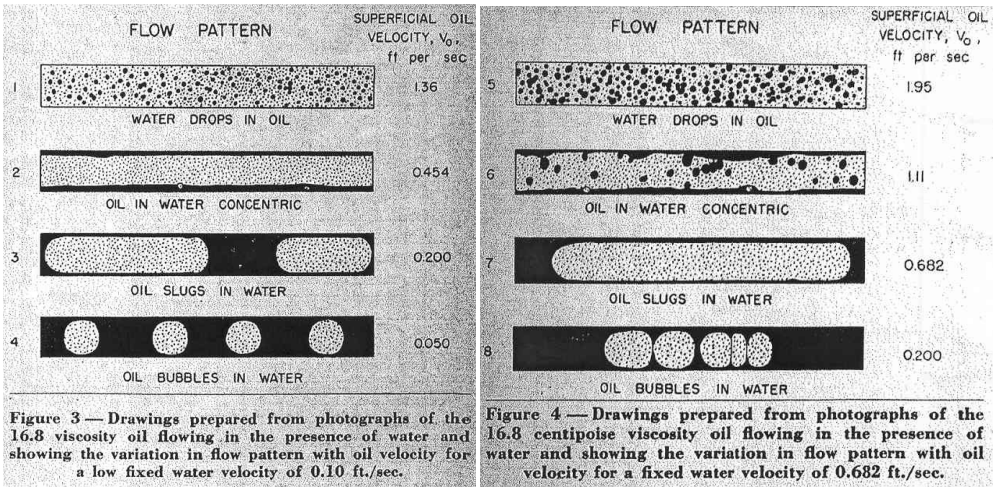

Figure 3 — Drawings prepared from photographs of the 16.8 viscosity oil flowing in the presence of water and showing the variation in flow pattern with oil velocity for a low fixed water velocity of 0.10 ft./sec.

Figure 4 — Drawings prepared from photographs of the 16.8 centipoise viscosity oil flowing in the presence of water and showing the variation in flow pattern with oil velocity for a fixed water velocity of 0.682 ft./sec.

FIGURE 2.2: *Sketches of horizontal oil-water flows (by Charles et al., 1961). The fixed water velocities are* $0.03\mathrm{ms}^{-1}$ *(left) and* $0.21\mathrm{ms}^{-1}$ *(right).*

Russel, Hodgson and Govier (1959) describe similar experiments, but here the oil density is smaller ($834\mathrm{kgm}^{-3}$) than that of the water. The pipe diameter in this experiment is somewhat smaller, $D = 2.45\mathrm{cm}$, and the pipe length slightly larger, $L = 8.6\mathrm{m}$. Figure 2.3 (right) shows sketches of the flow configurations for a fixed superficial water velocity of $0.86\mathrm{ms}^{-1}$ when the oil-water volume ratio takes the values $R_\mathrm{v} = 0.14$, $R_\mathrm{v} = 0.47$ and $R_\mathrm{v} = 0.92$. The influence of gravity is clearly visible. When the oil fraction is small the oil phase tends to form long elongated bubbles which develop into a more stratified pattern when the oil fraction is increased. By further increasing the oil fraction the flow takes a pattern consisting of three stratified layers where the one in the middle becomes *mixed*; the two phases occur as a dispersion in the other phase.

Other sketches of oil-water flow patterns where the phases have different densities are shown in figure 2.4, which was taken from a paper by Trallero et al. (1997). These authors studied the flow of a mineral oil and water in a horizontal pipe with an inner diameter of $5.01\mathrm{cm}$ and a length of $15.54\mathrm{m}$. The viscosity and the density of the oil were $28.8\mathrm{mPas}$ and $884\mathrm{kgm}^{-3}$, and those of the water $0.97\mathrm{mPas}$ and $1037\mathrm{kgm}^{-3}$, respectively. The superficial velocities of the two phases were in the range $0.01 - 1.60\mathrm{ms}^{-1}$. The upper two sketches in the left column of figure 2.4 show that for low and roughly equal volume flow rates of the two phases a stratified flow was observed. The oil was on top. As the flow rates were increased the interface became wavy and broke up. Near the interface oil droplets were found in the water, and water droplets in the oil. The other four sketches in the figure illustrate what was observed at high flow rates. When the volume fractions of the phases were rather different the liquid that has the lowest value formed droplets that were dispersed in

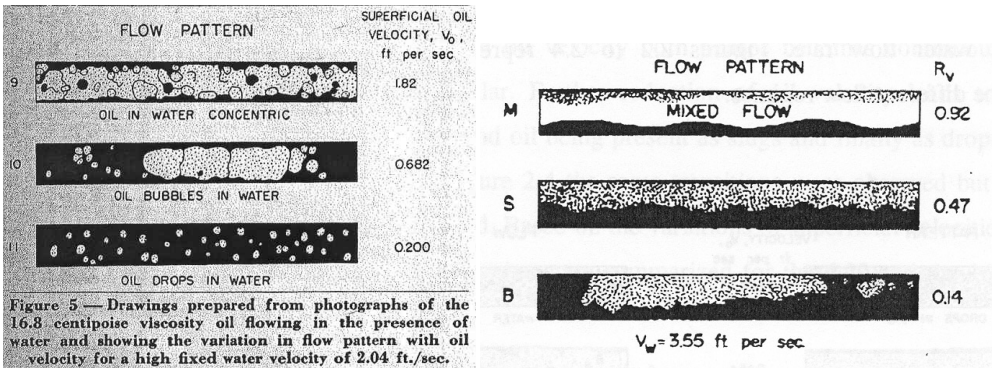

FIGURE 2.3: *Left: same as the in previous figure, but with a water velocity of* $0.62\,\mathrm{ms}^{-1}$. *Right: sketches of horizontal oil-water flows where the phases have different densities (by Russel et al., 1959); the water velocity is* $0.86\,\mathrm{ms}^{-1}$.

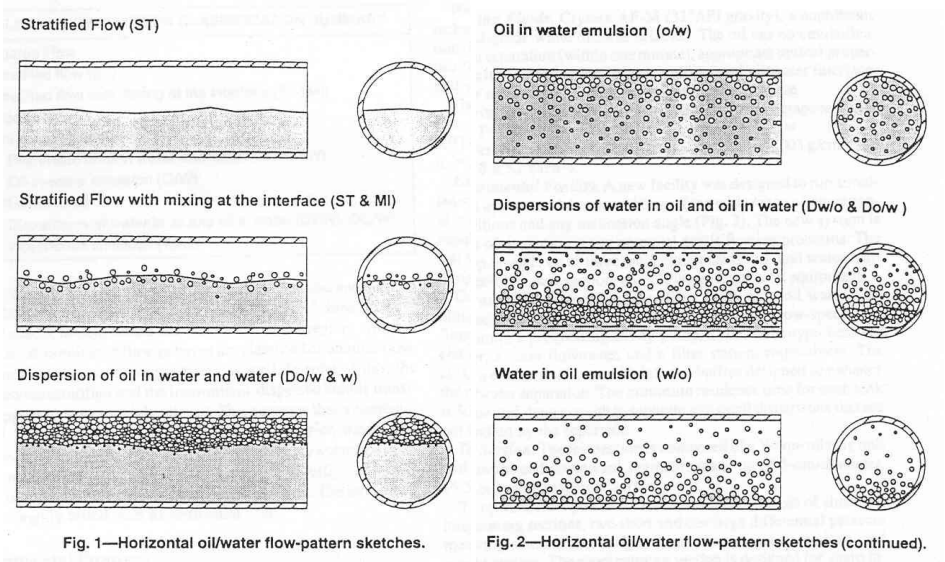

FIGURE 2.4: *Sketches of horizontal oil-water flows (by Trallero et al., 1997).*

the liquid with the high volume fraction. The authors called these flow configurations *emulsions* of water in oil or emulsions of oil in water. When the volume fractions were approximately equal complex patterns were found consisting of two separated layers in which droplets were densely dispersed.

Angeli and Hewitt (2000b) studied horizontal oil-water flows with a low viscosity contrast ($\mu_{\text{oil}} = 1.6\,\text{mPas}$, $\rho_{\text{oil}} = 801\,\text{kg}\,\text{m}^{-3}$) in steel and acrylic pipes. The mixture velocity was varied from $0.2\,\text{m}\,\text{s}^{-1}$ to $3.9\,\text{m}\,\text{s}^{-1}$ and the input water fraction ranged from 6% to 86%. Flow patterns are usually determined visually by means of a transparent pipe or window. However, due to multiple reflections it is often difficult to identify accurately the phase distribution, especially for complex and rapidly varying interfaces. Figures 2.5 and 2.6 make this point clear.

The flow patterns that were observed were various different forms of stratified flows: with a wavy interface; with drops at the interface, figure 2.5 (top); with three layers with a layer of drops in between layers of pure oil and pure water, figure 2.5 (bottom); with two layers where one layer with drops was on top of or below a layer of the continuous phase, figure 2.6 (top). When the mixture velocity was increased a fully dispersed or mixed pattern occurred of one phase into the other, figure 2.6 (bottom). Wether the oil or the water is the continuous phase depends on the input water volume fraction, low values yield a water in oil dispersion, high values an oil in water dispersion. The transition of the one dispersion into the other one (*phase inversion*) did not take place at a particular input water volume fraction. Within a certain intermediate regime the two phases were observed to be periodically continuous and dispersed in waves, see also figure 2.1p.

Although the flow regimes identified in the steel and in the acrylic pipe were observed to be similar, also some differences were found. The patterns in the steel pipe were more disturbed than those in the acrylic pipe; i.e. the stratified wavy regime was very narrow and the mixed region started at lower velocities. Angeli and Hewitt (2000b) attribute this difference to the higher, turbulence generating, wall roughness of the steel pipe wall. The second difference that they mention is that the oil continuous regimes are more persistent. These patterns change into other regimes only beyond a wide range of mixture velocities and water fractions, wider than in steel pipes. They explain this by the differences in wettability of the pipe wall. Since the oil more easily wets the acrylic wall than the steel wall the continuous oil patterns occurs over a wider range of flow conditions.

The flow patterns become very different when the oil is very viscous as shown by the sketches in figures 2.7 and 2.8 (by Joseph et al., 1997). The first figure shows sketches of regimes in horizontal pipes that resemble the patterns from figure 2.2 of equal density oil-water flows. Still, the influence of gravity is clearly visible as the oil phase has the tendency to rise towards the top of the pipe. Additionally, ripples are formed on the long oil bubbles or on the core while in the experiments

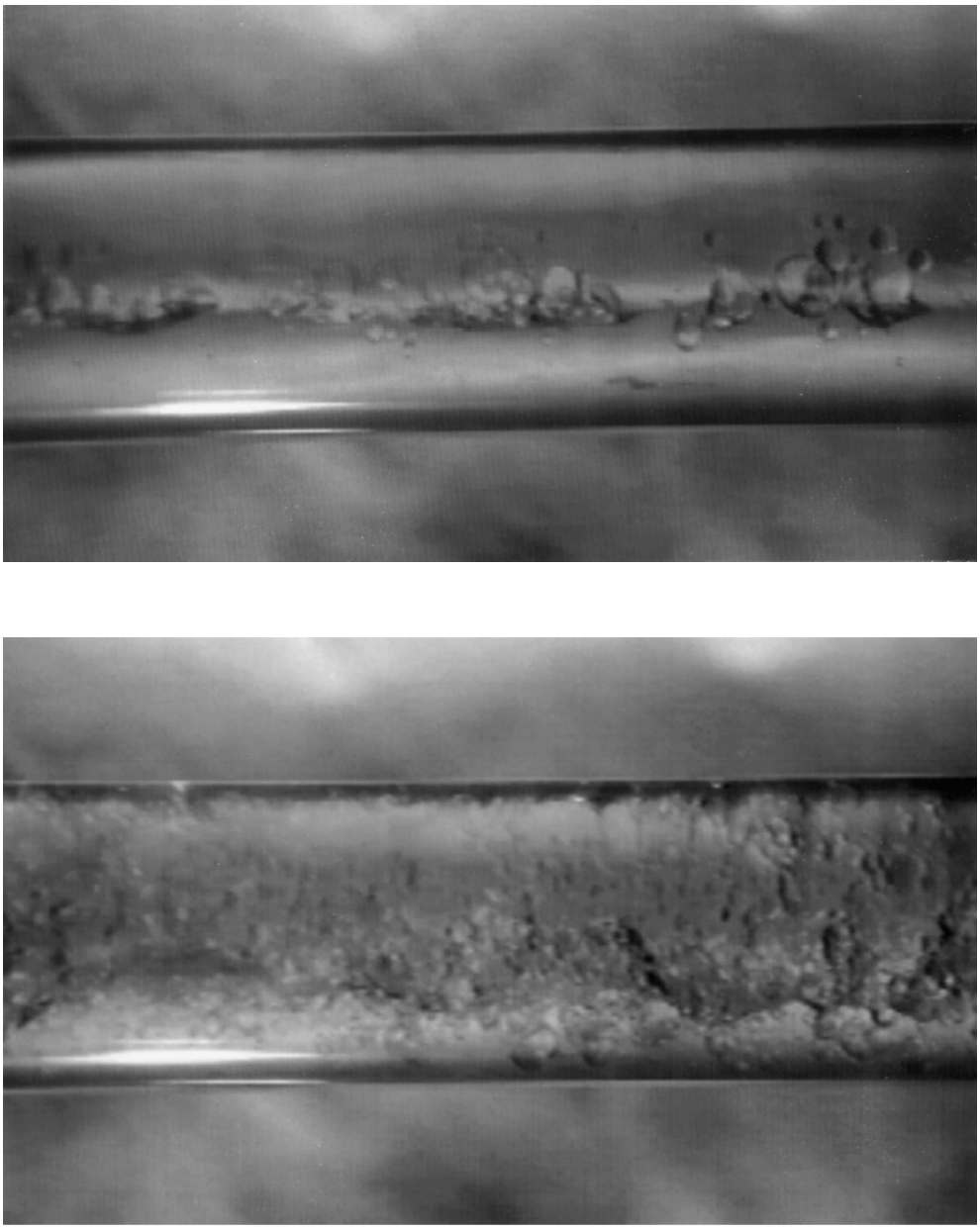

FIGURE 2.5: *Stratified Wavy with Drops (SWD) flow pattern (Top) and Three Layer (3L) flow pattern (Bottom) in an acrylic pipe (Angeli and Hewitt, 2000b).*

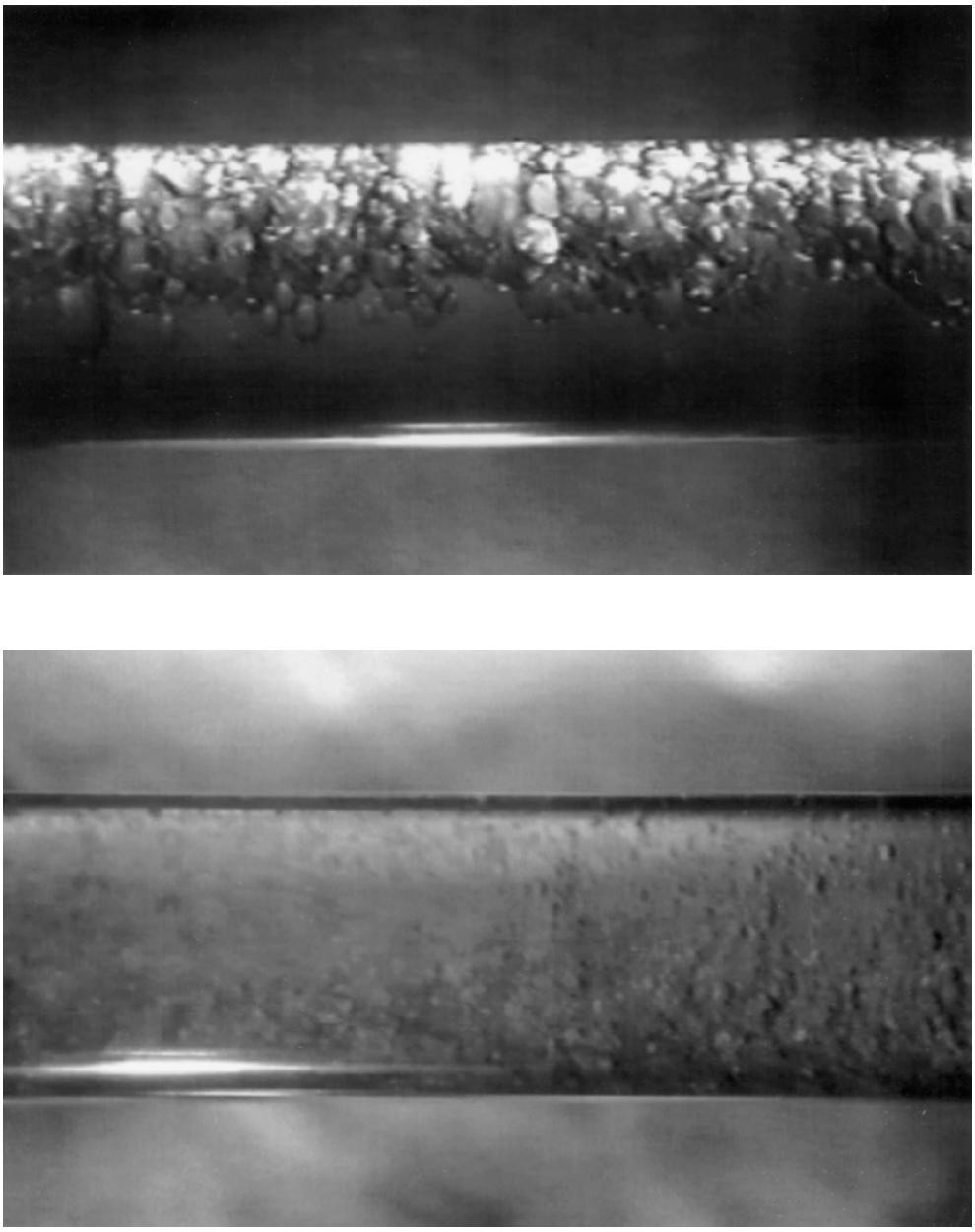

FIGURE 2.6: *Stratified Mixed with water layer (SM/water) flow pattern (Top) and Mixed (M) flow pattern (Bottom) in an acrylic pipe (Angeli and Hewitt, 2000b).*

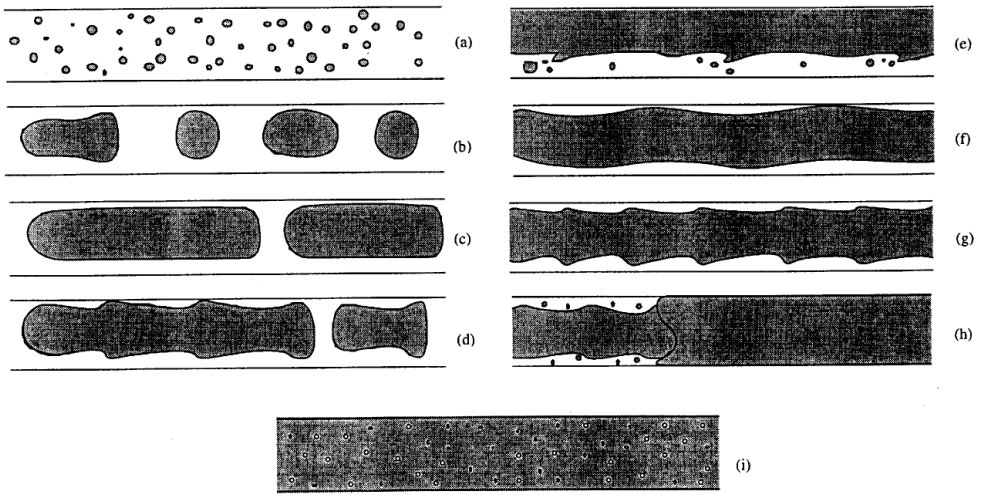

FIGURE 2.7: *Sketches of flow patterns in horizontal flows (flowing from the right to the left) with a lighter oil phase (from Joseph et al., 1997)*

of Charles et al. (1961) the bubbles rather break up into smaller bubbles. More in-depth analyzes of rippled cores lubricated by water can be found in for example Ooms, Segal, Meerhof and Oliemans (1984). A profound description of the vertical flows in figure 2.8 is given by Bai, Chen and Joseph (1992) who did experiments on water-lubricated pipelining of viscous oil, $\mu_{\text{oil}} = 601\,\text{mPas}$, in a vertical pipe where the flow rates were small, less than $0.9\,\text{ms}^{-1}$. The core in vertical up-flows often takes the shape of the so-called *bamboo* waves. In down-flow systems only the short bamboo waves appear and instead of the long bamboo waves *corkscrew* waves occur. Besides viscous oils the core can also consist of well-dispersed water drops in oil. These emulsions may be formed to have an effective high viscosity which has similar properties and patterns as described above, even though the viscosity of the pure oil phase itself is low (Ho and Li, 1994).

2.3 Drop sizes in dispersions

Many experiments on droplet sizes have been carried out (e.g. Collins and Knudsen, 1970; Karabelas, 1978; Angeli and Hewitt, 2000a; Simmons and Azzopardi, 2001). The order of magnitude of the drop sizes were in the range up to $0.5\,\text{mm}$ (e.g. Simmons and Azzopardi, 2001) and in the range up to several millimeters in other systems (Angeli and Hewitt, 2000a). Estimates of the droplet sizes are required to determine the attenuation of sound in dispersions. Therefore, relations that provide the drop size in terms of system parameter such as the flow rate and the physical properties of the phases would be advantageous.

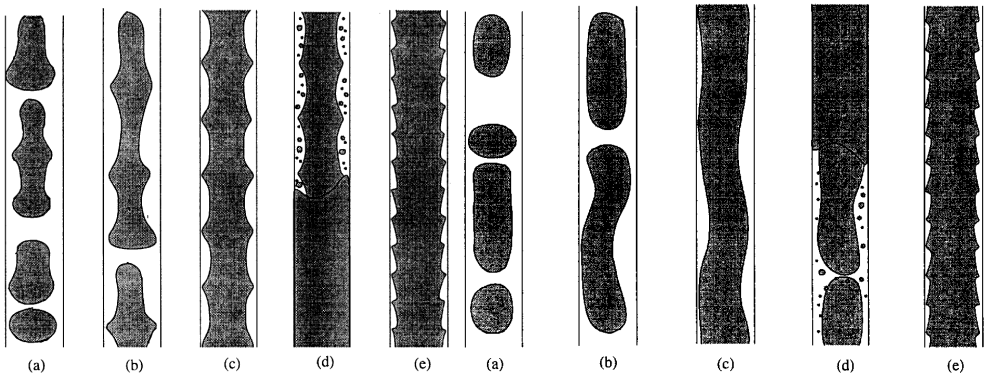

FIGURE 2.8: *Sketches of flow patterns in up-flows in a vertical pipe (left); in down-flows in a vertical pipe (right) (from Joseph et al., 1997)*

Theories on drop or bubble sizes in dispersions are mostly based on the work by Kolmogorov (1949) and Hinze (1955) who considered the breakup of a single drop in a infinite flow field where coalescence does not occur.

According to a brief review of Brauner (2001) of their theory, they argue that in turbulent flows regions where viscous shear is relevant are small compared to the size of the largest drops. Therefore, the dominant external stress working on the drops is the dynamic pressure of the turbulent eddies of the drop size d. The maximum drop size follows from a balance between the drop surface energy and the turbulent energy,

$$\frac{4\sigma}{d_{\max}} \approx \tfrac{1}{2}\rho_c u'^2, \tag{2.1}$$

with ρ_c the density of the continuous phase. For homogeneous isotropic turbulence the turbulent kinetic energy may be related to the rate of turbulent energy dissipation $\bar{e}$,

$$u'^2 = 2(\bar{e}d_{\max})^{2/3}, \tag{2.2}$$

as long as

$$l_k = \left(\frac{\mu_c^3}{\rho_c^3\bar{e}}\right)^{1/4} \ll d_{\max} < D/10, \tag{2.3}$$

where μ_c denotes the dynamic viscosity of the continuous phase, l_k the Kolmogorov microscale and $D/10$ the length scale of the energy containing eddies in a pipe with diameter D, (Hinze, 1959). The relation between the turbulent energy dissipation and the maximum drop diameter then follows from equations 2.1, 2.2,

$$d_{\max}\left(\frac{\rho_c}{\sigma}\right)^{3/5}\bar{e}^{2/5} = C. \tag{2.4}$$

The constant $C = 0.725$ is determined by fitting experimental data of various liquid-liquid dispersions. The corresponding critical Weber number, denoting the ratio between the external force τ that tends to deform the largest drops and the counteracting surface tension force,

$$\mathrm{We}_{\mathrm{crit}} = \frac{\tau d_{\max}}{\sigma}, \tag{2.5}$$

has the value 1.17. This value agrees with the theoretical value obtained when considering the resonance frequencies of liquid drops (Sevik and Park, 1973).

The turbulent energy dissipation in pipe flows may be related to the frictional pressure drop,

$$\bar{e} = \frac{4\tau U_c}{D\rho_c(1-\epsilon_d)} = \frac{2U_c^3 f}{D}\frac{\rho_m}{\rho_c(1-\epsilon_d)}. \tag{2.6}$$

Here f is the friction factor.

The maximum drop size prediction by Hinze (1955) then becomes

$$\left(\frac{d_{\max}}{D}\right)_0 = 0.55\mathrm{We}_c^{-0.6}\left(\frac{\rho_m}{\rho_c(1-\epsilon_d)}f\right)^{-0.4}, \tag{2.7}$$

with $\mathrm{We}_c = \rho_c U_c^2 D/\sigma$. Correlations for the friction factor f can be used to close equation 2.7, for instance by Blasius' equation $f = 0.046/\mathrm{Re}_c^{0.2}$, with $\mathrm{Re}_c = \rho_c D U_c/\mu_c$. In the dilute limit, $\epsilon_d \ll 1$, the mixture density may be approximated by

$$\rho_m = \epsilon_d\rho_d + (1-\epsilon_d)\rho_c \approx (1-\epsilon_d)\rho_c \tag{2.8}$$

and hence, the last term in equation 2.7 may be omitted as long as the bulk density of the dispersed phase is not much larger than that of the continuous phase, like in gas-liquid mist flow where the liquid forms the dispersed phase. Hinze's theory predicts the maximum drop size in dilute dispersions fairly well for a variety of two-phase systems, as long as $d_{\max} < D/10$, (e.g. Karabelas, 1978). The mechanisms that cause breakup in systems with larger drops or bubbles and denser dispersions are more complicated and still subject to research (e.g. Lasheras, Eastwood, Martínez-Bazán and Montañés, 2002; Risso and Fabre, 1998). For these flows Hinze's theory underpredicts the actual drop sizes as measured in experiments. Hence, it cannot be employed in the calculation of the attenuation of the sound waves in these dispersions.

ACOUSTICS OF DISPERSED AND SEPARATED FLOWS

CHAPTER 3

3.1 Introduction

In this chapter the acoustics of two-phase flows in pipes are considered for flow configurations that do not vary with position along the pipe. Examples of these configurations are dispersions where the volume fractions of the phases are constant with position along the pipe. Here the length scale of the phase distribution is very small compared to the wavelength such that the system resembles a single phase fluid with effective acoustic properties. Other examples are well-separated flows, such as core-annular flows or stratified flows. The latter may consist of two layers with the lighter fluid flowing on top of the heavier fluid, but also three layer systems where two layers of the pure phases are separated by a dispersion of the one fluid in the other or a mixed layer where the two phases are dispersed into each other.

In the next section the main properties of low frequency sound waves in pipes are briefly discussed focussing on the differences of the acoustics of single phase flows, dispersed flows and separated flows. In the following sections the propagation speed and the attenuation of sound waves will be analyzed in more detail for dispersed and separated systems illuminated by several examples of flows as described in the previous chapter.

3.2 Sound velocity in pipes

The *speed of sound* is usually meant to be the velocity of propagation of small amplitude pressure perturbations when non-equilibrium effects are negligibly small. However, in general only very low frequency sound waves actually do propagate with this velocity. For higher frequencies non-equilibrium effects affect the actual propagation speed of the waves.

Pierce (1981) gives limiting expressions for the speed of sound for very low and for very high frequencies for a medium that is in rest, unbounded and consists of a

single phase. In this case the linearized energy equation reads

$$\rho_0 T_0 \frac{\partial s}{\partial t} = \kappa_0 \nabla^2 T, \tag{3.1}$$

where s and T denote the entropy and the temperature perturbations, respectively. ρ_0, T_0 and κ_0 denote the density, the temperature and the thermal conductivity, respectively, evaluated for undisturbed conditions. Since the entropy and temperature perturbations vary on the acoustic time and length scales, time and the spatial coordinates should be expressed in terms of angular frequency ω and the wave number $k = \omega/c$ of the acoustic waves, respectively. As long as the waves have a constant amplitude the magnitude of the term in the left-hand side of equation 3.1 is proportional to the frequency whereas the magnitude of the term in the right-hand side varies proportionally to the square of the frequency. Then in the limit of very low frequencies the generation of heat through conduction becomes negligibly small from which it follows that the entropy must be constant. Therefore, in the zero frequency limit the *equilibrium* speed of sound is given by the derivative of the pressure to the density for isentropic conditions,

$$c_s^2 = \left(\frac{\mathrm{d}p}{\mathrm{d}\rho}\right)_s. \tag{3.2}$$

In the high frequency limit the conduction of heat fully dominates the energy balance. As a result the temperature remains constant and the speed of sound should be evaluated for isothermal conditions. The *frozen* sound speed is in this case given by

$$c_T^2 = \left(\frac{\mathrm{d}p}{\mathrm{d}\rho}\right)_T. \tag{3.3}$$

The equilibrium and the frozen speed of sound are the low and high frequency limits of the true propagation speed of sound waves in an infinite medium. In order to estimate whether the actual frequency is small or large the relaxation frequency of thermal conduction is introduced as the reciprocal of the time scale of thermal conduction in which locally heat is generated through conduction. An expression for this frequency follows from equation 3.1,

$$f_{\mathrm{tc}} = \frac{c^2}{2\pi k_H}, \tag{3.4}$$

where $k_H = \kappa_0/(\rho_0 C_p)$ denotes the thermal diffusivity of the fluid. For atmospheric conditions typical values for the relaxation frequency are $f_{\mathrm{tc}} \sim 10^9\,\mathrm{Hz}$ in air and even higher in water, $f_{\mathrm{tc}} \sim 10^{12}\,\mathrm{Hz}$. The equilibrium speed of sound is clearly the appropriate one when dealing with low frequency sound waves ($f \ll f_{\mathrm{tc}}$) in single

phase infinite media. Throughout this thesis the speed of sound of the pure fluids is evaluated for isentropic conditions.

The non-equilibrium effect of heat conduction plays a role in the attenuation and dispersion of acoustic waves in an infinite domain. However, when dealing with low frequency sound waves in pipes (compared to f_{tc}) its influence is negligible and will be ignored in this thesis. When sound propagates through a single phase fluid in a pipe the most significant non-equilibrium effect is associated with the adjustment of the fluid velocity and temperature to that of the pipe wall. The result is a frequency dependent small correction to the propagation speed that would occur for equilibrium conditions, and more importantly, a frequency dependent attenuation of the disturbances as they travel through the pipe. For a detailed discussion on the effects of heat conduction on the propagation of sound waves the reader is referred to, for instance, Pierce (1981) or Lighthill (1978), but also many other textbooks cover this topic.

If the medium consists of two phases the situation is more complicated, even without the presence of the pipe wall. When the phases are intimately connected, as when one of the phases is finely dispersed in the form of droplets in the other continuous phase, the equilibrium sound velocity of the medium should be considered as the velocity of propagation of pressure waves when the droplet temperature and size are always those that they would be for equilibrium conditions (given the actual value of the pressure that is imposed by the perturbation). When subject to pressure fluctuations the two phases would accelerate differently because of the contrast in density. However, at low frequencies the viscous forces dominate the inertial forces due to the intimate connection of the two phases. The velocity of the droplets is in that case equal to the velocity of the surrounding fluid. The influence of the density contrast increases with frequency and diminishes the effect of the viscous force. The result is that the drops cannot follow the surrounding fluid perfectly anymore and assume a different velocity than that of the surrounding fluid. The velocity difference between the two phases permanently tends to relax towards its equilibrium value of zero. Also the temperature difference between the two phases is in a permanent relaxation process towards its equilibrium value of zero. Yet, the two relaxation processes only reach full equilibrium in the zero frequency limit. In equilibrium the temperatures in the two phases are the same (Temkin, 1992).

It is these relaxation processes towards equilibrium that give pressure wave propagation in dispersions its interesting properties. These may be very different depending on the fluids that form the dispersion and on the constitution of the dispersion. In many cases the wave velocity and attenuation strongly depends on the frequency. The *equilibrium* sound velocity is then the low frequency extreme; the high frequency extreme, in which the phases are free to move relative to each other and the conduction of heat across the interfaces is absent, is the *frozen* sound velocity.

In annular flows or stratified flows the phases are not intimately connected, in other

words well-separated. Then the propagation of pressure waves is more reminiscent of that in single phase flows. The proper approach is to consider the sound propagation for equilibrium conditions as that when the phases are free to move relative to each other for the condition that the pressure be continuous across the interface as well as the component of the induced velocity that is normal to the interface. Non-equilibrium effects are now associated not only with adjustment of temperature and velocity near the wall of the pipe, but also at the interface between the fluids. These processes are similar in nature, and it is likely that the adjustment process near the wall is the dominant effect. After all, the velocity difference between the phases at the interface will be smaller than the velocities of the two phases near the wall of the pipe. It is noted that a brief discussion of what this approach would give in the case of gas-liquid flows is given by van Wijngaarden (1976).

3.2.1 Separated composition

Let us proceed by considering a composition where the phases are free to move relatively to each other and not intimately connected. Suppose that oil and water occupy well-separated parts of the cross-section of a pipe, as for instance in stratified flows, annular flows or slug flows. The two phases are denoted by the subscripts $i = 1, 2$. Let the undisturbed flow be at rest and the two phases in this undisturbed case have densities ρ_{0i} and occupy cross-sections A_{0i}. When the frequency tends to zero the motion is purely longitudinal. Then for each of the phases i the conservation equation of mass reads

$$\frac{\partial(\rho_i A_i)}{\partial t} + \frac{\partial(\rho_i A_i u_i)}{\partial x} = 0. \tag{3.5}$$

Upon linearizing and employing the definition of the *bulk modulus* K (also called the modulus of elasticity),

$$K_i = \left(\rho_i \frac{\mathrm{d}p_i}{\mathrm{d}\rho_i}\right)_0 = \rho_{0i} c_{0i}^2, \tag{3.6}$$

where the subscript 0 denotes the evaluation for undisturbed conditions, one obtains

$$\frac{A_{0i}}{K_i}\frac{\partial p_{e,i}}{\partial t} + \frac{\partial A_i}{\partial t} = -\frac{\partial(A_{0i} u_i)}{\partial x}, \tag{3.7}$$

with u_i the induced velocity and $p_{e,i}$ the excess pressure over the undisturbed value. In the following the subscript 0 is omitted as it is understood that all physical properties are to be evaluated for undisturbed conditions. It is recalled that the two phases are considered to be separately in thermodynamic equilibrium and have a different temperature since the conduction of heat across the interface is neglected. Since the wavelength is very long compared to the pipe diameter the pressures in the two phases must be the same. Then the condition that the pressure be continuous across the interface is automatically satisfied. The total area that is covered by the two phases is

just the cross-section of the pipe, which is a constant. Adding the linearized mass conservation equations of the two phases yields

$$\frac{\partial p_e}{\partial t} = -K\frac{\partial u}{\partial x}, \tag{3.8}$$

where, upon introducing the holdup $\alpha = A_1/A$ as the fraction of the cross-section that is covered by phase 1, the bulk modulus of the two-phase medium is given by

$$\frac{1}{K} = \frac{\alpha}{K_1} + \frac{1-\alpha}{K_2}, \tag{3.9}$$

and the mean induced velocity by

$$u = \alpha u_1 + (1-\alpha)u_2. \tag{3.10}$$

In each phase the momentum conservation equation reads

$$\rho_i\left(\frac{\partial u_i}{\partial t} + u_i\frac{\partial u_i}{\partial x}\right) = -\frac{\partial p_e}{\partial x}. \tag{3.11}$$

Linearizing and adding gives, with use of equation 3.10,

$$\frac{\partial u}{\partial t} = -\frac{1}{\rho}\frac{\partial p_e}{\partial x}, \tag{3.12}$$

where the effective density ρ is given by

$$\frac{1}{\rho} = \frac{\alpha}{\rho_1} + \frac{1-\alpha}{\rho_2}. \tag{3.13}$$

Combining equations 3.8, 3.12 yields the wave equation for the excess pressure,

$$\frac{\partial^2 p_e}{\partial t^2} = \frac{K}{\rho}\frac{\partial^2 p_e}{\partial x^2}. \tag{3.14}$$

It is clear that the sound velocity is given by $c^2 = K/\rho$. This expression can be written in terms of the holdup α as

$$\frac{c^2}{c_1^2} = \frac{\alpha + (1-\alpha)/\rho_*}{\alpha + (1-\alpha)/K_*}, \tag{3.15}$$

where $\rho_* = \rho_2/\rho_1$ and $K_* = K_2/K_1$ denote the density ratio and the ratio of the bulk moduli, respectively. Another quantity of interest is the acoustic *impedance*. Waves that have the form

$$p_e(\pm x/c - t), \;\; u(\pm x/c - t) \tag{3.16}$$

are solutions to equations 3.8, 3.12 if $p_e/u = \sqrt{K\rho}$. This ratio of the excess pressure and the induced velocity in the direction of sound propagation is called the acoustic impedance. For separated configurations the impedance, $Z = \sqrt{K\rho}$, is given by

$$\frac{Z^2}{Z_1^2} = \frac{1}{\alpha + (1-\alpha)/K_*} \frac{1}{\alpha + (1-\alpha)/\rho_*}, \tag{3.17}$$

where the impedance of phase 1 is given by $Z_1 = \rho_1 c_1$.

A different way of writing the equations above follows from introducing the acoustic *admittance* Y of the two phases as the reciprocal of the impedance Z,

$$Y_i = \frac{1}{\sqrt{K_i \rho_i}}, \tag{3.18}$$

i.e. in each phase as the ratio of the induced velocity in the direction of sound propagation and the pressure excess. Then K_i and ρ_i may be written in terms of the admittance and the speed of sound as $1/K_i = Y_i/c_i$ and $1/\rho_i = c_i Y_i$. The effective quantities now become, according to equations 3.9, 3.13,

$$\frac{1}{K} = \frac{Y}{c} = \alpha \frac{Y_1}{c_1} + (1-\alpha)\frac{Y_2}{c_2}, \quad \frac{1}{\rho} = cY = \alpha c_1 Y_1 + (1-\alpha) c_2 Y_2. \tag{3.19}$$

In terms of these new variables the wave equations 3.8, 3.12 yield

$$\frac{\partial p_e}{\partial t} = -\frac{c}{Y}\frac{\partial u}{\partial x}, \quad \frac{\partial u}{\partial t} = -cY\frac{\partial p_e}{\partial x}. \tag{3.20}$$

Lighthill (1978) explains that these are the general equations governing longitudinal pressure wave propagation in tubes and channels. Within this longitudinal theory the waveguide properties are even allowed to vary with the axial position in the pipe. The two-phase pipe flow problem that we are concerned with here is a special case in which *both* the local sound speed and the local admittance may vary with position along the tube, as a consequence of variations in the cross-sectional areas covered by the two phases.

3.2.2 Dispersed composition

In contrast to flows where the phases are able to move freely relatively to each other consider an oil-water flow where one of the fluids is homogeneously dispersed as droplets in the other fluid such that the phases are intimately connected and have the same velocity. In section 3.2 the influence of heat conduction on the speed of sound was briefly discussed for single phase flows. In that section it was explained that the linearized energy equation in the zero frequency limit yields a constant entropy because the temperature gradients are negligibly small for long wavelengths and so is

the conduction of heat. In dispersions the two phases respond differently to pressure perturbations since their thermodynamic properties differ. The result is a temperature jump across the interfaces which leads to the conduction of heat. The argument for single phase flows that the conduction of heat is negligible in equilibrium does not apply to heat conduction across interfaces in dispersions. Instead, in the fully relaxed state of equilibrium not only the pressure must be the same in the two fluids, but also the temperature.

Yet, the relaxation frequency of heat conduction across the interface is very small in oil-water flows according to a rough estimate of Temkin (1992),

$$f_{\mathrm{t}} = \frac{6\nu_2\rho_* C_{p,2}}{d^2 \mathrm{Pr}_2 C_{p,1}}, \tag{3.21}$$

where d denotes the diameter of the droplets, C_p the isobaric heat capacity, ν the kinematic viscosity and Pr the Prandtl number. It is recalled that the asterisk denotes the ratio of the particular fluid properties of phase 2 and phase 1; here the dispersed phase is taken as phase 1. To give an example suppose that the dispersion consists of water and kerosene in the extreme case of very small droplets, $d = 0.2\mathrm{mm}$. Then the estimate gives $f_{\mathrm{t}} = 1\mathrm{Hz}$ when it is the water that is the dispersed phase and $f_{\mathrm{t}} = 12\mathrm{Hz}$ when it is the oil that forms the dispersed phase. It is noted that f_{t} decreases with the square of increasing drop diameters, which means that the expected value of f_{t} will be much smaller in dispersions with larger drop diameters. Temkin (1992) also gives an estimate of the relaxation frequency of the relative motion between the phases,

$$f_{\mathrm{tr}} = \frac{18\nu_2\rho_*}{d^2(1+\rho_*/2)}. \tag{3.22}$$

Typical values for kerosene-water dispersions are $f_{\mathrm{tr}} = 173\mathrm{Hz}$ for water drops dispersed in kerosene and $f_{\mathrm{tr}} = 87\mathrm{Hz}$ when it is the oil that forms the dispersed phase. The frequency range of interest is much larger than these values of the relaxation frequencies. Since f_{t} is much smaller than f_{tr} and heat conduction significantly affects the speed of sound the conduction of heat is considered as frozen in the derivation of the equilibrium speed of sound that will be given below. Strictly, it is not the true equilibrium speed of sound, but the special limit where the relative motion between the phases is fully relaxed and the process of heat conduction is frozen. In bubbly liquids, air bubbles in water, say, the values of the relaxation frequencies according to the expressions above are about $f_{\mathrm{t}} = 9600\mathrm{Hz}$ and $f_{\mathrm{tr}} = 220\mathrm{Hz}$. It is clear that heat conduction cannot be ignored in this case.

Let α be the volume concentration of the droplets, and ρ_1 and ρ_2 the densities of the droplets and the continuous phase, respectively. Then the effective density ρ * of

*Note that here ρ denotes the effective density of a dispersion and should not be confused by the effective density of a separated flow as discussed in the previous section.

the oil-water dispersion equals

$$\rho = \alpha\rho_1 + (1-\alpha)\rho_2, \tag{3.23}$$

or in terms of the mass concentration of the droplets ϕ, i.e. the mass of droplets in a unit mass of the dispersion,

$$\frac{1}{\rho} = \frac{\phi}{\rho_1} + \frac{1-\phi}{\rho_2}. \tag{3.24}$$

For equilibrium conditions the droplets simply follow the motion of the surrounding fluid due to the viscous forces so that the mass fractions are constant,

$$\phi = \frac{\alpha\rho_1}{\rho} = \text{constant}. \tag{3.25}$$

An expression for the bulk modulus of the dispersion is now obtained by considering how the density changes due to a compression for isentropic conditions in the two phases separately. By means of differentiating equation 3.24 one finds

$$\begin{aligned} \frac{1}{K} = \frac{1}{\rho c^2} = \frac{1}{\rho}\frac{\mathrm{d}\rho}{\mathrm{d}p} &= \frac{\phi\rho}{\rho_1^2}\frac{\mathrm{d}\rho_1}{\mathrm{d}p} + \frac{(1-\phi)\rho}{\rho_2^2}\frac{\mathrm{d}\rho_2}{\mathrm{d}p} \\ &= \frac{\phi\rho}{\rho_1}\frac{1}{\rho_1 c_1^2} + \frac{(1-\phi)\rho}{\rho_2}\frac{1}{\rho_2 c_2^2}. \end{aligned} \tag{3.26}$$

This shows, by employing equations 3.25, 3.23, that

$$\frac{1}{K} = \frac{\alpha}{K_1} + \frac{1-\alpha}{K_2}, \tag{3.27}$$

which is the same expression for K as for separated compositions. Some manipulation yields two alternative expressions for the speed of sound,

$$\frac{c_1^2}{c^2} = \frac{\alpha^2}{\phi} + \frac{(1-\alpha)^2}{(1-\phi)c_*^2}, \tag{3.28}$$

and

$$\frac{c_1^2}{c^2} = \left(\alpha + (1-\alpha)/K_*\right)\left(\alpha + (1-\alpha)\rho_*\right). \tag{3.29}$$

In the literature equation 3.29 is referred to as Wood's equation (Wood, 1941). The acoustic impedance is in the case of dispersed flows given by

$$\frac{Z^2}{Z_1^2} = \frac{\alpha + (1-\alpha)\rho_*}{\alpha + (1-\alpha)/K_*}, \tag{3.30}$$

where it is recalled that $Z_1 = \rho_1 c_1$ denotes the impedance of the pure phase 1.

Temkin (1992) includes heat conduction across the interfaces at the calculation of the sound speed and derives expressions for the effective entropy and thermodynamic properties of suspensions. For the equilibrium sound speed he finds an expression that differs from Wood's equation. Only when the ratios of the isobaric and the isochoric specific heats, $\gamma = C_p/C_v$, are equal to one for the two phases then the two expressions for the sound speed are the same. This condition applies approximately to water but not in general for liquids; kerosene has for instance a specific heat ratio of about 1.2. The common assumption that the value of γ is close to one for liquids is not correct (see e.g. Garvin, 2002).

The difference between the two expressions for the equilibrium sound speeds are small for dilute dispersions of gas bubbles in water, or rather, 'conceptual' in the words of the author. Still, the author mentions (in Temkin, 2000) experimental data by Karplus (1961) of the speed of sound in bubbly liquids at low frequencies ($250\,\mathrm{Hz}$, which is smaller than f_t in bubbly liquids). The data is in agreement with his theoretical prediction of the sound speed whereas Wood's relation overestimates the data slightly. He also shows in the same paper (on theoretical grounds) that in oil-water dispersions the deviation is significant. Yet, the frequency range of interest is much higher than the relaxation frequency of heat conduction and it expected that Wood's relation gives better predictions on the sound speed as long as the frequencies are not too low. For frequencies that are much higher than the relaxation frequency of the relative motion between the two phases, $f \gg f_\mathrm{tr}$, the speed of sound as given by Wood (1941) should be corrected. This correction, however, is very small (see Temkin, 2000) and will be ignored in this thesis.

3.2.3 Examples

In this section we will give some examples of the above expressions for the sound velocity for the specific case of oil-water flows. In what follows we take the oil to have density $\rho_\mathrm{oil} = 800\,\mathrm{kg\,m^{-3}}$ and sound velocity $c_\mathrm{oil} = 1200\,\mathrm{m\,s^{-1}}$, while the water has density $\rho_\mathrm{water} = 1000\,\mathrm{kg\,m^{-3}}$ and sound velocity $c_\mathrm{water} = 1500\,\mathrm{m\,s^{-1}}$. Figure 3.1 shows that the effective density of the separated flow increases almost linear with the volume fraction of water. Moreover, the difference in effective density in a dispersed and a separated composition is very small. The modulus of elasticity is the same for the two configurations. Consequently, the difference in speed of sound and impedance for the two configurations is small as can be seen in figure 3.2 where the two quantities (in terms of those in pure water) of the two-phase flow smoothly increase from their value in pure oil to that in pure water as the volume fraction of water is increased from 0 to 1. In the two-phase flow literature equation 3.29 is sometimes taken to apply to all sorts of flow configurations. The figure shows that if that expression is used to infer the volume fraction of water from measurements of the sound speed this may lead to a very slight overestimate when the flow is separated.

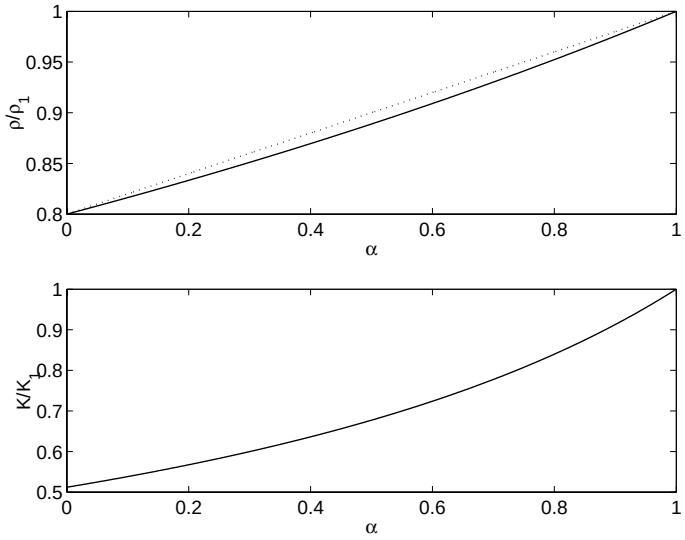

FIGURE 3.1: *Density and bulk modulus of a water-oil mixture for a dispersed (dotted) and a stratified (solid) flow in terms of their values in pure water.* $\rho_* = 800/1000$, $c_* = 1200/1500$.

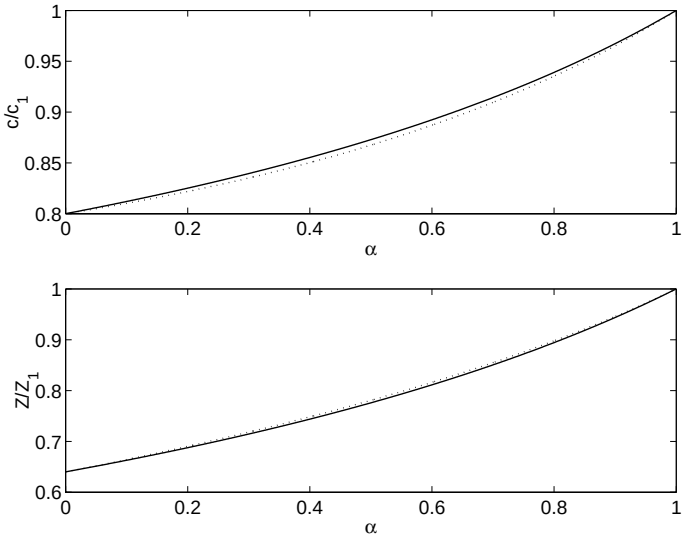

FIGURE 3.2: *Speed of sound and impedance of a water-oil mixture for a dispersed (dotted) and a stratified (solid) flow in terms of their values in pure water.* $\rho_* = 800/1000$, $c_* = 1200/1500$.

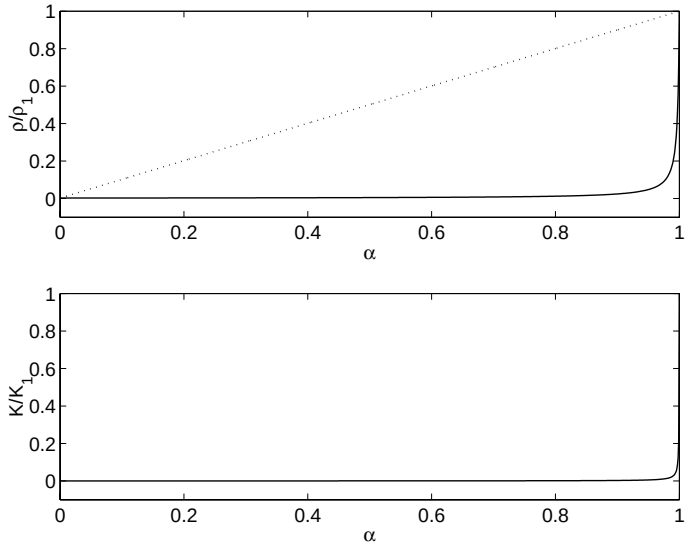

FIGURE 3.3: *Density and bulk modulus of an oil-gas mixture for a dispersed (dotted) and a stratified (solid) flow in terms of their values in pure oil.* $\rho_* = 2/800$, $c_* = 400/1200$.

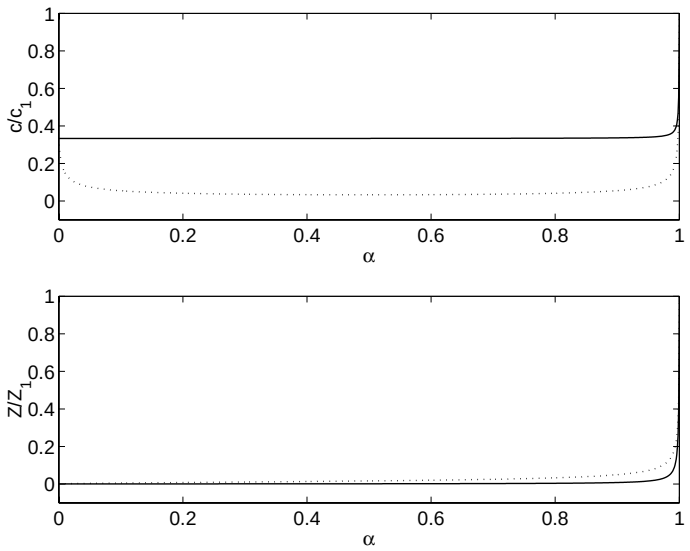

FIGURE 3.4: *Speed of sound and impedance of an oil-gas mixture for a dispersed (dotted) and a stratified (solid) flow in terms of their values in pure oil.* $\rho_* = 2/800$, $c_* = 400/1200$.

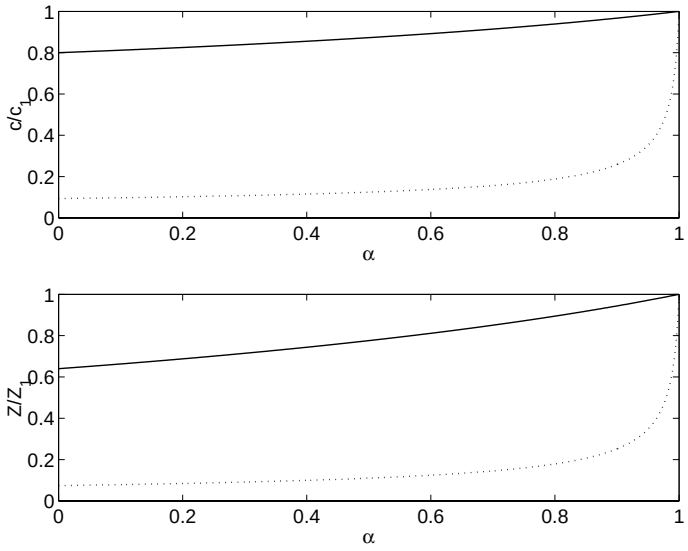

FIGURE 3.5: *Solid: speed of sound and impedance of an stratified water-oil flow in terms of their values in pure water,* $\rho_* = 800/1000$*,* $c_* = 1200/1500$*. Dotted: same with 1% gas dispersed in the oil,* $\rho_* = 792/1000$*,* $c_* = 140/1500$*.*

In practice small amounts of gas are sometimes dispersed through the oil. Figure 3.3 illustrates that the modulus of elasticity in this case is dominated by the gas and thus very small except for a very high volume fraction of oil. The effective density as function of the holdup has a similar shape for separated flows. However, in dispersed flows the effective density varies linearly with the holdup. This has a dramatic effect on the sound velocity, see figure 3.4. Here the gas is assumed to have density $\rho_{\mathrm{gas}} = 2\mathrm{kg}\mathrm{m}^{-3}$ and sound speed $c_{\mathrm{gas}} = 400\mathrm{ms}^{-1}$. In a dispersion the speed of sound drops down to a level even far below c_{gas}. For example when the gas volume fraction is increased from 0 to 0.01 (i.e. to 1%) the sound velocity of the dispersion drops from $1200\mathrm{ms}^{-1}$ to only about $200\mathrm{ms}^{-1}$. In separated configurations the speed of sound takes the (constant) sound velocity of the gas over almost the whole holdup range. Only when the medium is close to the liquid phase the speed of sound abruptly inclines to its value in pure oil. The impedance varies with the oil volume fraction in a similar way as the modulus of elasticity.

The reduced effective stiffness of liquids by the presence of gas substantially changes the sound speeds of oil-water flows when a small amount of gas is dispersed in the oil. In Figure 3.5 the speed of sound and impedance in a separated oil-water flow is compared to the same configuration but now with oil in which 1% of gas is present, so that the sound speed of the oil is reduced to $140\mathrm{ms}^{-1}$. It is clear that the influence of the presence of the gas on the acoustic properties of the three-phase

medium is huge. In fact, the presence of just a bit of gas reduces the effects of non-uniform liquid properties to higher order details. Note, equations 3.13, 3.23, that the effective density determines the difference in acoustic properties between a separated and a dispersed flow. Since the presence of a small amount of gas hardly affects the density of the oil phase the flow configuration, separated or dispersed, influences the acoustic properties in a similar small way as in the case where the gas is absent; i.e. a three phase dispersion yields approximately the same curves as in figure 3.5.

3.3 Attenuation of sound waves

Some sources of attenuation are related to the diffusion of momentum and heat within the bulk of the flow which would also occur in an infinite medium in the absence of walls. Additionally, dissipation of acoustic energy occurs in a boundary layer near the pipe wall. Pierce (1981) explains that in waveguides consisting of a single phase medium it is the attenuation due to the presence of the wall that is dominant. Both the velocity and the temperature fluctuations are adjusted to the value of zero at the wall when it is hard and conducts heat well. This leads to the formation of a thermal and a viscous boundary layer. According to Morse and Ingard (1968) the thicknesses of the viscous and the thermal boundary layers, also called the *penetration depths*, may be estimated by

$$d_{\mathrm{v}} = \sqrt{\frac{2\nu}{\omega}}, \quad d_{\mathrm{t}} = \sqrt{\frac{2\nu}{\omega \mathrm{Pr}}}, \tag{3.31}$$

respectively. In the case of liquids the Prandtl number Pr is usually larger than one. Therefore in liquids the viscous boundary layer is thicker than the thermal one and contributes the dominant part to the attenuation of sound waves. In dispersions the dissipation in the bulk of the flow is larger than in single phase flows because of the friction between the two phases when the drops move relative to the surrounding fluid. Moreover, the adjustment of the temperature difference between the two phase through heat conduction is a significant source of dissipation. These two effects produce substantial contributions to the total attenuation of the sound waves, this besides the friction near the wall.

It is noted that at very low frequencies the penetration depths may become in the order of magnitude of the pipe diameter. Obviously, the non equilibrium effects are no longer confined in thin boundary layers at the all but are present in the entire cross-section of the pipe (e.g. Tijdeman, 1975). However, this plays only a role for frequencies below the frequency range of interest.

3.3.1 Frictional attenuation near the wall

According to Lighthill (1978) the viscous boundary layer in single phase flows generates a defect of volume flow as induced by the excess pressure. For monochromatic

waves this defect may be incorporated in the linearized momentum equation of a single phase flow,

$$\frac{\partial u}{\partial t} = -\frac{1}{\rho}\frac{\partial p_e}{\partial x}\left[1 - \frac{s}{A_0}\sqrt{\frac{\mathrm{i}\nu}{\omega}}\right], \tag{3.32}$$

where s and A_0 are the perimeter and the cross-section of the pipe, respectively, and ν the kinematic viscosity. It is noted that the monochromatic waves are proportional to $\mathrm{e}^{-\mathrm{i}\omega t}$ instead of the convention $\mathrm{e}^{\mathrm{i}\omega t}$ that is used by Lighthill (1978). For circular ducts the ratio A_0/s can be written in terms of the diameter of the pipe as $A_0/s = D/4$. It follows from equation 3.32 that the reciprocal of the density, $1/\rho$, may be replaced by

$$\frac{1}{\rho}\left[1 - \frac{4}{D}\sqrt{\frac{\mathrm{i}\nu}{\omega}}\right] \tag{3.33}$$

to include the wall friction. Since the linearized equation of continuity remains unaltered and so does the bulk modulus, the speed of sound $c = \sqrt{K/\rho}$ and the impedance $Z = \sqrt{K\rho}$ are to be replaced by

$$c\left[1 - \frac{4}{D}\sqrt{\frac{\mathrm{i}\nu}{\omega}}\right]^{\frac{1}{2}} \quad \text{and} \quad Z\left[1 - \frac{4}{D}\sqrt{\frac{\mathrm{i}\nu}{\omega}}\right]^{-\frac{1}{2}}, \tag{3.34}$$

respectively.

When the medium consists of two separated fluids the wall boundary layer is similar in nature. The defect of the volume flow then consist of two contributions. For each of the phases the associated defects are included in the linearized momentum equation as,

$$\frac{\partial \alpha u_1}{\partial t} = -\frac{\alpha}{\rho_1}\frac{\partial p_e}{\partial x}\left[1 - \frac{s_1}{A_1}\sqrt{\frac{\mathrm{i}\nu_1}{\omega}}\right], \tag{3.35}$$

$$\frac{\partial (1-\alpha) u_2}{\partial t} = -\frac{(1-\alpha)}{\rho_2}\frac{\partial p_e}{\partial x}\left[1 - \frac{s_2}{A_2}\sqrt{\frac{\mathrm{i}\nu_2}{\omega}}\right]. \tag{3.36}$$

Adding these two equation yields a modified form of equation 3.12,

$$\frac{\partial u}{\partial t} = -\frac{1}{\rho}\frac{\partial p_e}{\partial x} + \frac{1}{\rho}\frac{\partial p_e}{\partial x}\left[\frac{\rho}{\rho_1}\frac{s_1}{s}\sqrt{\nu_1} + \frac{\rho}{\rho_2}\frac{s_2}{s}\sqrt{\nu_2}\right]\frac{4}{D}\sqrt{\frac{\mathrm{i}}{\omega}}. \tag{3.37}$$

Upon introducing the perimeter fraction

$$\sigma = s_1/s, \quad \text{and thus} \quad s_2/s = 1 - \sigma, \tag{3.38}$$

the reciprocal of the effective density of the separated composition may be replaced in the same way as above but now with an effective viscosity that is given by

$$\sqrt{\nu} = \frac{\rho}{\rho_1}\sigma\sqrt{\nu_1} + \frac{\rho}{\rho_2}(1-\sigma)\sqrt{\nu_2}. \tag{3.39}$$

For a given flow configuration the volume fraction α is related to the perimeter fraction. In core-annular flows only the annulus wets the wall. The perimeter fraction is thus equal to zero (given that phase 2 covers the annulus). In order to obtain the relation between α and σ for stratified flows consider the sketch of the cross-section of the pipe in figure 3.6 (left). The fraction σ of the perimeter s that is covered by phase 1 may be expressed in terms of the angle θ,

$$\sigma = \frac{s_1}{s} = \frac{2\theta R}{2\pi R} = \frac{\theta}{\pi}. \tag{3.40}$$

Then the area that is covered by phase 1 is equal to

$$A_1 = \frac{2\theta}{2\pi}\pi R^2 - R^2\sin\theta\cos\theta = R^2\left(\theta - \tfrac{1}{2}\sin 2\theta\right). \tag{3.41}$$

Dividing A_1 by the total cross-section of the pipe leads to an expression of the volume fraction α of phase 1 in terms of the angle θ,

$$\alpha = \frac{A_1}{A} = \frac{1}{\pi}\left(\theta - \tfrac{1}{2}\sin 2\theta\right). \tag{3.42}$$

Combining equations 3.40, 3.42 yields

$$\alpha = \sigma - \frac{1}{2\pi}\sin 2\pi\sigma. \tag{3.43}$$

Unfortunately, its analytical inverse cannot be written down in closed form. Therefore expressing σ in terms of α has been done numerically. The result is shown in figure 3.6 (right).

For harmonic waves, $p \sim \mathrm{e}^{\mathrm{i}\omega(x/c-t)}$, the corrected factor $1/c$ in the exponent can be approximated as

$$\frac{1}{c}\left[1 + \tfrac{1}{2}(1+\mathrm{i})\tfrac{4}{D}\sqrt{\tfrac{\nu}{2\omega}}\,\right]. \tag{3.44}$$

The real part of the correction means a (usually negligibly small) reduction of the wave speed, the imaginary part describes the attenuation of the waves due to wall friction. Substituting the imaginary part in the exponent of a harmonic wave,

$$p \sim \mathrm{e}^{-x\frac{\sqrt{2\nu\omega}}{Dc}}, \tag{3.45}$$

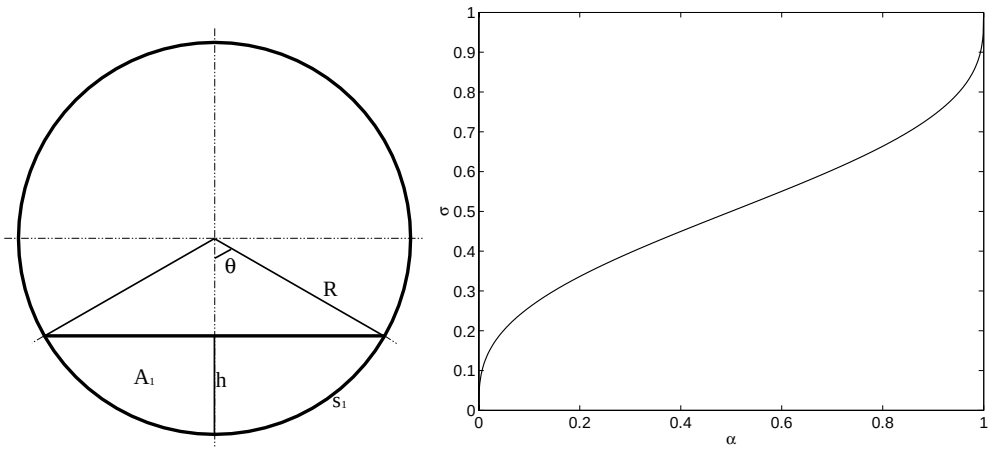

FIGURE 3.6: *Left: cross-section of the pipe containing a stratified configuration. Right: perimeter fraction σ in terms of the volume fraction α for a stratified configuration in a circular pipe.*

shows that the attenuation length, being the reciprocal of the attenuation coefficient, due to wall friction should be taken as

$$L_{\mathrm{wf}} = 1/\gamma_{\mathrm{wf}} = \frac{Dc}{\sqrt{2\nu\omega}}. \tag{3.46}$$

The adjustment of the velocities of the two phases to each other at the interface is a similar process as the adjustment of velocity at the pipe walls. In the absence of friction the velocity difference between the two phases follows from the linearized momentum equation. Since the pressure tends to be uniform over the cross-section for low frequencies and so its derivative with respect to x the mass flow in the two phases must be the same, $\rho_1 u_1 = \rho_2 u_2$, and hence the velocity difference becomes $u_1 - u_2 = u_2(\rho_* - 1)$. For liquid-liquid flows the density ratio ρ_* is close to one which results in a small velocity difference compared to u_1 and u_2 which are to be adjusted near the wall. The friction near the wall clearly dominates the viscous attenuation above the friction at the interface in this case. It is noted that this is not the case for separated gas-liquid flows.

3.3.2 Attenuation in dispersions

In dispersions the attenuation in the bulk of the flow cannot be neglected with respect to the dissipation near the wall of the pipe. The relative motion between the drops and the surrounding fluid causes a viscous dissipation of sound waves. In addition, the sound waves attenuate through the conduction of heat across the interfaces. These two mechanisms are the main two non-equilibrium effects next to the adjustment of the velocity and the temperature perturbations to their values at the wall. The two

effects are essentially correlated but within the approximation where the dimensionless parameter $(\gamma-1)\nu\omega/(c\mathrm{Pr})$, evaluated for the surrounding fluid, is small the two effects may be treated separately (Epstein and Carhart, 1953).

The most widely used theory on dissipation of sound waves in dilute dispersions is the ECAH-theory, named after Epstein and Carhart (1953) and Allegra and Hawley (1972). The first paper is concerned with absorbtion of sound by water fog in air. In the second paper the theory is generalized to suspensions of rigid particles in a fluid, but is also, according to the authors, generally applicable to dilute dispersions consisting of two fluids. In the paper they present experiments on the attenuation of sound in an emulsion of toluene droplets in water, an emulsion of liquid and solid hexadecane particles in water and suspensions of polystyrene spheres in water. The results are in agreement with the theory. Furthermore, the authors show that the ECAH-theory is equivalent to the work by Isakovich (1948) in the limit of long wavelengths.

In the theory the attenuation produced by the presence of particles is written in terms of three contributions to the attenuation coefficient. In this linear theory the different attenuation coefficients being the reciprocals of the associated attenuation lengths of the particular process, may be added to give the total attenuation coefficient,

$$1/L_{\mathrm{att}} = 1/L_{\mathrm{wf}} + 1/L_{01} + 1/L_{02} + 1/L_1. \tag{3.47}$$

The terms denote attenuation through wall friction, heat conduction in the pure phases, heat conduction across the interfaces and viscous dissipation at the interfaces, respectively. The attenuation due to the conduction of heat in the pure phases is negligibly small and therefore the term $1/L_{01}$ is omitted. The final two contributions to the attenuation in equation 3.47 are given in terms of the wavelength by

$$\lambda/L_{02} = \tfrac{3}{2}\pi\alpha c^2 T_0 C_{p,2}\rho_2^2\left[\tfrac{\beta_2}{\rho_2 C_{p,2}} - \tfrac{\beta_1}{\rho_1 C_{p,1}}\right]^2 \tfrac{\mathrm{Re}H(X_2,X_1)}{X^2}, \tag{3.48}$$

$$\lambda/L_1 = 3\pi\alpha\left(\rho_* - 1\right)\mathrm{Re}(\mathrm{i}F(Y_2,Y_1)), \tag{3.49}$$

where β denotes the coefficient of thermal expansion, T_0 the undisturbed temperature and $X = R/d_t$ and $Y = R/d_v$ the ratio of the droplet radius and the penetration depths (see equation 3.31) of thermal and shear waves, respectively. Hence

$$X = R\sqrt{\frac{\omega\mathrm{Pr}}{2\nu}},\;\; Y = R\sqrt{\frac{\omega}{2\nu}}. \tag{3.50}$$

The functions H and F are given by

$$H = H_n/H_d, \quad F = F_n/F_d, \tag{3.51}$$

where

$$H_n = \left[1 + (1-\mathrm{i})X_2\right]\left[(1-\mathrm{i})X_1 - \tanh((1-\mathrm{i})X_1)\right], \tag{3.52}$$

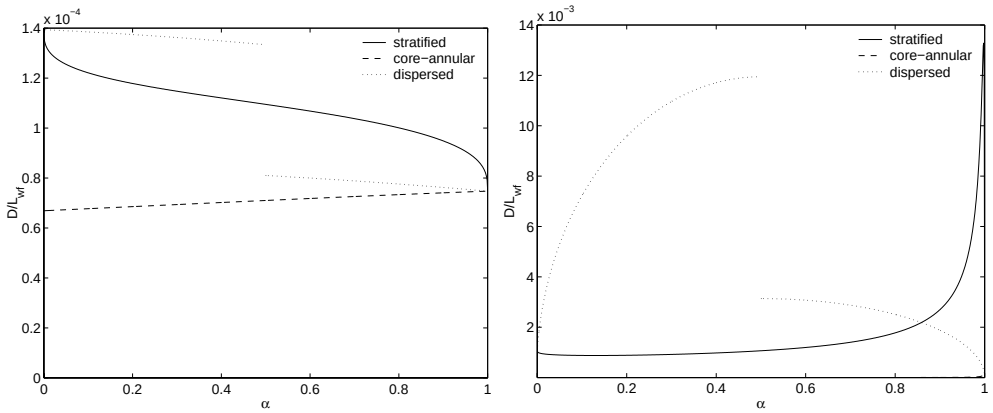

FIGURE 3.7: *Left graph: attenuation per diameter due to wall friction of a* $1000\,\mathrm{Hz}$ *sound wave varying with the volume fraction of water in a stratified flow (solid), in a kerosene core surrounded by a water annulus (dashed), in a dispersion of water in kerosene (dotted left), in a dispersion of kerosene in water (dotted right). Right graph: the same but with the kerosene replaced by gas.*

$$H_d = [(1-\mathrm{i})X_1 - \tanh((1-\mathrm{i})X_1)] + [1 + (1-\mathrm{i})X_2]\,\kappa_* \tanh((1-\mathrm{i})X_1) \quad (3.53)$$

and κ denotes the thermal conductivity. Furthermore,

$$F_n = h_2(\hat{Y}_2)Q - \nu_*\rho_*\hat{Y}_2 h_1(\hat{Y}_2) j_2(\hat{Y}_1), \quad (3.54)$$

$$F_d = \left[3\rho_* h_2(\hat{Y}_2) + 2(\rho_* - 1)h_0(\hat{Y}_2)\right] Q - \nu_*\rho_*\hat{Y}_2 h_1(\hat{Y}_2) j_2(\hat{Y}_1)(\rho_* + 2), \quad (3.55)$$

with

$$Q = \hat{Y}_1 j_1(\hat{Y}_1) - 2(1 - \nu_*\rho_*) j_2(\hat{Y}_1), \;\; \hat{Y}_1 = (1+\mathrm{i})Y_1, \;\; \hat{Y}_2 = (1+\mathrm{i})Y_2. \quad (3.56)$$

The functions j_k, h_k denote the k^{th}-order spherical Bessel functions of the first and the third kind (1^{st} spherical Hankel function), respectively. In the relations on the damping per wavelength, equations 3.48, 3.49, the drop radius R and the frequency f only appear in the penetration depths X and Y. Since they are both proportional to $R\sqrt{f}$ also the damping per wavelength is a function of $R\sqrt{f}$, or alternatively, of $R^2 f$. The attenuation coefficients per unit length of the pipe ($1/L_{02}$ and $1/L_1$) are found by dividing equations 3.48, 3.49 over the wavelength $\lambda = c/f$.

3.3.3 Examples

In order to estimate the importance of the different sources of attenuation in specific configurations as described in Chapter 2 some examples are given of flows consisting of kerosene and water. In addition, systems are considered where the flow consists of water and gas in order to illustrate what this approach means when the properties

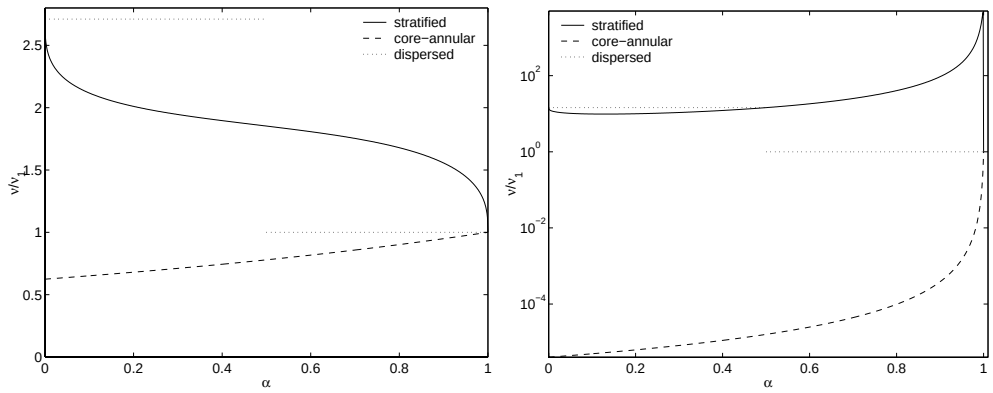

FIGURE 3.8: *Effective viscosity varying with α corresponding to the configurations as in figure 3.7 for kerosene-water (left) and for gas-water (right).*

of the fluids have a larger contrast. It is noted that in the approach of determining the attenuation in separated configurations, only the friction near the wall is taken into account. The effects of damping at the interface between the two fluids is neglected. For gas-liquid systems the dissipative effects at the interface are substantial and should not be ignored. The properties of all fluids are tabulated below.

	$\rho_{[\mathrm{kg\,m^{-3}}]}$	$c_{[\mathrm{m\,s^{-1}}]}$	$\nu_{[10^{-6}\,\mathrm{m^2\,s^{-1}}]}$	$C_{p\,[\mathrm{J\,kg^{-1}\,K^{-1}}]}$	Pr	$\beta_{[10^{-3}\,\mathrm{K^{-1}}]}$	γ
water	1000	1500	1.0	4190	8.1	0.21	1.0
kerosene	790	1324	2.7	2010	28	0.99	1.2
gas	2	400	15	1012	0.7	3.48	1.4

Let us start with some examples of the friction near the wall according to equations 3.46, 3.39. Three different flow configurations are considered. The first is a stratified flow of kerosene flowing on top of a layer of water. In this case the perimeter fraction σ of phase 1, the water, is related to volume fraction α according to equation 3.43. In figure 3.6 (right) this relation is visualized. The second flow configuration is a core consisting of kerosene embedded in a water annulus. Here the wall is wetted by the water and thus is the perimeter fraction always equal to 1 and does not depend on the volume fraction, except for, of course, the situation where α takes a value close to one such that width of the annulus becomes smaller than the boundary layer thickness. This effect is ignored in the following; i.e for all values of α, even for $\alpha = 1$, it is the water that is assumed to wet the pipe wall. For these two cases the wall friction is calculated by employing the effective viscosity and equations 3.13, 3.15. In the third example the medium consists of a dispersion of water drops in kerosene for $\alpha < 0.5$ and a dispersion of kerosene drops in water when $\alpha > 0.5$. The corresponding phases that wet the wall and determine the viscosity in equation 3.46 are the kerosene and the water, respectively. Wood's relation is used for the speed of sound c in this case.

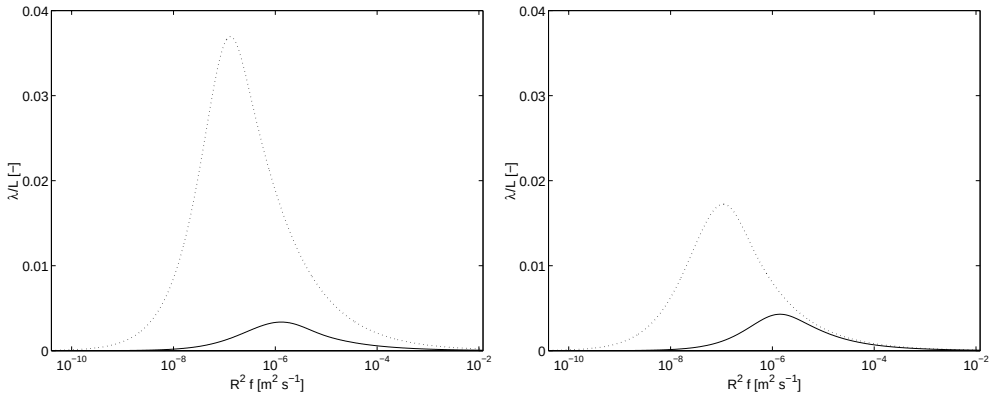

FIGURE 3.9: *Attenuation per wavelength in a dispersion of* 10% *kerosene in water (left) and* 10% *water in kerosene (right) by thermal conduction (dotted) and by viscous shear (solid). The range of* $R^2 f$ *covers frequencies up to* $3000\,\mathrm{Hz}$ *and droplet radii up to* $2\,\mathrm{mm}$.

In figure 3.7 (left) the attenuation coefficients of the three configurations are plotted against the volume fraction of the water, in terms of the pipe diameter D. The frequency of sound waves is taken as $1000\,\mathrm{Hz}$. The largest damping occurs in the dispersion of water in kerosene. At $\alpha = 0.5$ the attenuation coefficient obviously drops. After all for $\alpha > 0.5$ the dispersion is considered to consist of kerosene drops in water. The water wets the pipe wall in that case and since water has a smaller viscosity than kerosene the damping coefficient will be smaller. For all volume fractions of the water the damping remains decreasing with α. This can be explained by noting that the sound speed of these dispersions slightly increases with α and that the attenuation coefficient is proportional to the reciprocal of the speed of sound.

In figure 3.7(right) the kerosene has been replaced by gas. In this case the damping in dispersions of gas in water increases with α because here the speed of sound does not increase but drops (quite steeply for small α) with the volume fraction of the water. When the volume fraction is larger than 0.5 the situation is similar, but now the sound speed increases and consequently the attenuation decreases. The other lines in the figures clearly show the influence of the effective density on the effective viscosity. For the core-annular configuration the perimeter fraction has a constant value of one and thus, see equation 3.39 and figure 3.8, is the square root of the effective viscosity proportional to the effective density; hence, $D/L_{\mathrm{wf}} \sim \rho/c$. For kerosene and water the increasing density 'wins' slightly over the increasing speed of sound. In the gas-water analogue the effective density and the sound speed hardly vary except for values of α that are close to one. The attenuation coefficient in stratified water-kerosene flows diminishes gradually with α. Only close to $\alpha = 0$ and $\alpha = 1$ the curve becomes steep. Upon considering the relation for the effective viscosity, equation 3.39, and noting that the effective density changes almost linearly with α,

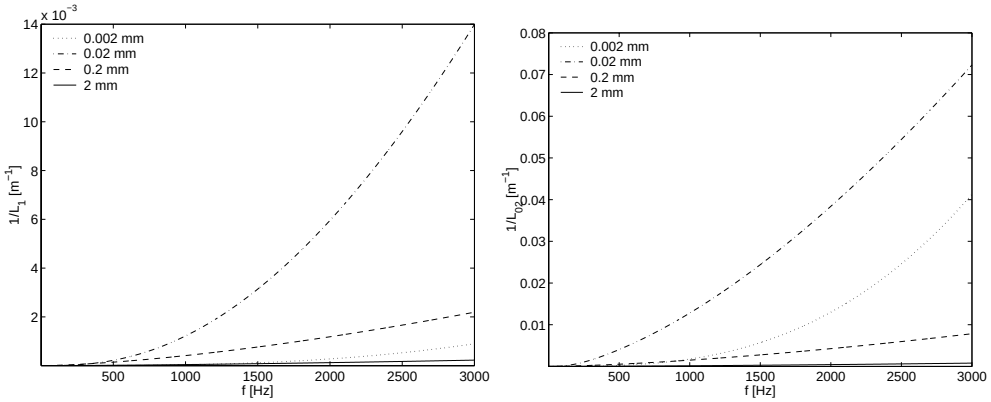

FIGURE 3.10: *Attenuation coefficient in a dispersion of* 10% *kerosene in water due to viscous shear (left) and due to thermal conduction (right) for several drop radii.*

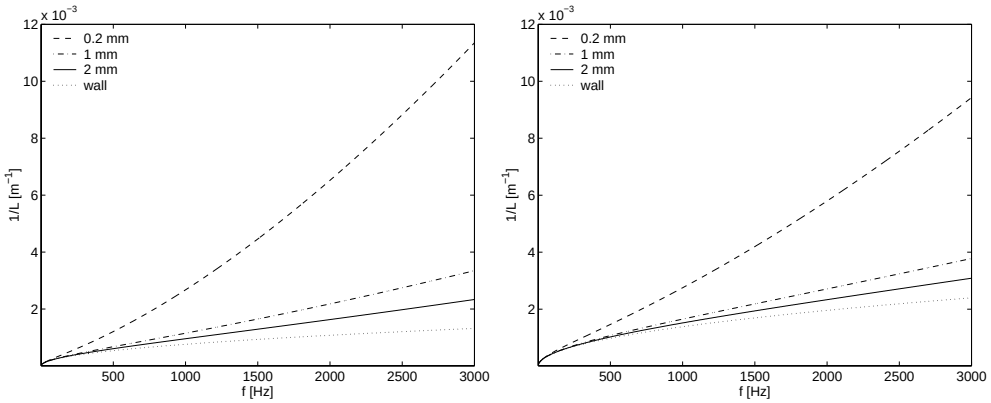

FIGURE 3.11: *Total attenuation in a dispersion of* 10% *kerosene in water (left) and* 10% *water in kerosene (right) due to viscous shear, thermal conduction and wall friction for several drop radii. The dotted lines denote the wall friction only.*

see figure 3.1, it becomes clear that the reason for this sudden change of slope has to be sought in the dependency of the perimeter fraction σ on α. Figure 3.6 (right) shows that the graph of $\sigma(\alpha)$ is very steep at the domain boundaries of α. Consequently, the transition of the viscosity of pure water towards that of the pure kerosene takes place rapidly near the boundaries of α.

In the gas-water analogue the effective density is almost constant up to $\alpha = 0.9$ and then increases abruptly to its value of pure water. This means that the ratio of the effective density and the density of the pure gas, ρ/ρ_2, in the second term in equa-

tion 3.39 corresponding to the gas phase becomes very large. This is clearly visible in the graph where the attenuation coefficient increases rapidly to values beyond those of the pure fluids and then falls back to the value of the pure water.

The next example is concerned with the attenuation in dispersions. Also here the dispersion consists of kerosene and water. Since in the ECAH-theory the interaction between the drops is neglected the attenuation coefficient is proportional to the volume fraction. In this example it has the value of 10%. Figure 3.9 shows the attenuation per wavelength varying with $R^2 f$ as a result of thermal conduction (dotted) and of viscous shear (solid). The dispersion plotted in the left figure is that of kerosene in water while in the right figure it is opposite. It appears that the damping in the kerosene in water dispersion is approximately a factor two larger. The shape of all curves is similar and it is clear that the thermal damping is dominant. Moreover, the two damping coefficients per wavelength have a maximum. Figure 3.10 visualizes the damping per unit length of the pipe for several drop sizes ranging from $R = 210^{-3}\mathrm{mm}$ to $R = 2\mathrm{mm}$. The maxima in figure 3.9 are also recognized in figure 3.10 as for increasing drop size the damping goes up to its largest value for $R = 0.02\mathrm{mm}$ and then decreases again. As discussed in section 2.3, in experiments drop sizes have been observed in the range up to $R = 0.3\mathrm{mm}$ and in the range up to several millimeters in other experiments. Figure 3.11 shows the total attenuation, including wall friction, of sound waves in dispersion for drops that have the sizes as observed. In addition, the attenuation due to the friction near the wall is included separately in the graphs. In the two graphs in the figure the damping in the bulk of the dispersion is in the same order of magnitude as the damping due to the wall friction. Yet, for the smallest drops the wall friction contributes only to a small extent to the total attenuation.

3.4 Discussion

In this chapter the propagation properties of low frequency sound waves in separated and dispersed two-phase flows in pipes were considered. Expressions were derived for the density, the bulk modulus, the speed of sound and the impedance of the two-phase configurations as mentioned above. The derived relations suggest that these acoustic properties of oil-water flows for the two considered configurations are almost the same. Gas-water systems, however, do exhibit differences. Whilst the speed of sound in dispersions drops to values even below the sound speed of the pure fluids in stratified flows the sound speed is very close to that of the gas, except for very large volume fractions of water.

Non-equilibrium effects due to viscous friction near the wall and relaxation mechanisms in dispersions result mainly in the dissipation of sound; the speed of sound and the impedance as in the equilibrium situation are hardly affected. The attenu-

ation length due to wall friction was for the analyzed systems about $700 - 1400\,\mathrm{m}$ in oil-water flows and $10 - 1000\,\mathrm{m}$ in gas-water systems at $1000\,\mathrm{Hz}$. However, friction at the interfaces between the phases was not taken into account. Especially for gas-water flows the associated damping is presumably significant. For the attenuation in dispersions the theory of Epstein and Carhart (1953) and Allegra and Hawley (1972) was employed. At $1000\,\mathrm{Hz}$ the attenuation length was found to be in the range $500 - 1000\,\mathrm{m}$ for dispersions of 10% kerosene in water and only slightly smaller for dispersions of 10% water in kerosene for drop sizes of $0.2 - 2\,\mathrm{mm}$.

WAVEGUIDE MODES

CHAPTER 4

4.1 Introduction

The previous chapter involved the propagation properties of sound waves in pipes containing a two phase composition whose phase distribution does not vary with the position along the pipe. The wavelengths were supposed to be long compared to the diameter of the pipe, which justifies the approach of considering longitudinal waves. In this chapter it will be investigated to what extent this one-dimensional approach is judicious and to what degree the sound speed depends on the frequency. In addition, it will be shown how the *waveguide modes* as for single phase flows are affected when the flow consists of two phases.

In the next section the maximum frequency for which the propagation of sound is purely one-dimensional, i.e. the *cutoff frequency*, will be calculated analytically for single phase compositions. Above this cutoff frequency also the higher dimensional waveguide modes may propagate through the pipe in addition to the one-dimensional *fundamental* mode. In literature the fundamental mode is often called the *plane* wave. Presumably, the low frequency range of interest ($200 - 2000\,\mathrm{Hz}$), compared to the cutoff frequency, warrants to restrict attention to the purely longitudinal modes of sound propagation. Yet, it is expected that in two-phase flow configurations the cut-off frequencies differ from the ones in single phase flows, although the differences are probably small in oil-water flows where the two phases have similar acoustical properties. A second difference is that the waves in single phase flows are, in the absence of non-equilibrium effects, not dispersive below the smallest cutoff frequency. This is not obvious in two-phase flows. To what extent the cutoff frequencies of the waveguide modes are affected by medium inhomogeneities will be considered in the following sections as well as the effect on the propagation of the fundamental mode.

Calculating the waveguide modes of two-phase configurations is more complicated than those of single phase flows. Exceptions of this are uniform dispersions, which may be considered as single phase flows that have particular effective acoustic properties as derived in the previous chapter. The waveguide modes will therefore be the same as the ones of single phase flows. Calculating the modes of well-separated

configurations by means of the same analytical method that is used for single phase flows is only possible for some particular flow configurations. One of these configurations is the core-annular configuration whose waveguide modes are discussed in section 4.3. Unfortunately, the modes of stratified flows cannot be computed analytically in this way, at least not in circular waveguides. Instead, a numerical approach will be employed.

To the author's knowledge, among the first who have investigated the waveguide modes of stratified flows are Morioka and Matsui (1975). They derived analytically the dispersion relation for two-dimensional ducts containing a stratified gas-liquid configuration and solved it numerically. The fact that the density ratio is very small in gas-liquid flows has not been employed in their work and, hence, their dispersion relation also holds for oil-water systems. Sinai (1984) solved the dispersion relation as well and noticed a second class of solutions. The appearance of two classes of solutions is due to the huge density contrast between liquids and gases. The author argues by means of asymptotic solutions that the waveguide should in fact be considered as two separate waveguides that are coupled only slightly; one waveguide contains pure gas and the other pure liquid. In oil-water systems the contrast in density is much smaller and as a consequence only one class of solutions is expected. In section 4.4 the dispersion relation found by Morioka and Matsui (1975) will be extended to the three-dimensional case of a square duct containing a stratified configuration. The results give much insight into the acoustics of stratified flows in circular ducts as will become clear upon comparing them to the results of the numerical computations for circular ducts.

4.2 Single phase composition

The behavior of sound waves in waveguides is described by many authors (e.g. Morse and Ingard, 1968; Lighthill, 1978; Pierce, 1981) in terms of waveguide modes. Consider for instance a circular waveguide with a constant radius R filled with a single phase medium with sound speed c. Then any travelling monochromatic sound wave with an angular frequency ω may be expressed in terms of an expansion in waveguide modes,

$$p = \sum_{m=0}^{\infty} \sum_{n=0}^{\infty} a_{mn} p_{mn}(r,\theta) \mathrm{e}^{\mathrm{i}(k_{mn}x - \omega t)}, \tag{4.1}$$

where $p_{mn}(r,\theta)$ expresses the shape of the mode and k_{mn} denotes the corresponding wavenumber. This expression satisfies the wave equation in cylindrical coordinates if

$$\left(\frac{\partial^2}{\partial r^2} + \frac{1}{r}\frac{\partial}{\partial r} + \frac{1}{r^2}\frac{\partial^2}{\partial \theta^2} + \frac{\omega^2}{c^2} \right) p_{mn} = k_{mn}^2 p_{mn}. \tag{4.2}$$

The squares of the wavenumbers, k_{mn}^2, are the eigenvalues to the Helmholtz operator in the left-hand side of equation 4.2; p_{mn} are the corresponding eigenfunctions. This eigenvalue problem may be written in terms of the resonance frequencies ω_{mn} or wavenumbers κ_{mn},

$$\omega_{mn}^2 = \omega^2 - k_{mn}^2 c^2, \quad \kappa_{mn} = \omega_{mn}/c. \tag{4.3}$$

In terms of the latter equation 4.2 becomes

$$\left(\frac{\partial^2}{\partial r^2} + \frac{1}{r}\frac{\partial}{\partial r} + \frac{1}{r^2}\frac{\partial^2}{\partial \theta^2} \right) p_{mn} = -\kappa_{mn}^2 p_{mn}. \tag{4.4}$$

It is clear that $-\kappa_{mn}^2$ are the eigenvalues to the Laplace operator whereas the associated eigenfunctions p_{mn} are, obviously, identical to the ones of the related Helmholtz operator. Equation 4.4 has the form of the Helmholtz equation and its solutions are readily found to be

$$p_{mn}(r,\theta) = \mathrm{e}^{-\mathrm{i}m\theta} \left[J_m(\kappa_{mn} r) + b_{mn} Y_m(\kappa_{mn} r) \right], \tag{4.5}$$

where J_m and Y_m are the m^{th} order Bessel functions of the first and of the second kind, respectively. The coefficient b_{mn} must be zero since the functions Y_m are singular at the origin while the solution must remain finite. In addition, for a hard-walled pipe the eigenfunctions p_{mn} should satisfy the boundary condition of zero normal derivative on the wall. For these conditions the eigenfunctions become

$$p_{mn}(r,\theta) = \mathrm{e}^{-\mathrm{i}m\theta} J_m(\kappa_{mn} r), \tag{4.6}$$

where the values of κ_{mn} are to be determined from the condition

$$J_m'(\kappa_{mn} R) = 0. \tag{4.7}$$

Here J_m' denotes the derivative of J_m with respect to its argument. For each integer value of m there exists a discrete set of values κ_{mn}, each of which satisfies equation 4.7. Introduce the notation

$$\alpha_{mn} = \frac{\kappa_{mn} R}{\pi} = \frac{\omega_{mn} R}{\pi c}. \tag{4.8}$$

Then for a few of the smallest κ_{mn} the corresponding numerical values of α_{mn} can be inferred from table 4.1.

The fundamental mode, $p_{00}(r,\theta) = 1$, has $\omega_{00} = 0$ and corresponds to strictly one-dimensional waves with angular frequency ω and propagating with the sound speed c of the medium. For $k_{mn} > 0$ the waveguide modes travel with phase velocity

$$\frac{\omega}{k_{mn}} = c \, \frac{\omega}{(\omega^2 - \omega_{mn}^2)^{\frac{1}{2}}}, \tag{4.9}$$

$$\begin{array}{lll} \alpha_{00} = 0.0000 & \alpha_{01} = 1.2197 & \alpha_{02} = 2.2331 \\ \alpha_{10} = 0.5861 & \alpha_{11} = 1.6970 & \alpha_{12} = 2.7140 \\ \alpha_{20} = 0.9722 & \alpha_{21} = 2.1346 & \alpha_{22} = 3.1734 \end{array}$$

TABLE 4.1: *Values of α_{mn} for a single phase configuration.*

exceeding the sound speed c. These modes are dispersive, and have group velocity (energy propagation velocity)

$$\frac{\mathrm{d}\omega}{\mathrm{d}k_{mn}} = c\frac{(\omega^2 - \omega_{mn}^2)^{\frac{1}{2}}}{\omega}, \tag{4.10}$$

which is always lower than c. Equation 4.9 shows that a waveguide mode can only propagate when $\omega > \omega_{mn}$. The modes for which the cutoff frequency is greater than the frequency, $\omega_{mn} > \omega$ are evanescent waves. These modes attenuate,

$$p_e \sim \mathrm{e}^{-x/L_{\mathrm{att}}}, \text{ with } L_{\mathrm{att}} = \frac{c}{(\omega_{mn}^2 - \omega^2)^{\frac{1}{2}}} \tag{4.11}$$

the attenuation length. For frequencies less than ω_M, where ω_M is the smallest positive eigenfrequency, wave motion is confined to strictly one-dimensional propagation. For the cylindrical hard-walled pipe $\omega_M = \omega_{10}$, so that for frequencies

$$f < f_M = \frac{0.5861c}{2R} \tag{4.12}$$

it is permissible to restrict attention to strictly one-dimensional propagation. In oil-water flows the sound speeds c lie within the range $1200 - 1500\mathrm{ms}^{-1}$. For a typical experiment in a pipe with diameter $2R = 0.1\mathrm{m}$, say, the lowest cutoff frequency is about $7033\mathrm{Hz}$, much higher than the frequencies that concern us here. Still, the cutoff frequency as derived above is only valid for a single phase systems and not for a two-phase configurations.

4.3 Waveguide modes in a core-annular composition

The analytical modal expansion as derived in the previous section is based on the circular symmetry of the waveguide walls; that is in cylindrical coordinates the pipe wall is located along a curve of a constant radius $r = R$. Then equation 4.2, or rather equation 4.4, may be solved by means of separation which means that the modes are of the form $p_{mn}(r, \theta) = F_{mn}(r)G_{mn}(\theta)$. The modes of a two-phase configuration still satisfy equation 4.2 but with the difference that now the speed of sound varies over the cross-section of the pipe, so

$$\left(\frac{\partial^2}{\partial r^2} + \frac{1}{r}\frac{\partial}{\partial r} + \frac{1}{r^2}\frac{\partial^2}{\partial \theta^2} + \frac{\omega^2}{c(r,\theta)^2}\right) p_{mn} = k_{mn}^2 p_{mn}. \tag{4.13}$$

A consequence is that separation is in general not possible for an arbitrary phase distribution over the cross-section. Therefore the analytical modal expansion for a single phase configuration cannot easily be extended to pipes with a two-phase composition. Exceptions, however, are configurations with a particular (cylindrical) symmetry; i.e. the interfaces between the phases must be located along surfaces of constant radius r or angle θ.

A physically relevant example of a configuration that satisfies this condition is a core-annular flow where the core consists of fluid 1 and is surrounded by an annulus of fluid 2, see figure 2.1 (k,l) and figure 2.2 (2). The interface is located at $r = \sqrt{\alpha}R$, where α denotes the volume fraction of phase 1. The speed of sound $c(r, \theta)$ then takes the value c_1 for $r < \sqrt{\alpha}R$ and c_2 for $r > \sqrt{\alpha}R$. In each phase $i = 1, 2$ the general solution to equation 4.13 may be written as

$$p_{mn,i} = a_{mn,i} \mathrm{e}^{-\mathrm{i}m\theta} \left[J_m(\kappa_{mn,i} r) + b_{mn,i} Y_m(\kappa_{mn,i} r) \right], \tag{4.14}$$

where

$$\kappa_{mn_i}^2 = \frac{\omega^2}{c_i^2} - k_{mn}^2, \tag{4.15}$$

This equation relates κ_{mn_1} to κ_{mn_2},

$$k_{mn}^2 = \frac{\omega^2}{c_1^2} - \kappa_{mn,1}^2 = \frac{\omega^2}{c_2^2} - \kappa_{mn,2}^2, \tag{4.16}$$

or, alternatively,

$$\kappa_{mn,2}^2 = \kappa_{mn,1}^2 + \frac{\omega^2}{c_1^2} \left(\frac{1}{c_*^2} - 1 \right). \tag{4.17}$$

As before $c_* = c_2/c_1$ denotes the ratio of the speed of sound in the annulus to that in the core.

As a first condition we again require a finite pressure everywhere in the core and since the functions Y_m are singular in the origin the coefficient $b_{mn,1}$ must be zero. In the annulus the normal component of the velocity must be zero at the (hard) wall which determines $b_{mn,2}$,

$$J'_m(\kappa_{mn,2} R) + b_{mn,2} Y'_m(\kappa_{mn,2} R) = 0. \tag{4.18}$$

It is recalled that the prime denotes differentiation with respect to the argument. Along the interface between the core and the annulus continuity of pressure requires that m must have the same value in the two solutions (as already anticipated in the notation). The waveguide modes are specified by connecting the solutions in the two phases via the coefficients $a_{mn,1}$, $a_{mn,2}$ by requiring continuity of pressure and of normal velocity across the interface. This yields

$$a_{mn,1} J_m(\kappa_{mn,1}\sqrt{\alpha}R) = a_{mn,2} \left[J_m(\kappa_{mn,2}\sqrt{\alpha}R) + b_{mn,2} Y_m(\kappa_{mn,2}\sqrt{\alpha}R) \right] \tag{4.19}$$

and

$$a_{mn,1}\kappa_{mn,1}\rho_1^{-1}J'_m(\kappa_{mn,1}\sqrt{\alpha}R) = a_{mn,2}\kappa_{mn,2}\rho_2^{-1}\left[J'_m(\kappa_{mn,2}\sqrt{\alpha}R) + b_{mn,2}Y'_m(\kappa_{mn,2}\sqrt{\alpha}R)\right], \quad (4.20)$$

respectively. The amplitudes $a_{mn,i}$ may be cancelled from equations 4.19, 4.20 to get the dispersion relation

$$\frac{J_m(\kappa_{mn,1}\sqrt{\alpha}R)}{J'_m(\kappa_{mn,1}\sqrt{\alpha}R)} = \rho_* \frac{\kappa_{mn,1}}{\kappa_{mn,2}} \frac{J_m(\kappa_{mn,2}\sqrt{\alpha}R) + b_{mn,2}Y_m(\kappa_{mn,2}\sqrt{\alpha}R)}{J'_m(\kappa_{mn,2}\sqrt{\alpha}R) + b_{mn,2}Y'_m(\kappa_{mn,2}\sqrt{\alpha}R)}, \quad (4.21)$$

where $\rho_* = \rho_2/\rho_1$ denotes the density ratio. An important difference between the dispersion relation for the single phase composition and equation 4.21 is the explicit appearance of the frequency via $\kappa_{mn,1}$, and $\kappa_{mn,2}$ (see equation 4.17). This means that $\kappa_{mn,1}(\omega)$, and $\kappa_{mn,2}(\omega)$ depend on the frequency and so does the shape of the mode, given by equation 4.14. The phase velocity follows from one of equation 4.15,

$$\frac{\omega}{k_{mn}} = c_1 \frac{\omega}{(\omega^2 - c_1^2\kappa_{mn_1}^2(\omega))^{\frac{1}{2}}}. \quad (4.22)$$

The group velocity becomes

$$\frac{\mathrm{d}\omega}{\mathrm{d}k_{mn}} = c_1 \frac{(\omega^2 - c_1^2\kappa_{mn_1}^2(\omega))^{\frac{1}{2}}}{\omega - \frac{1}{2}\frac{\mathrm{d}}{\mathrm{d}\omega}(c_1^2\kappa_{mn_1}^2(\omega))}. \quad (4.23)$$

Alternatively, the phase velocity and the group velocity may be expressed in terms of c_2 and κ_{mn_2}. The frequency dependency of κ_{mn_1}, κ_{mn_2} implies that even the fundamental mode is essentially dispersive unlike the fundamental mode of single phase configurations. Moreover, the relation for the group velocity of single phase configurations, equation 4.10, differs from equation 4.23 by the second term in the denominator. The product of the phase speed and the group velocity is no longer equal to the square of the equilibrium speed of sound c as given by equation 3.15 as in the single phase case.

4.3.1 Dispersion of the fundamental mode

In the limit of very low frequencies, $\omega \to 0$, sound waves only propagate in the fundamental mode ($m = n = 0$). Also, the associated wavenumber must be real and therefore the term $c_1\kappa_1$ must even be smaller than the frequency, see equation 4.16. In other words the arguments of the Bessel functions in equation 4.21 must be small. In order to find an approximation to the propagation speed of low frequency waves

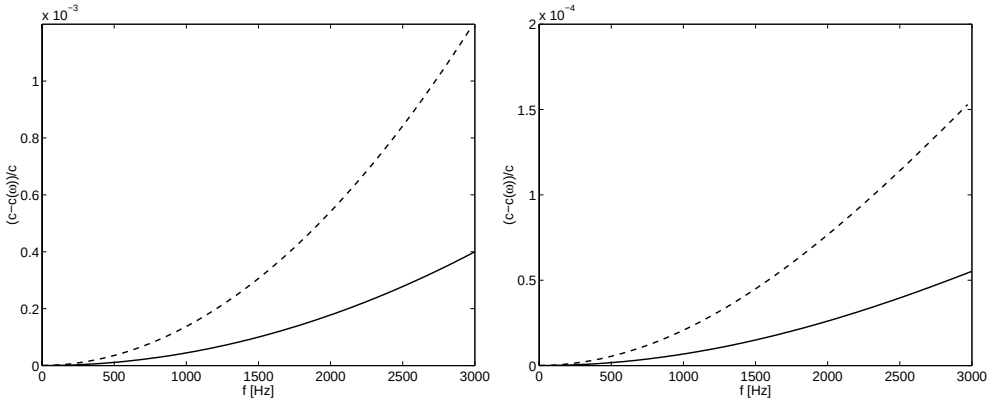

FIGURE 4.1: *Reduction of the phase speed (solid) and the group velocity (dashed) in terms of equilibrium sound speed varying with the frequency for a core-annular configuration with* $\alpha = 0.6$ *for oil in water with* $c_* = 1500/1200$*,* $\rho_* = 1000/800$ *(left); for gas in water with* $c_* = 1500/400$*,* $\rho_* = 1000/2$ *(right).*

the Bessel functions are expanded in the neighborhood of zero by means of Maple,

$$J_0(z) = 1 - \frac{z^2}{4} + \mathcal{O}(z^4), \quad J_1(z) = \frac{z}{2} + \mathcal{O}(z^3),$$
$$\frac{Y_0(qz)}{Y_1(z)} = \mathcal{O}(z), \quad \frac{Y_1(qz)}{Y_1(z)} = \frac{1}{q} + \mathcal{O}(z^2). \tag{4.24}$$

Then the dispersion relation, equation 4.21, reduces to

$$\kappa_{00,2}^2(1-\alpha) + \rho_*\kappa_{00,1}^2 = \mathcal{O}(\omega^4). \tag{4.25}$$

Substitution of equation 4.16 yields an expression that gives the phase velocity,

$$\frac{\omega^2}{k^2} = c_1^2 \frac{(1-\alpha)/\rho_* + 1}{(1-\alpha)/(\rho_* c_*^2) + 1} + \mathcal{O}(\omega^4), \tag{4.26}$$

which is the same as equation 3.15 in section 3.2.1 but demonstrates that the fundamental mode is dispersive unlike the fundamental modes of single phase waveguides. Unfortunately, an analytical expression of the dispersion term is hard to find due to the nonlinearity in the dispersion relation, even in the approximated form. A numerical solution as visualized in figure 4.1, however, shows that the decrease of the phase speed and the group velocity with the frequency is extremely small. Further parameters of the configuration are given in the caption of the figure. For the oil-core surrounded by water (left) the phase speed (solid) is at $3000\,\mathrm{Hz}$ about 0.04% smaller than the equilibrium sound speed as given by equation 3.15. The maximum drop of the group velocity (dashed) is about 0.12%. For a configuration with gas surrounded

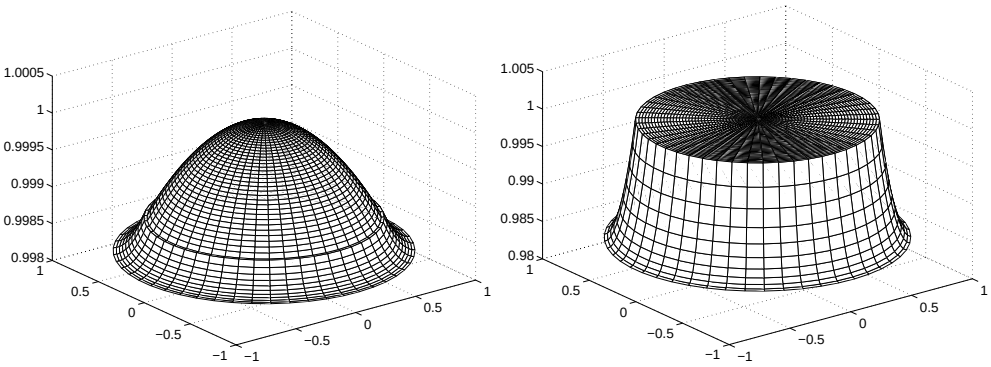

FIGURE 4.2: *Shape of the fundamental mode, p_{00}, for the configurations as described in figure 4.1 for $f = 1000\,\mathrm{Hz}$.*

by water the decrease is even smaller, namely about 0.005% for the phase speed and 0.015% for the group velocity. So here *both* the phase and the group velocity are smaller than the equilibrium sound speed. It is clear that dispersive effects of the fundamental mode are negligibly small in the frequency range of interest. That also the shape of the fundamental mode varies with the frequency is visualized in figure 4.2. The graphs in the figure shows the real part of p_{mn} (see equation 4.14), normalized upon the maximum value of the mode for a frequency of $f = 1000\,\mathrm{Hz}$. The left graph shows the case where the core consists of oil surrounded by water while the right graph corresponds to the system where the oil is replaced by gas. In both cases the shapes of the modes are almost plane although the graphs might give the impression that this is not the case. In contrast to the oil-water system where the pressure varies gradually over the whole cross-section of the pipe the mode of the gas-water system is more or less plane in the core compared to the pressure variation in the water annulus. In the core the mode actually resembles the fundamental mode of a pipe that contains a single phase medium; i.e. the water acts as a hard wall to the gas.

4.3.2 Cutoff frequencies

Sound only propagates in the fundamental mode when the frequency is below the smallest of the cutoff frequencies. Analogues to the cutoff frequencies in single phase configurations, see equation 4.3, the terms $c_1\kappa_1(\omega)$ and $c_2\kappa_2(\omega)$ in equation 4.15 may be considered as resonance frequencies. Yet, since they depend on the frequency itself this notation might be confusing. The true resonance frequencies satisfy, see equation 4.16,

$$\omega_{mn} = c_1\kappa_1(\omega_{mn}) \quad \text{or, equivalently,} \quad \omega_{mn} = c_2\kappa_2(\omega_{mn}). \tag{4.27}$$

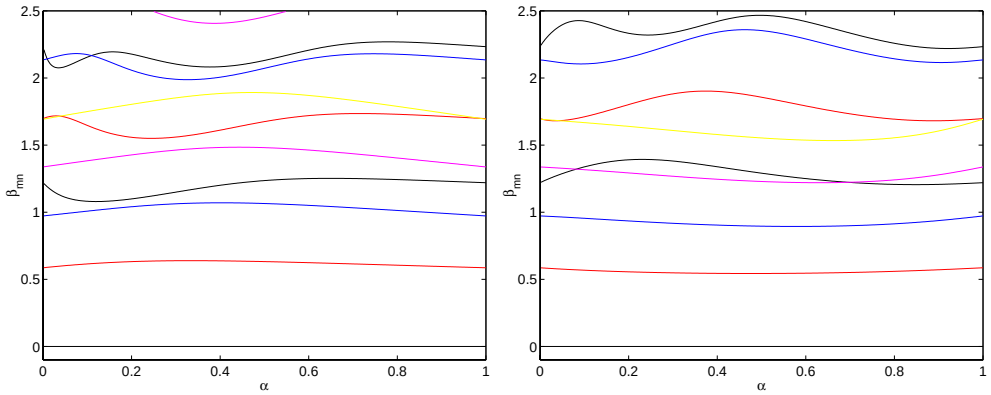

FIGURE 4.3: *Smallest values of α_{mn} as a function of the holdup. Oil core in a water annulus, $\rho_* = 1000/800$, $c_* = 1500/1200$ (left); Water core in a oil annulus, $\rho_* = 800/1000$, $c_* = 1200/1500$ (right); $m = 0$ (black), $m = 1$ (red), $m = 2$ (blue), $m = 3$ (magenta), $m = 4$ (yellow).*

Then substitution of $\omega_{mn} = c_1\kappa_{mn,1}$ *and* $\omega_{mn} = c_2\kappa_{mn,2}$ in equation 4.21 leaves an equation that expresses the cutoff frequencies (in the dimensionless form $\hat{\omega}_{mn} = \omega_{mn}R/c_1$) in terms of the holdup α, the density ratio ρ_* and the speed of sound ratio c_*,

$$\frac{J_m(\hat{\omega}_{mn}\sqrt{\alpha})}{J'_m(\hat{\omega}_{mn}\sqrt{\alpha})} = \rho_* c_* \frac{J_m(\hat{\omega}_{mn}\sqrt{\alpha}/c_*) + b_{mn,2}Y_m(\hat{\omega}_{mn}\sqrt{\alpha}/c_*)}{J'_m(\hat{\omega}_{mn}\sqrt{\alpha}/c_*) + b_{mn,2}Y'_m(\hat{\omega}_{mn}\sqrt{\alpha}/c_*)}, \tag{4.28}$$

For a single phase composition the eigenfrequencies are proportional to the equilibrium speed of sound. In order to compare the eigenfrequencies of a core-annular composition to those of a single phase flow the sound velocity c_1 appearing in the non-dimensional eigenfrequency should be replaced by the equilibrium speed of sound c of the two-phase medium, given by equation 3.15. Similar to the definition of α_{mn} (see equation 4.8) we introduce the notation

$$\beta_{mn} = \frac{\hat{\omega}_{mn}c_1}{\pi c} = \frac{\omega_{mn}R}{\pi c}. \tag{4.29}$$

Then the cutoff frequencies are given by

$$f_{mn} = \frac{\beta_{mn}c}{2R}. \tag{4.30}$$

It is noted that the limiting values of β_{mn} for $\alpha \to 0$ or $\alpha \to 1$ must tend to the values of α_{mn} of a single phase configuration.

As an example consider the core and the annulus consisting of oil and water, respectively. Then for a few of the smallest cutoff frequencies the corresponding values

of β_{mn} varying with α are presented in figure 4.3 (left). For $\alpha = 0$, $\alpha = 1$ the corresponding values of β_{mn} are, as expected, those of the single phase medium. The lowest cutoff frequency increases at most about 9% for $\alpha = 0.33$ compared to the single phase case. Figure 4.3 (right) shows the values of β_{mn} for the same system but now with the phases exchanged. Although core-annular configurations with a water core and an oil annulus have, to our knowledge, not been observed in experiments it indicates that when $c_* < 1$ and $\rho_* < 1$ the lowest cutoff frequency is smaller than the corresponding value for a single phase composition. In this case the lowest cut off frequency is about 8% *smaller* (for $\alpha = 0.48$) than that for a single phase composition. The shape of the smallest waveguide modes (besides the fundamental mode) at the corresponding resonance frequencies are shown in figures 4.5 and 4.6 (middle) for the configuration where the oil covers the core ($\alpha = 0.6$). The modes are almost identical to the modes of a single phase configuration (top). Only at the interface between the phases the pressure derivative normal to the interface jumps in order to satisfy the continuity of normal velocity. This jump, however, is small because of the small density ratio. Being ahead of the following example, in the gas-liquid case the density ratio is large. The corresponding modes at the bottom of the figures indeed kink much more.

The next example involves a gas core surrounded by a water annulus. In this flow the contrast of the phase properties is large compared to the previous example, typically $\rho_* = 1000/2$, $c_* = 1500/400$. Figure 4.4 suggests that the graphs of β_{mn} varying with α may be split up in two branches. One branch starts at $\alpha = 0$ and the second one at $\alpha = 1$. The values of β_{mn} are larger than one would expect based on single phase flows. An explanation for this is that for a large density ratio the coupling between the waves in the two phases through the conditions at the interface becomes weak and, in fact, the waveguide should be viewed as two separate waveguides. Sinai (1984) who studied the modes of a two-dimensional waveguide consisting of a stratified composition with a light fluid above a layer of a heavy fluid called these two branches the lighter-fluid modes and the heavy-fluid modes. The reason for this naming becomes clear by taking the limit $\rho_* \to \infty$. The dispersion relation, equation 4.21, then simplifies into

$$J'_m(\kappa_{mn,1}\sqrt{\alpha}R)\left(J_m(\kappa_{mn,2}\sqrt{\alpha}R) + b_{mn,2}Y_m(\kappa_{mn,2}\sqrt{\alpha}R)\right) = 0. \tag{4.31}$$

The first term,

$$J'_m(\kappa_{mn,1}\sqrt{\alpha}R) = 0, \tag{4.32}$$

corresponds to the gas modes and may be viewed as the dispersion relation of a single phase composition in a hard-walled pipe with radius $\sqrt{\alpha}R$ as discussed in section 4.2. For these modes we recall the notation as for single phase systems,

$$\alpha_{mn} = \frac{\kappa_{mn}\sqrt{\alpha}R}{\pi} = \frac{\omega_{mn}\sqrt{\alpha}R}{\pi c_1}. \tag{4.33}$$

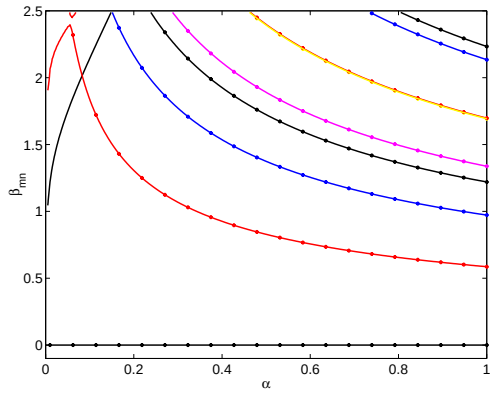

FIGURE 4.4: *Smallest values of β_{mn} varying with α for a gas core in a water annulus according to equation 4.29. The dots denote the approximation of equation 4.35. $\rho_* = 1000/2$, $c_* = 1500/400$; $m = 0$ (black), $m = 1$ (red), $m = 2$ (blue), $m = 3$ (magenta), $m = 4$ (yellow).*

Then the cutoff frequencies corresponding to the gas modes are given by

$$f_{mn} = \frac{\alpha_{mn} c_1}{2R\sqrt{\alpha}}, \tag{4.34}$$

where the values of α_{mn} can be found in table 4.1. It is clear in figure 4.4 that when $\alpha \to 1$ the values of α_{mn} indeed tend to the values in table 4.1. The cutoff frequencies according to equation 4.34 are related to β_{mn} as

$$\beta_{mn} = \frac{\alpha_{mn} c_1}{\sqrt{\alpha} c}. \tag{4.35}$$

This expression is visualized in the form of the dots in figure 4.4 and it is clear that equation 4.34 gives a good approximation to the cutoff frequencies of the gas modes of the gas-liquid core-annular configuration.

Setting the second term in equation 4.31 to zero yields

$$J_m(\kappa_{mn,2}\sqrt{\alpha}R)Y'_m(\kappa_{mn,2}R) - J'_m(\kappa_{mn,2}R)Y_m(\kappa_{mn,2}\sqrt{\alpha}R) = 0. \tag{4.36}$$

This relation corresponds to the liquid modes and is the same as the dispersion relation of an annular waveguide with outer diameter R surrounded by a hard wall and a free surface at $r = \sqrt{\alpha}R$, thus with $p = 0$ on the inner radius instead of the boundary conditions as given by equations 4.19, 4.20. An exact solution to equation 4.36 has not been found, only limiting values for $\alpha \to 0$ and for $\alpha \to 1$.

In the limit $\alpha \downarrow 0$ the second term in equation 4.36 becomes dominant through Y_m which is singular in the origin yielding $J'_m(\kappa_{mn,2}R) = 0$. Hence, the dispersion

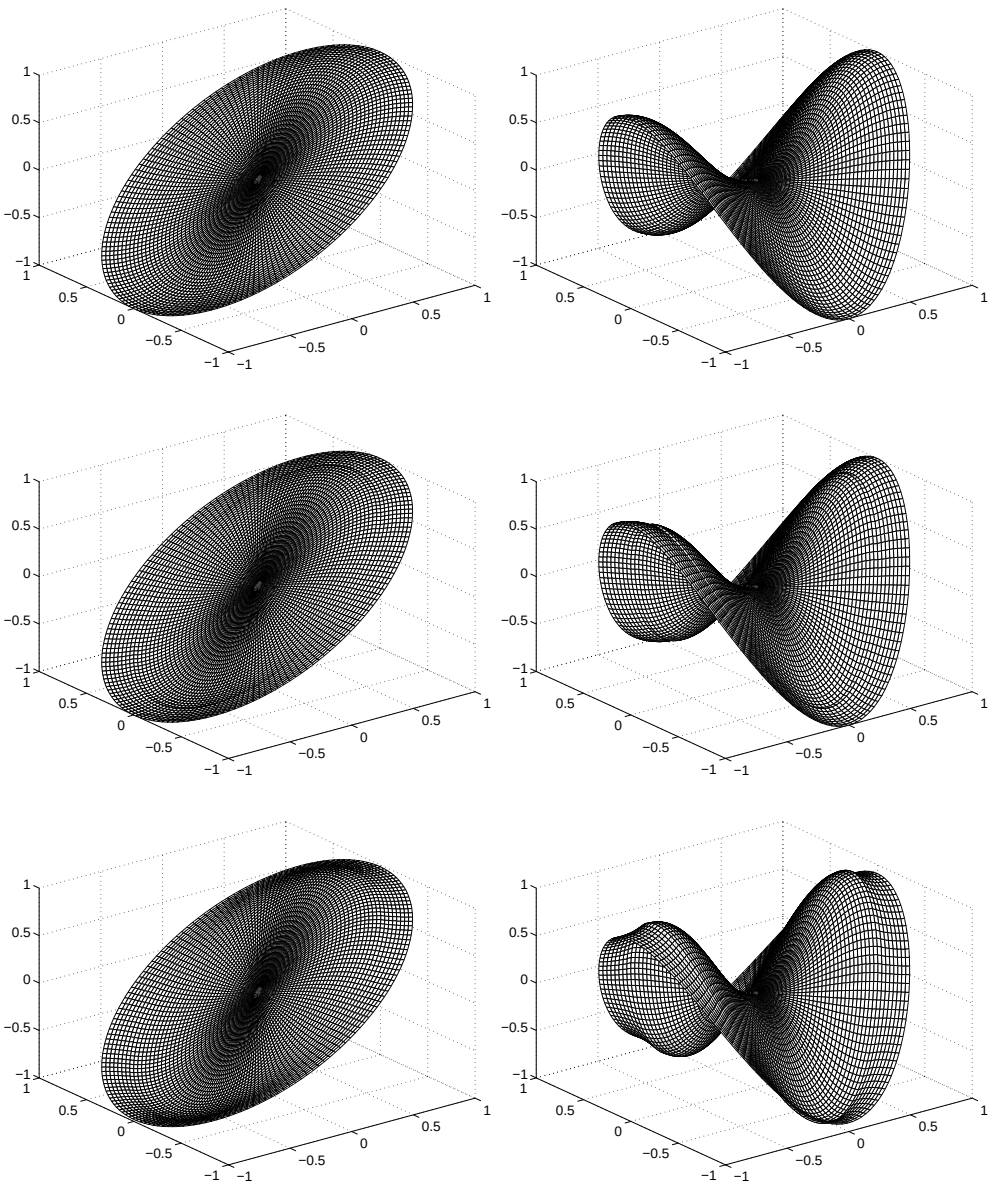

FIGURE 4.5: *Shape of the smallest waveguide modes. Top: a single phase system; middle: the oil-water configuration as in figure 4.3 (left) for* $\alpha = 0.6$*; bottom: the gas-liquid configuration as in figure 4.4 (left) for* $\alpha = 0.6$*; left:* p_{10}*, right:* p_{20}*.*

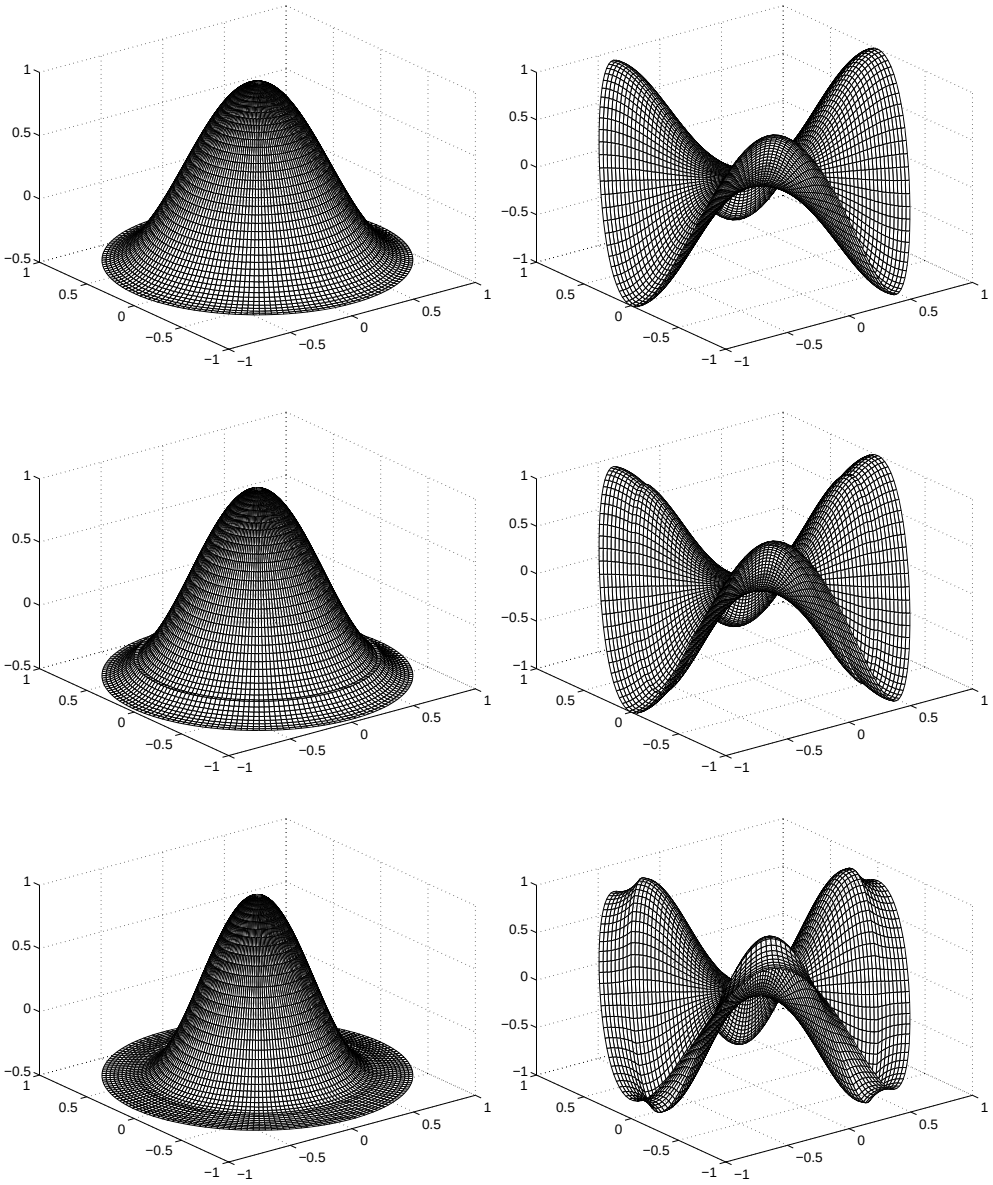

FIGURE 4.6: *Continuation of figure 4.5; left:* p_{01}*, right:* p_{30}*.*

relation for a single phase medium is recovered as it should be. The cutoff frequencies corresponding to the liquid modes when $\alpha \to 0$ are thus given by

$$f_{mn} = \frac{\alpha_{mn} c_2}{2R}, \tag{4.37}$$

where the values of α_{mn} are given in table 4.1. Unfortunately, the limiting values are not clearly visible in the figure 4.4 since the curves are quite steep near $\alpha = 0$.

The limiting values of the cutoff frequencies for $\alpha \to 1$ are found by noting that then $\kappa_{mn,2} R$ becomes very large and therefore the Bessel functions in equation 4.36 may be approximated by (Abramowitz and Stegun, 1965)

$$\begin{aligned} J_m(bz) &\approx \sqrt{\frac{2}{\pi bz}} \left[\cos(z-q)\cos([1-b]z) + \sin(z-q)\sin([1-b]z)\right], \\ Y_m(bz) &\approx \sqrt{\frac{2}{\pi bz}} \left[\sin(z-q)\cos([1-b]z) - \cos(z-q)\sin([1-b]z)\right], \\ J'_m(z) &\approx -\sqrt{\frac{2}{\pi z}}\sin(z-q), \quad Y'_m(z) \approx \sqrt{\frac{2}{\pi z}}\cos(z-q), \end{aligned} \tag{4.38}$$

where $q = (m + 1/2)\pi/2$, $b = \sqrt{\alpha}$, $z = \kappa_{mn,2} R$. Substitution of these approximations in equation 4.36 results, after some manipulation, in

$$\cos\left((1-b)z\right) = \cos\left((1-\sqrt{\alpha})\kappa_{mn,2} R\right) = 0. \tag{4.39}$$

The cutoff frequencies are now given by

$$f_{mn} = \frac{(1/2+n)c_2}{2(1-\sqrt{\alpha})R}. \tag{4.40}$$

Remarkable is the fact that the subscript m has dropped out of the equation; i.e. all cutoff frequencies associated with a particular value of m converge to the same value when $\alpha \to 1$.

In practice, the volume fraction of the gas phase will not assume the small values for which the liquid modes govern the smallest cutoff frequencies. It is the cutoff frequencies of the gas modes as approximated well by equation 4.34 that govern the resonances of the waveguide.

4.4 Waveguide modes in a stratified composition

When the composition of the medium in the pipe is stratified the circular symmetry is broken and analytical solutions cannot be obtained by separating the Helmholtz equation. A numerical solution, however, is obtained by means of a finite element

method which is included in Matlab. In order to gain insight into the sound transmission in stratified pipe flows the similar case of a square duct of width $L = 1$ is considered as well. The main advantage of a square duct is that the interface between the phases coincides with a line of constant y and accordingly the solutions to the Helmholtz equation (in cartesian coordinates),

$$\left(\frac{\partial^2}{\partial x^2} + \frac{\partial^2}{\partial y^2} + \frac{\omega^2}{c_i^2} - k_{mn}^2\right) p_{mn,i} = 0, \tag{4.41}$$

may be calculated in the two phases i separately and be connected. The two solutions $p_{mn,i}$ that satisfy the hard-wall condition read

$$p_{mn,1} = a_{mn,1} \cos(m\pi y) \cos(\kappa_{mn,1} z), \tag{4.42}$$

$$p_{mn,2} = a_{mn,2} \cos(m\pi y) \cos(\kappa_{mn,2}(1 - z)), \tag{4.43}$$

where

$$\kappa_{mn,1}^2 = \frac{\omega^2}{c_1^2} - k_{mn}^2 - (m\pi)^2, \quad \kappa_{mn,2}^2 = \frac{\omega^2}{c_2^2} - k_{mn}^2 - (m\pi)^2. \tag{4.44}$$

Consequentially, κ_{mn_1} and κ_{mn_2} are related,

$$\kappa_{mn,2}^2 = \kappa_{mn,1}^2 + \frac{\omega^2}{c_1^2}\left(\frac{1}{c_*^2} - 1\right). \tag{4.45}$$

Upon requiring continuity of pressure and the normal component of induced velocity across the interface at $y = \alpha$ one finds the dispersion relation

$$\kappa_{mn,1}\rho_* \tan(\kappa_{mn,1}\alpha) + \kappa_{mn,2} \tan(\kappa_{mn,2}(1 - \alpha)) = 0. \tag{4.46}$$

This dispersion relation was found earlier by Morioka and Matsui (1975) who considered pressure-wave propagation in two-dimensional separated gas-liquid flows. The exact form differs slightly, however, as they used exponential functions in equations 4.42, 4.43 instead of harmonic functions. Moreover, the value of m is equal to zero in two dimensions whereas the effect of the third dimension is simply caught by taking nonzero values of m.

4.4.1 Cutoff frequencies

Again, the cutoff frequencies ω_{mn} follow from equation 4.44 by setting $k = 0$ yielding

$$\omega_{mn}^2 = c_1^2\left(\kappa_{mn,1}^2 + (m\pi)^2\right) = c_2^2\left(\kappa_{mn,2}^2 + (m\pi)^2\right). \tag{4.47}$$

The values of β_{mn}, defined as before, become

$$\beta_{mn} = \frac{\omega_{mn} R}{\pi c} \tag{4.48}$$

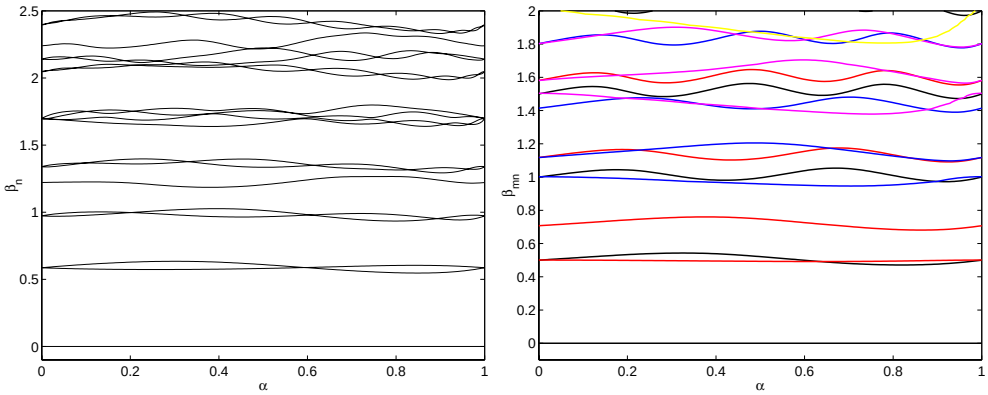

FIGURE 4.7: *Smallest values of α_{mn} as a function of the holdup for a stratified composition of oil and water in a circular pipe (left) and in a square duct (right); $\rho_* = 800/1000$, $c_* = 1200/1500$. $m = 0$ (black), $m = 1$ (red), $m = 2$ (blue), $m = 3$ (magenta), $m = 4$ (yellow).*

for the circular duct, and

$$\beta_{mn} = \frac{\omega_{mn} L}{2\pi c} \tag{4.49}$$

for the square duct. They are visualized as a function of the holdup α in figure 4.7 for an oil-water system, $\rho_* = 800/1000$, $c_* = 1200/1500$. It is noted that exchanging the phases gives the same solution to β_{mn} (when α is replaced by $1-\alpha$) in contrast to the core-annular composition. The left graph shows the numerically calculated cutoff frequencies for a circular pipe. Here the lines are all black since the labels m are, of course, not present in the finite element approach. The right plot shows the values of β_{mn} for the square duct. A remarkable difference with core-annular systems is that the modes which are the same at $\alpha = 0$ split up in two different curves and come back together at $\alpha = 1$. This can be explained by considering a hard-walled square duct filled with a single phase medium. Then the eigenfunctions read

$$p_{mn} = \cos(m\pi y)\cos(n\pi z), \tag{4.50}$$

and it is clear that exchanging particular values of m and n yields the same eigenfrequency; i.e. the modes may be rotated over 90° and still satisfy the Helmholtz equation. However, for a two-phase stratified composition the value of $\kappa_{mn,1}$ is in general not an integer and can, consequently, not be exchanged with m. The rotated mode only satisfies the Helmholtz equation in a modified form. When ρ_* and c_* are close to one (close to a single phase medium) the modification will be small, at least at low frequencies, and the two corresponding cutoff frequencies will differ only slightly. In core-annular system this splitting up does not occur because of the axial symmetry. That ρ_* and c_* must be close to one can be illuminated by considering a gas-liquid system. The shape of the modes that correspond to the four smallest cutoff

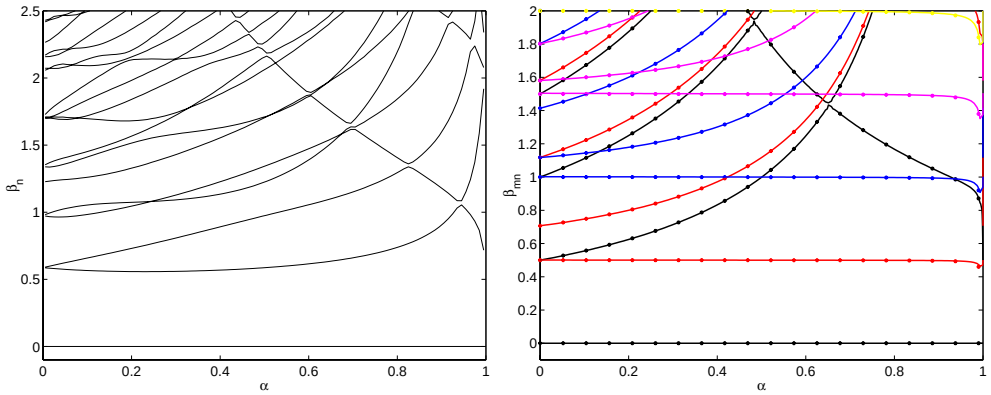

FIGURE 4.8: *Smallest values of α_{mn} as a function of the holdup for a stratified composition of gas and water in a circular pipe (left) and in a square duct (right). The dots denote the approximations of equations 4.54, 4.56; $\rho_* = 2/1000$, $c_* = 400/1500$; $m = 0$ (black), $m = 1$ (red), $m = 2$ (blue), $m = 3$ (magenta), $m = 4$ (yellow).*

frequencies are plotted in figure 4.9. The two modes at the top seem rotated versions of each other but are actually slightly different. The same can be observed at the second pair of modes (middle). The bottom of the figure shows the first two modes of the configuration where the oil has been replaced by gas. These modes differ so much that they cannot be regarded as a pair.

Figure 4.8 shows the values of β_{mn}, according to equations 4.48, 4.49, for the same systems but with $\rho_* = 2/1000$, $c_* = 400/1500$. Also here the liquid modes and the gas modes are recognized as well as modes that are independent of α except, perhaps, when α is close to one.

These modes have not been detected in two-dimensional analyzes, (e.g. Morioka and Matsui, 1975; Sinai, 1984) and are due to the third dimension. The importance of these modes is clearly visible in the figure; they correspond to the smallest cutoff frequencies! In particular for larger volume fractions the cutoff frequencies are factors smaller than the cutoff frequencies following from the two-dimensional approach.

In the limit $\rho_* \to 0$ the dispersion relation, equation 4.46, may be approximated by

$$\sin(\kappa_{mn,2}(1-\alpha))\cos(\kappa_{mn,1}\alpha) = 0. \tag{4.51}$$

The gas modes are given by $\sin(\kappa_{mn,2}(1-\alpha)) = 0$, exactly the dispersion relation for a rectangular hard-walled duct with an aspect ratio of $1/(1-\alpha)$ filled with a single phase medium. Upon defining

$$\beta_{g,mn} = \frac{\omega_{mn} L}{2\pi c_2} = \tfrac{1}{2}\sqrt{\tfrac{n^2}{(1-\alpha)^2} + m^2}, \tag{4.52}$$

the cutoff frequencies of the gas modes become

$$f_{mn} = \frac{\beta_{g,mn} c_2}{L}. \tag{4.53}$$

For $n = 0$ the cutoff frequencies are independent of the holdup for all values of m. When $\alpha = 0$ the values of $\beta_{g,mn}$ become $0, \frac{1}{2}, \frac{1}{2}\sqrt{2}, 1, \ldots$, exactly the values of a single phase configuration. Substitution of $\beta_{g,mn}$ in equation 4.49 for β_{mn} gives

$$\beta_{mn} = \frac{c_2}{c} \frac{1}{2} \sqrt{\frac{n^2}{(1-\alpha)^2} + m^2}, \tag{4.54}$$

This approximation to the cutoff frequencies is visualized in figure 4.8 (right) in the form of the dots and they clearly fit the curves very well.

The liquid modes follow from $\cos(\kappa_{mn,1}\alpha) = 0$, the dispersion relation for an open rectangular duct with aspect ratio $1/\alpha$,

$$\beta_{l,mn} = \frac{\omega_{mn} L}{2\pi c_1} = \frac{1}{2} \sqrt{\frac{(n+1/2)^2}{\alpha^2} + m^2}. \tag{4.55}$$

Numerical values of $\beta_{l,mn}$ at $\alpha = 1$ are approximately: $\frac{1}{4}, 0.559, \frac{3}{4}, \ldots$. These values can hardly be observed in figure 4.8 (right) because of the large inclination of the curves. Yet, closer inspection showed that the curves associated with the liquid modes indeed assume these values at $\alpha = 1$. The value of β_{mn} according to these liquid modes,

$$\beta_{mn} = \frac{c_1}{c} \frac{1}{2} \sqrt{\frac{(n+1/2)^2}{\alpha^2} + m^2}, \tag{4.56}$$

is shown in figure 4.8 (right) in the form of dots. Also the liquid modes are approximated very well by equation 4.56.

4.5 Discussion

The smallest of the cutoff frequencies is the upper limit to the frequency range in which only the fundamental mode propagates. In single phase configurations this fundamental mode has a shape that is plane and is not dispersive. In contrast, the fundamental modes in core-annular and in stratified flows do not have a uniform pressure over the cross-section. The deviation from plane and the differences in the dispersive properties, however, are negligibly small for gas-water and oil-water systems, at least for frequencies that are smaller than, roughly, a few times the smallest cutoff frequency. Therefore, the frequency range of interest warrants to restrict attention to one-dimensional waves only.

The cutoff frequencies as those of a single phase flow are hardly affected by medium inhomogeneities when the flow consists of oil and water, two fluids with

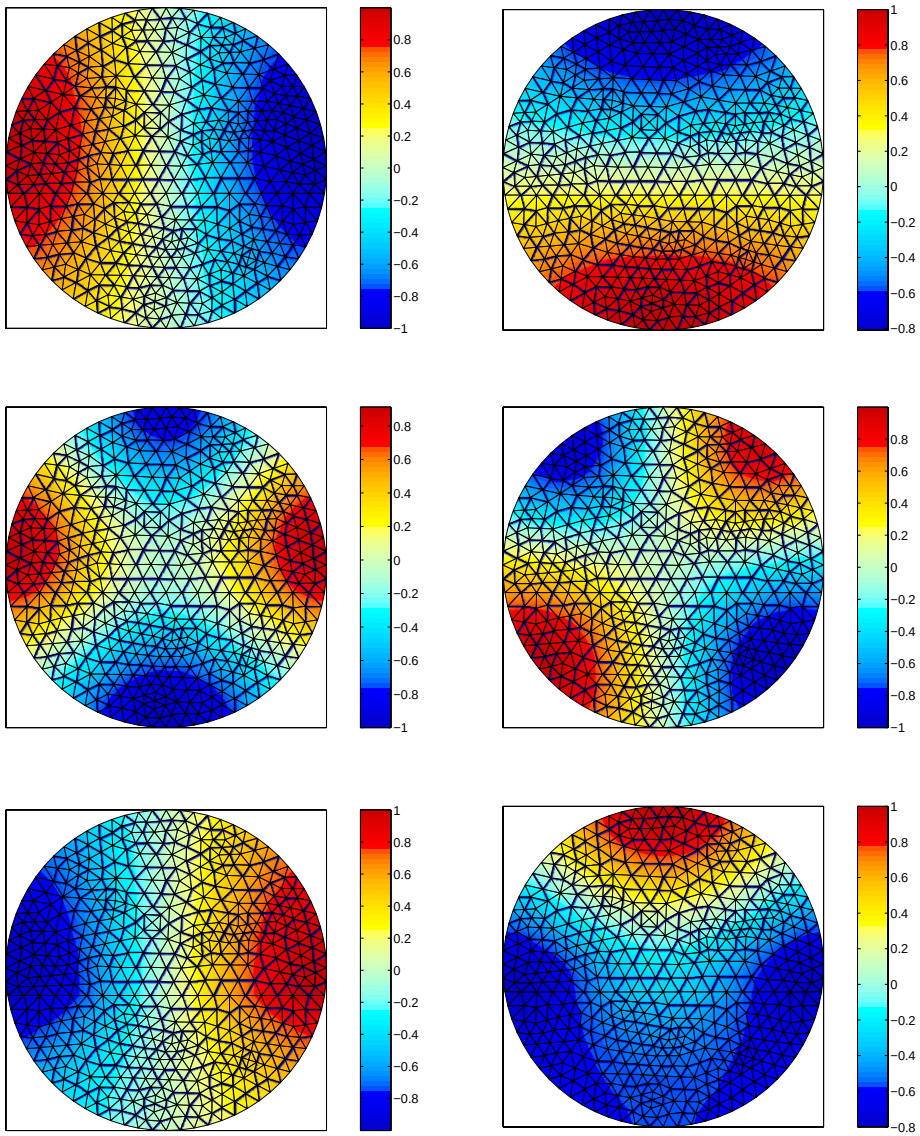

FIGURE 4.9: *Shape of the first four waveguide modes for a stratified configuration of oil on top of water. The volume fraction of the water is* $\alpha = 0.4$*. Top:* p_1*,* p_2*; middle:* p_3*,* p_4*. Bottom: the shape of the first two waveguide modes,* p_1 *and* p_2*, for the same system but with the oil replaced by gas.*

similar acoustic properties. This is not the case for gas-water flows. In core-annular flows it is the gas that basically forms the waveguide as long as the volume fraction of the gas is larger than roughly 0.1. Below this value the liquid phase comes into play and determines the smallest cutoff frequency instead of the gas phase. Core-annular configurations for which the gas volume fraction is smaller than 0.1 have, to the author's knowledge, not been observed in experiments. The cutoff frequencies of the gas modes are well approximated by a simple relation.

For stratified flows a numerical approach demonstrated that also here the gas modes cause the smallest cutoff frequency. Above a volume fraction of the water of about 0.9 it is a liquid mode that determines the smallest cutoff frequency. Stratified configurations of oil and water have modes that occur in pairs of two almost identical modes. This can be explained by effects of symmetry. These pairs do not occur in core-annular flows nor in stratified gas-water flows.

A square duct containing a stratified composition has similar acoustic properties as the same configuration in a circular pipe and is an extension of the analyzes of Morioka and Matsui (1975) and Sinai (1984) of a two-dimensional duct. The third dimension yields the appearance of a new branch of gas modes. The associated cutoff frequencies are the smallest of the system and resemble the ones of stratified gas-water flows in a circular pipe; they should not be ignored upon estimating the upper limit of the frequency range where only the fundamental mode propagates. The cutoff frequencies corresponding to the two branches of modes of the square duct containing a stratified gas-liquid flow are approximated well by means of simple relations.

ACOUSTICS OF AXIALLY VARYING SYSTEMS

CHAPTER 5

5.1 Introduction

In the previous two chapters the propagation of sound was discussed for two-phase flows whose phase distribution does not vary with the axial position along the pipe; e.g. separated flow and dispersed flows as sketched in figure 2.1 (a, c, i, k, etc.). In addition, flows have been observed whose composition does vary along the pipe. Examples of these flows are intermittent flows where the one phase forms large bubbles in the other phase, see figure 2.1 (q,r), figure 2.2 (3,4,7,8). Another example of intermittent configurations are flows whose composition alternates between single phase parts and dispersed parts, see figure 2.1 (p). Intermittent flows have the special property of being more or less periodic. Their characteristic acoustic properties will be analyzed in detail in the next two chapters. Also separated flows that have a wavy interface are examples of (more or less) periodically varying systems. Other examples of systems where the composition varies are separated flows in which the interface exhibits a form of mixing of the one phase into the other, see figure 2.1 (b, c, d). These volume fraction fluctuations have a random character of which the length scale is small.

In this chapter we will develop mathematical tools to analyze the propagation of longitudinal waves through axially varying configurations. Two types of variations in acoustic properties may be distinguished. The first type is concerned with a varying speed of sound c, resulting in changes of the local wavenumber. The second type is the variation in impedance. When waves propagating through a medium reach a change in impedance they are reflected.

If the impedance of the system varies only gradually within the wavelength of the sound waves these reflections are minimal. Section 5.3 concerns configurations where the acoustic properties of the flow vary only gradually within a wavelength. In this case the small effects of reflections are neglected.

The resulting approximation, however, breaks down when the impedance fluctuates *abruptly*; i.e. the impedance varies substantially within one wavelength. Then reflections must not be neglected. Also, when waves propagate over (small), but

many, impedance fluctuations the net effect upon the propagating waves may become significant over distances that cover many wavelengths because of effects of *multiple scattering*.

A more general technique than the one mentioned above is the transfer-matrix method, which describes the propagation of longitudinal waves through waveguides essentially containing an arbitrarily axially varying medium. This method includes the reflections of waves and thus the effects of multiple scattering. In this method the configuration is regarded as a stepwise varying medium; i.e. the waveguide consists of a sequence of sections with constant (effective) acoustic properties ρ and K (or alternatively c and Z) that change abruptly at interfaces with the subsequent sections. Expressions for the effective acoustic properties in each section were found in Chapter 3 for separated and dispersed configurations. Besides these also other expressions may be used. For instance a section that consists of three stratified layers where a dispersion of oil and water is located between a layer of pure oil and one of pure water as a generalized form of the relations for separate systems as discussed in Chapter 3.

Within these sections the exact solution to the Helmholtz equation is readily found in terms of two constants that are expressed in terms of the wave field in the sections up- and downstream. All of these constants are related to each other since pressure and induced velocity are continuous across the interfaces.

5.2 Longitudinal waves

In Chapter 3 expressions have been found that describe the propagation of longitudinal sound waves through some relatively simple flow configurations such as separated and dispersed flows. These equations have the generic form

$$\frac{\partial}{\partial t}\begin{pmatrix} p \\ u \end{pmatrix} = \begin{bmatrix} 0 & -K \\ -1/\rho & 0 \end{bmatrix} \frac{\partial}{\partial x}\begin{pmatrix} p \\ u \end{pmatrix}, \tag{5.1}$$

where K denotes the bulk modulus of the two-phase medium and ρ the effective density. Both depend on the flow configuration. p and u are the excess pressure and the mean induced velocity, respectively. When K and ρ do not vary along the pipe the equation simplifies into

$$\frac{\partial^2 p}{\partial t^2} = \frac{K}{\rho}\frac{\partial^2 p}{\partial x^2}, \tag{5.2}$$

which is the usual wave equation. The term K/ρ is the square of the sound speed c of the two-phase flow. The product $K\rho$ equals the square of the impedance Z, which is the ratio of the pressure excess and the mean induced velocity in the direction of sound propagation.

As mentioned briefly in section 3.2.1, within the one-dimensional theory K and ρ are even allowed to vary with the axial position along the pipe. In that case the

wave equation governing the excess pressure becomes, upon eliminating u from equation 5.1,

$$\frac{\partial^2 p}{\partial t^2} = K(x)\frac{\partial}{\partial x}\left(\frac{1}{\rho(x)}\frac{\partial p}{\partial x}\right) \tag{5.3}$$

as the equation describing sound waves in two-phase pipe flows.

Instead of studying the acoustic field varying with position and time it is common to choose position and frequency as variables by applying the Fourier transform. Upon taking the disturbances harmonic in time, i.e. proportional to $\exp(-\mathrm{i}\omega t)$, the mass and momentum conservation equations reduce to two coupled linear ordinary differential equations,

$$\frac{\mathrm{d}}{\mathrm{d}x}\begin{pmatrix} p \\ \mathrm{i}u \end{pmatrix} = \begin{bmatrix} 0 & \rho(x)\omega \\ -\omega/K(x) & 0 \end{bmatrix}\begin{pmatrix} p \\ \mathrm{i}u \end{pmatrix}, \tag{5.4}$$

which may be written as the Helmholtz equation,

$$\rho(x)\frac{\mathrm{d}}{\mathrm{d}x}\left(\frac{1}{\rho(x)}\frac{\mathrm{d}p}{\mathrm{d}x}\right) + \frac{\omega^2}{c^2(x)}p = 0. \tag{5.5}$$

In case the densities of the two fluids are identical as in the experiments by Charles et al. (1961) (see section 2.2), the density can be taken out of the derivative. The result is the usual Helmholtz equation but with a speed of sound that varies with position along the pipe.

5.3 Gradually varying composition

Simple approximate solutions to equation 5.3 exists for the case in which the flow properties vary only gradually. Then one would expect that the wave propagates with the local sound speed $c(x)$, and with only very little reflection of energy. Thus, if it is assumed that the energy flux, i.e. p^2/Z, remains constant an approximate solution to equation 5.3, for a wave moving downstream*, should have the form (see Lighthill, 1978)

$$p(x,t) = \sqrt{\frac{Z(x)}{Z(0)}}f\left(t - \int_0^x c(x')^{-1}\mathrm{d}x'\right), \tag{5.6}$$

where $f(t)$ is the waveform at $x = 0$ and $\int_0^x c(x')^{-1}\mathrm{d}x'$ is the time it takes for the wave to travel from 0 to x. The corresponding expression for a wave travelling

*Downstream denotes the direction of positive x, upstream the direction of negative x.

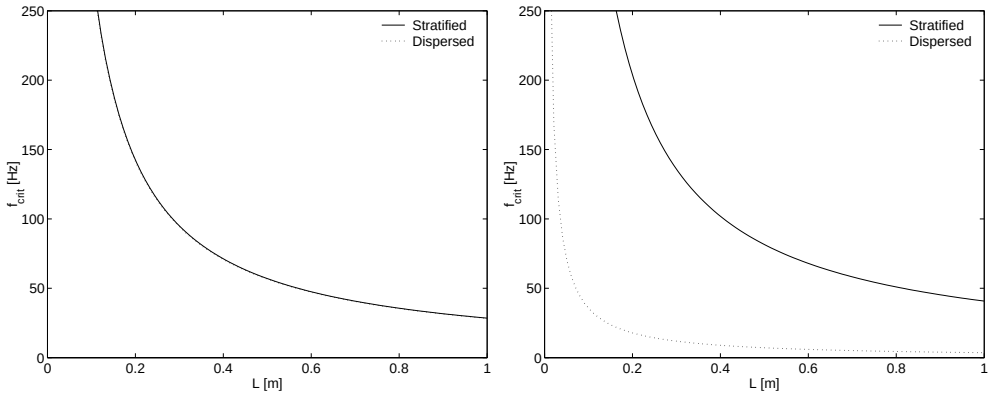

FIGURE 5.1: *Critical frequency as given by equation 5.12 varying with the wavelength of the interface waves. (left) oil-water system; (right) gas-water system.*

upstream is

$$p(x,t) = \sqrt{\frac{Z(x)}{Z(0)}} g\left(t + \int_0^x c(x')^{-1} \mathrm{d}x'\right). \tag{5.7}$$

Substitution of either of these approximations into the exact equation 5.3 shows that the relative error is, for a monochromatic wave with radian frequency ω,

$$\frac{cZ^{\frac{1}{2}}}{\omega^2} \frac{\mathrm{d}}{\mathrm{d}x}\left(\frac{1}{2} cZ^{\frac{1}{2}} \frac{\mathrm{d}Z^{-1}}{\mathrm{d}x}\right), \tag{5.8}$$

or alternatively,

$$\frac{1}{2}\left[\frac{3}{2}\frac{1}{Z}\frac{\mathrm{d}Z}{\mathrm{d}x} - \frac{\mathrm{d}^2 Z}{\mathrm{d}x^2} \Big/ \frac{\mathrm{d}Z}{\mathrm{d}x} - \frac{1}{c}\frac{\mathrm{d}c}{\mathrm{d}x}\right] \frac{1}{Z}\frac{\mathrm{d}Z}{\mathrm{d}x} \Big/ \left(\frac{\omega}{c}\right)^2. \tag{5.9}$$

This implies that the accuracy is good when the relative rates of change of c and of Z and of the derivative of Z all have small ratios to the wavenumber $\omega/c = 2\pi/\lambda$, where λ is the wavelength of the monochromatic wave. In other words, the wavelength should be small compared to the length scales that characterize the relative rates of change of these quantities. Equations 5.6, 5.7 are equivalent to the usual geometrical acoustics approximation. A formal WKB-approach to the solution of equation 5.3 would yield these as a first-order solution.

As a practical example to get some insight in the significance of equation 5.9 when the volume fractions of an oil-water system vary with the axial position, consider a stratified oil-water system; $\rho_2/\rho_1 = 800/1000$, $c_2/c_1 = 1200/1500$. Suppose that to the mean volume fraction, $\alpha = 0.5$ say, a small periodic component with a wavelength L and an amplitude of 0.1 is added, so

$$\alpha(x) = 0.5 + 0.1\sin(2\pi x/L). \tag{5.10}$$

Upon introducing the following frequencies,

$$f_c = \frac{c}{2\pi}\frac{1}{c}\frac{\mathrm{d}c}{\mathrm{d}x}, \quad f_Z = \frac{c}{2\pi}\frac{1}{Z}\frac{\mathrm{d}Z}{\mathrm{d}x}, \quad f_{Z'} = \frac{c}{2\pi}\frac{\mathrm{d}^2Z}{\mathrm{d}x^2}\Big/\frac{\mathrm{d}Z}{\mathrm{d}x}, \tag{5.11}$$

the frequency of the sound waves must be much larger than the critical frequency, defined as

$$f \gg f_{\text{crit.}} = \max(|f_c|, |f_Z|, |f_{Z'}|), \tag{5.12}$$

in order to have a small relative error on applying the approximation to the acoustics of this system. Figure 5.1 (left) shows the critical frequency varying with the wavelength L of the interface waves. In addition, the graph is given for basically the same system but now for a dispersion with a periodically fluctuating volume fraction. Wether the oil-water system is stratified or dispersed has not much influence on the critical frequencies. Figure 5.1 (right) shows the results when the oil is replaced by gas, $\rho_2/\rho_1 = 2/1000$, $c_2/c_1 = 400/1500$. In these gas-water systems the dispersions have a lower and the stratified flows a higher critical frequency than the ones of oil-water systems. Experiments by Trallero (1995) suggest that the wavelength of the interfacial waves in an oil-water stratified wavy flow is roughly two pipe diameters. That would mean that for a pipe with a diameter of $D = 0.1\,\mathrm{m}$ the frequency must be much larger than about $150\,\mathrm{Hz}$.

All these values of $f_{\text{crit.}}$ suggest that the theory is probably applicable to these flows. Yet, effects of multiple scattering are not taken into account. Especially in periodic flows the many small reflections may add up to significant values. This example should be considered as an indication of the magnitude of the relative error varying with α according to equation 5.9. In this sense the figure shows that even a small variation (0.1) of the volume fraction over distances smaller than about $0.1\,\mathrm{m}$ results in unacceptably large relative errors in the frequency range of interest when this method is applied.

5.4 Sound transmission as matrix multiplication

A method that does include reflections is the transfer-matrix method. Figure 5.2 visualizes what this method means. The left figure (top) shows a flow of oil bubbles (grey) in water which is regarded as a stepwise varying medium (bottom) consisting of stratified oil-water sections (grey) and sections of pure water. In the figure also the convention is given for the numbering of the interfaces and the sections. The plot at the right shows how a more gradually varying flow may be considered as a stepwise varying medium.

5.4.1 Transfer matrices

Suppose that the waveguide consists of a number of sections with constant properties, separated by acoustically compact discontinuities. Let section n have length l_n,

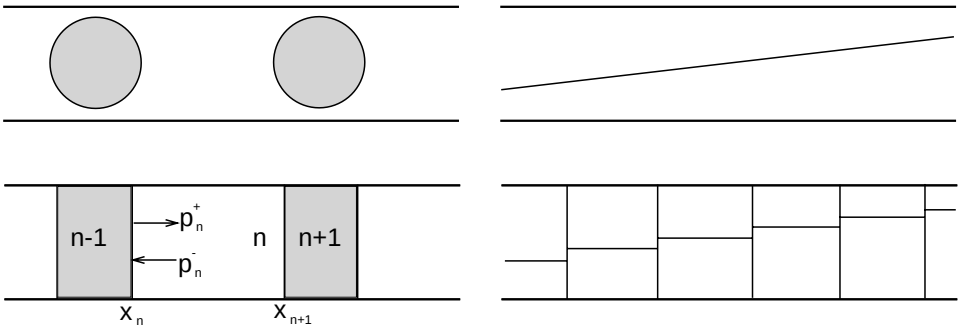

FIGURE 5.2: *Examples of how the two-phase flow is regarded as a stepwise varying medium. Flow with oil bubbles in water (left); Linearly increasing volume fraction (right).*

sound speed c_n and impedance Z_n. The interface at $x = x_n$ separates section $n-1$ upstream from section n downstream, see figure 5.2 (left). The pressure within each section may be taken to consist of the sum of a wave moving in the downstream direction (denoted $+$) and a wave moving in the upstream direction (denoted $-$). Then it follows from equation 5.4 that for a monochromatic component with frequency ω the pressure and induced velocity in section n between x_n and x_{n+1} may be expressed as

$$p_n(x) = p_n^+ \mathrm{e}^{\mathrm{i}\omega(x-x_n)/c_n} + p_n^- \mathrm{e}^{-\mathrm{i}\omega(x-x_n)/c_n}, \tag{5.13}$$

$$u_n(x) = \frac{p_n^+}{Z_n} \mathrm{e}^{\mathrm{i}\omega(x-x_n)/c_n} - \frac{p_n^-}{Z_n} \mathrm{e}^{-\mathrm{i}\omega(x-x_n)/c_n}. \tag{5.14}$$

Imposing continuity of pressure and induced velocity at each of the discontinuities, which is consistent with equation 5.4, yields at $x = x_{n+1}$

$$p_{n+1}^+ + p_{n+1}^- = p_n^+ \mathrm{e}^{\mathrm{i}\omega l_n/c_n} + p_n^- \mathrm{e}^{-\mathrm{i}\omega l_n/c_n}, \tag{5.15}$$

$$\frac{1}{Z_{n+1}} \left(p_{n+1}^+ - p_{n+1}^-\right) = \frac{1}{Z_n} \left(p_n^+ \mathrm{e}^{\mathrm{i}\omega l_n/c_n} - p_n^- \mathrm{e}^{\mathrm{i}\omega l_n/c_n}\right). \tag{5.16}$$

For N discontinuities this gives $2N$ equations for the $2N+2$ unknowns p_n^+ and p_n^-, $(n = 0, 1, \ldots, N)$, in terms of given values for Z_n and l_n. The system of equations may for instance be closed by setting $p_N^- = 0$ (no wave coming from far downstream) and specifying the value of p_0^+ (the incident signal on $x = x_1$).

An elegant way of formulating this scheme is by introducing the state variable $\boldsymbol{p}_n$, a vector whose components are p_n^+ and p_n^-. The equations 5.15, 5.16 can then be written as the transformation

$$\boldsymbol{p}_{n+1} = \boldsymbol{T}_n \boldsymbol{p}_n. \tag{5.17}$$

To obtain the transfer matrix $\boldsymbol{T}_n$, first write the two equations 5.13, 5.14 as a relationship between the state vectors $\boldsymbol{y}_n = [p_n, \mathrm{i}u_n]^T$ and $\boldsymbol{p}_n$:

$$\boldsymbol{y} = \boldsymbol{C}_n(x)\boldsymbol{p}, \tag{5.18}$$

where

$$\boldsymbol{C}_n(x) \equiv \begin{bmatrix} \mathrm{e}^{\mathrm{i}\omega(x-x_n)/c_n} & \mathrm{e}^{-\mathrm{i}\omega(x-x_n)/c_n} \\ \frac{\mathrm{i}}{Z_n}\mathrm{e}^{\mathrm{i}\omega(x-x_n)/c_n} & -\frac{\mathrm{i}}{Z_n}\mathrm{e}^{-\mathrm{i}\omega(x-x_n)/c_n} \end{bmatrix}. \tag{5.19}$$

The transformation (5.17) now follows from

$$\boldsymbol{p}_{n+1} = \boldsymbol{C}_{n+1}^{-1}(x_{n+1})\boldsymbol{C}_n(x_{n+1})\boldsymbol{p}_n = \boldsymbol{T}_n\boldsymbol{p}_n, \tag{5.20}$$

with the transfer matrix

$$\boldsymbol{T}_n \equiv \frac{1}{2}\begin{bmatrix} (1+Z_{n+1}/Z_n)\mathrm{e}^{\mathrm{i}\omega\tau_n} & (1-Z_{n+1}/Z_n)\mathrm{e}^{-\mathrm{i}\omega\tau_n} \\ (1-Z_{n+1}/Z_n)\mathrm{e}^{\mathrm{i}\omega\tau_n} & (1+Z_{n+1}/Z_n)\mathrm{e}^{-\mathrm{i}\omega\tau_n} \end{bmatrix}. \tag{5.21}$$

Here we have introduced the transit time $\tau_n = l_n/c_n$ as the time it takes for the sound wave to pass through layer n. The $\boldsymbol{T}_n$ matrix may also be written in terms of the transmission and reflection coefficients of a wave in a medium with intrinsic impedance Z_{n+1} incident upon a discontinuity to a medium with impedance Z_n. These are

$$\mathcal{T}_{n+1,n} = \frac{2Z_n}{Z_n + Z_{n+1}}, \quad \mathcal{R}_{n+1,n} = \frac{Z_n - Z_{n+1}}{Z_n + Z_{n+1}}, \tag{5.22}$$

respectively. In terms of these the transfer matrix reads

$$\boldsymbol{T}_n = \frac{1}{\mathcal{T}_{n+1,n}}\begin{bmatrix} \mathrm{e}^{\mathrm{i}\omega\tau_n} & \mathcal{R}_{n+1,n}\mathrm{e}^{-\mathrm{i}\omega\tau_n} \\ \mathcal{R}_{n+1,n}\mathrm{e}^{\mathrm{i}\omega\tau_n} & \mathrm{e}^{-\mathrm{i}\omega\tau_n} \end{bmatrix}. \tag{5.23}$$

The determinant of the transfer matrix $\boldsymbol{T}_n$ equals $\det(\boldsymbol{T}_n) = Z_{n+1}/Z_n$.

Note that when one prefers to work with the state variable $\boldsymbol{y}_n$ one can express the state at x_{n+1} in terms of the state at x_n as

$$\boldsymbol{y}(x_{n+1}) = \boldsymbol{C}_n(x_{n+1})\boldsymbol{C}_n^{-1}(x_n)\boldsymbol{y}(x_n) = \boldsymbol{M}_n\boldsymbol{y}(x_n), \tag{5.24}$$

with

$$\boldsymbol{M}_n \equiv \begin{bmatrix} \cos(\omega\tau_n) & Z_n\sin(\omega\tau_n) \\ -1/Z_n\sin(\omega\tau_n) & \cos(\omega\tau_n) \end{bmatrix}. \tag{5.25}$$

Since the pressure and the induced velocity are continuous across a discontinuity, i.e. $p_n(x_{n+1}) = p_{n+1}(x_{n+1})$ and $u_n(x_{n+1}) = u_{n+1}(x_{n+1})$, the subscript n of p and u is dropped. The determinant of this transfer matrix is $\det(\mathbf{M}_n) = 1$. Its eigenvalues are $\mathrm{e}^{\pm\mathrm{i}\omega\tau_n}$.

Suppose now that the medium has N compact variations of acoustic properties. In other words, the medium consists of $N-1$ sections that all may have a different sound speed and impedance. Repeated application of the transfer matrices then yields the state of the medium at x_N in terms of that at x_1 as

$$\boldsymbol{y}(x_N) = \boldsymbol{M}_{N-1}\boldsymbol{M}_{N-2}\ldots\boldsymbol{M}_2\boldsymbol{M}_1\boldsymbol{y}(x_1), \tag{5.26}$$

or,

$$\boldsymbol{p}_N = \boldsymbol{T}_{N-1}\boldsymbol{T}_{N-2}\ldots\boldsymbol{T}_2\boldsymbol{T}_1\boldsymbol{p}_1. \tag{5.27}$$

5.4.2 Effective impedances

To see what this entails and to establish the relation with methods using effective impedances, consider a wave of pressure I incident from the right, i.e. propagating in the upstream direction, on the discontinuity at x_N. This results in a reflected downstream propagating wave of pressure R, and a transmitted upstream propagating wave of pressure T to the left of x_1.

First we look at a description using the transfer matrix $\mathbf{M}$. The states at x_1 and at x_N are prescribed by

$$\boldsymbol{y}_1 = \begin{bmatrix} T \\ -\mathrm{i}T/Z_0 \end{bmatrix}, \quad \boldsymbol{y}_N = \begin{bmatrix} R+I \\ \mathrm{i}(R-I)/Z_N \end{bmatrix}, \tag{5.28}$$

respectively. The problem is to express T and R in terms of I. Substitution of equation 5.28 in equation 5.26 gives

$$\begin{bmatrix} R+I \\ \mathrm{i}(R-I)/Z_N \end{bmatrix} = \mathbf{M}_{N-1}\mathbf{M}_{N-2}\ldots\mathbf{M}_2\mathbf{M}_1 \begin{bmatrix} T \\ -\mathrm{i}T/Z_0 \end{bmatrix}. \tag{5.29}$$

Upon defining a vector $\boldsymbol{W}$ as

$$\begin{bmatrix} W_1 \\ \mathrm{i}W_2 \end{bmatrix} = \mathbf{M}_{N-1}\mathbf{M}_{N-2}\ldots\mathbf{M}_2\mathbf{M}_1 \begin{bmatrix} -Z_0 \\ \mathrm{i} \end{bmatrix}, \tag{5.30}$$

it follows from equation 5.29 that

$$(R+I) = W_1\frac{T}{-Z_0}, \quad (R-I)/Z_N = W_2\frac{T}{-Z_0}, \tag{5.31}$$

or equivalently,

$$\frac{R}{I} = \frac{W_1/W_2 - Z_N}{W_1/W_2 + Z_N}, \quad \frac{T}{I} = \frac{-Z_0(R/I+1)}{W_1}. \tag{5.32}$$

The ratio R/I may be interpreted as the effective reflection coefficient for the layered medium; i.e it is the reflection coefficient for a wave in a medium with impedance

Z_N incident on a medium with effective impedance $Z_e = W_1/W_2$ (in accordance with equation 5.22).

The appearance of an effective impedance may be explained by substituting the definition of the effective impedance $Z_e(x) \equiv p(x)/u(x)$ in (5.24),

$$\begin{bmatrix} 1 \\ \mathrm{i}/Z_e(x_{n+1}) \end{bmatrix} p(x_{n+1}) = \boldsymbol{M}_n \begin{bmatrix} 1 \\ \mathrm{i}/Z_e(x_n) \end{bmatrix} p(x_n). \tag{5.33}$$

The recurrence relation for the effective impedance is recovered by taking the ratio of these two equations,

$$Z_e(x_{n+1}) = Z_n \frac{Z_e(x_n) + \mathrm{i}Z_n \tan(\omega\tau_n)}{Z_n + \mathrm{i}Z_e(x_n)\tan(\omega\tau_n)}. \tag{5.34}$$

The transmission through the system can now be evaluated as follows. If one defines the effective impedance of the medium at x_1 as $Z_e(x_1) = Z_0$ then repeated application of equation 5.34 yields the effective impedance $Z_e(x_N)$. This immediately gives the amplitude of the reflected wave,

$$\frac{R}{I} = \frac{Z_e(x_N) - Z_N}{Z_N + Z_e(x_N)}. \tag{5.35}$$

The transmission through one layer follows equations 5.33, 5.25 as

$$\frac{p(x_n)}{p(x_{n+1})} = \left(\cos(\omega\tau_n) + \mathrm{i}\frac{Z_n}{Z_e(x_n)}\sin(\omega\tau_n)\right)^{-1}. \tag{5.36}$$

At x_N one has $p(x_N) = R + I$ so that repeated application of (5.36) yields the transmitted wave as

$$\frac{T}{I} = (R/I + 1)\prod_{n=1}^{N-1}\left(\cos(\omega\tau_n) - \mathrm{i}\frac{Z_n}{Z_e(x_n)}\sin(\omega\tau_n)\right)^{-1}. \tag{5.37}$$

The acoustic field within the system for instance at x_i follows from

$$\frac{p(x_i)}{I} = (R/I + 1)\prod_{n=i}^{N-1}\left(\cos(\omega\tau_n) - \mathrm{i}\frac{Z_n}{Z_e(x_n)}\sin(\omega\tau_n)\right)^{-1}. \tag{5.38}$$

Moreover, in the same fashion the pressure can be calculated within a section, at $x = x_j$ in layer i say, by splitting the section i in two sections. Then the local effective impedance is given as by equation 5.34,

$$Z_e(x_j) = Z_i \frac{Z_e(x_i) + \mathrm{i}Z_i \tan(\omega(x_j - x_i)/c_i)}{Z_i + \mathrm{i}Z_e(x_i)\tan(\omega(x_j - x_i)/c_i)}, \tag{5.39}$$

and hence $p(x_j)$ becomes

$$\frac{p(x_j)}{I} = \frac{p(x_{i+1})}{I}\left(\cos(\omega\tau_{j,i+1}) - \mathrm{i}\frac{Z_i}{Z_e(x_j)}\sin(\omega\tau_{j,i+1})\right)^{-1}, \tag{5.40}$$

where $\tau_{j,i+1} = (x_{i+1} - x_j)/c_i$.

5.4.3 Effective reflection and transmission coefficients

The same problem can be described in terms of $\boldsymbol{T}$ matrices. Instead of effective impedances, now effective reflection coefficients appear which can be calculated recursively as well. This approach for computing the reflection and transmission through a layered medium has recently been applied by Munday, Brad Bennett and Robertson (2002) to study the effects of small defects on the propagation characteristics in an acoustic band gap system. We will make further reference to this work in Chapter 6.

In terms of the state vectors $\boldsymbol{p}_i$ the state immediately to the right of x_N is now given by

$$\boldsymbol{p}_N = \begin{bmatrix} R \\ I \end{bmatrix}, \tag{5.41}$$

whereas the state immediately to the right of x_1 may be found by means of equation 5.18,

$$\boldsymbol{p}_1 = \boldsymbol{C}_1^{-1}(x_1)\boldsymbol{y}_1 = \boldsymbol{C}_1^{-1}(x_1)\begin{bmatrix} T \\ -\mathrm{i}T/Z_0 \end{bmatrix} = \frac{T}{\mathcal{T}_{1,0}}\begin{bmatrix} \mathcal{R}_{1,0} \\ 1 \end{bmatrix}. \tag{5.42}$$

Similar as in the precious section a vector $\boldsymbol{W}$ is defined as

$$\begin{bmatrix} W_1 \\ W_2 \end{bmatrix} = \mathbf{T}_{N-1}\mathbf{T}_{N-2}\ldots\mathbf{T}_2\mathbf{T}_1\begin{bmatrix} \mathcal{R}_{1,0} \\ 1 \end{bmatrix}, \tag{5.43}$$

in terms of which equation 5.27 can simply be written as

$$\begin{bmatrix} R \\ I \end{bmatrix} = \frac{T}{\mathcal{T}_{1,0}}\begin{bmatrix} W_1 \\ W_2 \end{bmatrix}. \tag{5.44}$$

The pressures of the reflected and transmitted waves therefore follow from

$$R/I = W_1/W_2, \quad T/I = \mathcal{T}_{1,0}/W_2. \tag{5.45}$$

In this description the ratio W_1/W_2 plays the role of an effective reflection coefficient, which is defined as $\mathcal{R}_e^-(x_n) = p_n^+/p_n^-$. Here, the minus sign corresponds to the negative direction in which the incident propagates.

Upon inserting the effective reflection coefficient in equation 5.20,

$$\begin{bmatrix} \mathcal{R}_e^-(x_{n+1}) \\ 1 \end{bmatrix} p_{n+1}^- = \boldsymbol{T}_n \begin{bmatrix} \mathcal{R}_e^-(x_n) \\ 1 \end{bmatrix} p_n^-, \tag{5.46}$$

one finds by taking the ratio of these equations and using equation 5.23 a recurrence relation for the effective reflection coefficient,

$$\mathcal{R}_e^-(x_{n+1}) = \frac{\mathcal{R}_e^-(x_n) + \mathcal{R}_{n+1,n}\,\mathrm{e}^{-2\mathrm{i}\omega\tau_n}}{\mathcal{R}_e^-(x_n)\mathcal{R}_{n+1,n} + \,\mathrm{e}^{-2\mathrm{i}\omega\tau_n}}. \tag{5.47}$$

The relation is closed according to equation 5.43 by specifying the effective reflection coefficient at $x = x_1$, $\mathcal{R}_e^-(x_1) = \mathcal{R}_{1,0}$. Then the reflection from the entire medium follows from applying equation 5.47 $N-1$ times.

The transmission through one section follows from equation 5.46 in the form of an effective transmission coefficient,

$$\mathcal{T}_e^-(x_{n+1}) = \frac{p_n^-}{p_{n+1}^-} = \frac{\mathcal{T}_{n+1,n}}{\mathcal{R}_e^-(x_n)\mathcal{R}_{n+1,n}\mathrm{e}^{\mathrm{i}\omega\tau_n} + \mathrm{e}^{-\mathrm{i}\omega\tau_n}}. \tag{5.48}$$

At an arbitrary interface at $x = x_n$ the wave p_n^- may be written in terms of p_k^- at an arbitrary interface at $x = x_k$ downstream,

$$\frac{p_n^-}{p_k^-} = \prod_{m=n+1}^{k} \mathcal{T}_e^-(x_m). \tag{5.49}$$

For $k = N$ equation 5.49 expresses p_n^- in terms of the incident wave $p_N^- = I$. The wave T/I that is transmitted through the entire medium, also through $x = x_1$, becomes $\mathcal{T}_{1,0}p_1^-/p_N^-$, see equation 5.42.

Instead of having an incident wave I immediately to the right of $x = x_N$ one may also have an incoming wave from far upstream incident on the interface at $x = x_1$. The state immediately to the right of x_N is now given by

$$\boldsymbol{p}_N = \begin{bmatrix} T \\ 0 \end{bmatrix}, \tag{5.50}$$

whereas the state immediately to the right of x_1 may be found by means of equation 5.18,

$$\boldsymbol{p}_1 = \boldsymbol{C}_1^{-1}(x_1)\boldsymbol{y}_1 = \boldsymbol{C}_1^{-1}(x_1)\begin{bmatrix} I+R \\ \mathrm{i}(I-R)/Z_0 \end{bmatrix} = \frac{1}{\mathcal{T}_{1,0}}\begin{bmatrix} I+R\mathcal{R}_{1,0} \\ I\mathcal{R}_{1,0}+R \end{bmatrix}. \tag{5.51}$$

Similar to the previous case an effective reflection coefficient is defined as

$$\mathcal{R}_e^+(x_n) = p_n^-/p_n^+, \tag{5.52}$$

where the plus-sign corresponds to the positive direction in which the incident wave propagates. It is noted that in general $\mathcal{R}_e^+(x_n) \neq 1/\mathcal{R}_e^-(x_n)$ since the layered medium is subject to different boundary conditions. Substitution of $\mathcal{R}_e^+(x_n)$ in equation 5.20 yields

$$\begin{bmatrix} 1 \\ \mathcal{R}_e^+(x_n) \end{bmatrix} p_n^+ = \boldsymbol{T}_n^{-1}\begin{bmatrix} 1 \\ \mathcal{R}_e^+(x_{n+1}) \end{bmatrix} p_{n+1}^+. \tag{5.53}$$

Again by taking the ratio of these equations one obtains a recurrence relation for the effective reflection coefficient,

$$\mathcal{R}_e^+(x_n) = \frac{\mathcal{R}_{n,n+1} + \mathcal{R}_e^+(x_{n+1})}{(1 + \mathcal{R}_{n,n+1}\mathcal{R}_e^+(x_{n+1}))\ \mathrm{e}^{-2\mathrm{i}\omega\tau_n}}, \tag{5.54}$$

which is closed by $p_N^- = 0$ (no wave from far downstream) and therefore $\mathcal{R}_e^+(x_N) = 0$. Applying equation 5.54 $N-1$ times gives the effective reflection coefficient $\mathcal{R}_e^+(x_1)$, which gives the reflected wave at the left of $x = x_1$,

$$\mathcal{R}_e^+(x_1) = \frac{I + R\mathcal{R}_{1,0}}{I\mathcal{R}_{1,0} + R}, \ \text{ so } \ \frac{R}{I} = \frac{1 - \mathcal{R}_e^+(x_1)\mathcal{R}_{0,1}}{\mathcal{R}_e^+(x_1) - \mathcal{R}_{0,1}}. \tag{5.55}$$

By defining an effective transmission coefficient as

$$\mathcal{T}_e^+(x_{n+1}) = \frac{p_{n+1}^+}{p_n^+} = \frac{\mathcal{T}_{n,n+1}}{(1 + \mathcal{R}_e^+(x_{n+1})\mathcal{R}_{n,n+1})\mathrm{e}^{-\mathrm{i}\omega\tau_n}}, \tag{5.56}$$

the transmission through some number of layers, e.g. from x_k to x_n downstream, is caught by multiplying these effective transmission coefficients,

$$p_n^+/p_k^+ = \prod_{m=k+1}^{n} \mathcal{T}_e^+(x_m). \tag{5.57}$$

The transmitted wave to the right of $x = x_N$ follows from equation 5.51,

$$T/I = \frac{1 + \mathcal{R}_{1,0}R/I}{\mathcal{T}_{1,0}} \prod_{m=2}^{N} \mathcal{T}_e^+(x_m). \tag{5.58}$$

5.5 Green function

When subject to a distribution of sources the sound field is obtained by calculating the convolution integral of the source distribution and the Green function, which is the solution to equation 5.5 where the Dirac delta function $\delta(x - x_s)$ is added to the right-hand side.

In order to calculate the Green function let us introduce subfield 1 as the acoustic field from the first case in section 5.4.3, thus induced by an incoming wave I^-, incident from far downstream on $x = x_N$ and the second case as subfield 2; i.e. the acoustic field induced by an incoming wave I^+, incident from far upstream on $x = x_1$. Then due to the linearity of the governing equations an arbitrary field can be written as a linear combination of these two subfields. Instead of by an incoming wave the field may also be induced by a source located in layer n, say, at x_s

between x_n and x_{n+1}. The induced upstream and downstream propagating waves p_n^- and p_n^+ may be viewed as incoming waves incident on $x = x_n$ and $x = x_{n+1}$, respectively. In the following we will determine how the sound energy delivered by the source is divided between these upstream and downstream propagating waves.

If the medium were homogeneous and had a sound speed of the layer in which the source is located the Green function would be

$$g_n(x, x_s) = \frac{c_n}{2\mathrm{i}\omega} \begin{cases} \mathrm{e}^{-\mathrm{i}\omega(x-x_s)/c_n} & x < x_s \\ \mathrm{e}^{\mathrm{i}\omega(x-x_s)/c_n} & x > x_s \end{cases} . \tag{5.59}$$

The presence of the discontinuities can now be accounted for by adding the homogeneous solution,

$$p_n(x, x_s) = \hat{p}_n^+ \mathrm{e}^{\mathrm{i}\omega(x-x_n)/c_n} + \hat{p}_n^- \mathrm{e}^{-\mathrm{i}\omega(x-x_n)/c_n} + g_n(x, x_s), \tag{5.60}$$

or, alternatively,

$$p_n(x, x_s) = \begin{cases} \hat{p}_n^+ \mathrm{e}^{\mathrm{i}\omega(x-x_n)/c_n} + (\hat{p}_n^- + g_n^-)\mathrm{e}^{-\mathrm{i}\omega(x-x_n)/c_n} & x_n < x < x_s, \\ (\hat{p}_n^+ + g_n^+)\mathrm{e}^{\mathrm{i}\omega(x-x_n)/c_n} + \hat{p}_n^- \mathrm{e}^{-\mathrm{i}\omega(x-x_n)/c_n} & x_s < x < x_{n+1} \end{cases}, \tag{5.61}$$

where

$$g_n^- = \frac{c_n}{2\mathrm{i}\omega} \mathrm{e}^{\mathrm{i}\omega(x_s-x_n)/c_n}, \quad g_n^+ = \frac{c_n}{2\mathrm{i}\omega} \mathrm{e}^{-\mathrm{i}\omega(x_s-x_n)/c_n}. \tag{5.62}$$

For $x_n < x < x_s$ the terms $(\hat{p}_n^- + g_n^-)$ and $\hat{p}_n^+$ may be considered as the incoming wave incident on $x = x_n$ and its reflected wave, respectively. Their ratio is equal to the effective reflection coefficient, $\hat{p}_n^+ = \mathcal{R}_e^-(x_n)(\hat{p}_n^- + g_n^-)$, representing the medium at $x < x_n$. The medium downstream, $x > x_{n+1}$, is included by the effective reflection coefficient, $\mathcal{R}_e^+(x_n) = \hat{p}_n^-/(\hat{p}_n^+ + g_n^+)$. Upon expressing $\hat{p}_n^+$ and $\hat{p}_n^-$ in terms of g_n^+, g_n^- and $\mathcal{R}_e^+(x_n)$, $\mathcal{R}_e^-(x_n)$ one obtains

$$\begin{bmatrix} \hat{p}_n^+ \\ \hat{p}_n^- \end{bmatrix} = \frac{1}{1 - \mathcal{R}_e^-(x_n)\mathcal{R}_e^+(x_n)} \begin{bmatrix} \mathcal{R}_e^-(x_n)(g_n^- + \mathcal{R}_e^+(x_n)g_n^+) \\ \mathcal{R}_e^+(x_n)(g_n^+ + \mathcal{R}_e^-(x_n)g_n^-). \end{bmatrix}. \tag{5.63}$$

The pressure distribution in the layered system can be calculated by applying the method given in the previous section separately to the systems to the left of x_n and to the right of x_{n+1}. Upon inserting the above expressions for $\hat{p}_n^+$ and $\hat{p}_n^-$ in equation 5.61 it becomes clear that amplitude of the upstream running wave incident on the medium to the left of x_n is

$$p_n^- = \hat{p}_n^- + g_n^- = \frac{g_n^- + g_n^+ \mathcal{R}_e^+(x_n)}{1 - \mathcal{R}_e^+(x_n)\mathcal{R}_e^-(x_n)} \tag{5.64}$$

and that the amplitude of the downstream running wave incident on the medium to the right of x_{n+1} is

$$p_n^+ = \hat{p}_n^+ + g_n^+ = \frac{g_n^+ + g_n^- \mathcal{R}_e^-(x_n)}{1 - \mathcal{R}_e^+(x_n)\mathcal{R}_e^-(x_n)}. \tag{5.65}$$

Equations 5.64, 5.65 show that resonances occur when the two effective reflection coefficients are reciprocals, $\mathcal{R}_e^-(x_n) = 1/\mathcal{R}_e^+(x_n)$, and since the modulus of the effective reflection coefficients is smaller or equal than 1 this condition is only satisfied if $|\mathcal{R}_e^-(x_n)| = |\mathcal{R}_e^+(x_n)| = 1$ and if $\arg(\mathcal{R}_e^-(x_n)) + \arg(\mathcal{R}_e^+(x_n)) = 0$. It is noted that if the effective reflection coefficients are reciprocals somewhere in the pipe they must be everywhere, see section 5.4.3.

5.6 Discussion

Two methods have been presented that describe the acoustics of longitudinal acoustic waves in pipe flows whose composition varies with axial position in the pipe. In the first method, presented in section 5.3, reflections of waves are neglected and the energy flux is assumed to remain constant. This method fails when the impedance fluctuations are substantial within a wavelength of the sound waves. Also, many negligibly small impedance fluctuations may add up to substantial reflections when the pipe is long enough. In these two cases reflections cannot be ignored.

The second method is the transfer-matrix method, presented in section 5.4, which governs the acoustics of basically all phase distributions for frequencies smaller than the smallest cutoff frequencies of the system. In this method the medium is regarded as stepwise varying. The resulting transfer matrices express the wave amplitudes in one section to those in neighboring sections. The complete field may be computed by first determining the effective reflection coefficients of all layers and then the effective transmission coefficients through a recurrence relation. Also, the Green function for this stepwise varying medium was derived. This revealed that the medium upstream, say, is fully characterized by the effective reflection coefficient $\mathcal{R}_e^-(x_n)$ and only affects the (complex) amplitude of the sound field downstream. The acoustic field upstream and downstream of the source may, except for their amplitudes, be calculated separately as if the medium at the other side of the source is absent.

Although the one-dimensional approach is justifiable to waves having a frequency below the cutoff frequency the longitudinal wave approximation in spatially varying systems is more complicated. When the sections consist of pure fluids or dispersions, the shape of the fundamental mode over the cross-section is plane. If also the interfaces are plane then the shape of the wave front will remain plane and taking into account the higher waveguide modes is not required to ensure continuity of pressure and induced velocity *everywhere* across the interface. In this case the one-dimensional formulation as presented is generally applicable. When sections consist of a stratified composition the shape of the fundamental mode is not perfectly plane, see Chapter 4. This leads to a 'mismatch' of the mode at plane interfaces to sections containing a single phase medium, a dispersion or a stratified composition with a different composition. Due to this mismatch higher modes come into play

and although these modes are attenuating they might still be present at the next interface, especially for frequencies close to the cutoff frequency, and affect the acoustic field resulting from this one-dimensional approach. Yet, these effects are very small since the shapes of the fundamental modes in two-phase flows are all very close to plane. Moreover, the evanescent modes attenuate in the sections and may be ignored when the sections are much longer than the attenuation length. This is referred to in literature as the wide spacing approximation, (e.g. Devillard, Dunlop and Souillard, 1988; Evans and Linton, 1994).

ACOUSTICS OF PERIODIC FLOWS

CHAPTER 6

6.1 Introduction

Flows of large bubbles of oil in water, see figure 2.1 (q,r) and figure 2.2 (3,4,7,8), are examples of intermittent flows. In these flows the composition changes abruptly with time when one observes the flow at a certain fixed position in the pipe. Other intermittent configurations are flows whose composition alternates between single phase parts and dispersed parts, see figure 2.1 (p). Intermittency also occurs in gas-liquid systems. *Slug flows* for instance consist of alternating parts of a liquid or a dispersion of gas bubbles in water (the liquid slug) and a stratified part of liquid and gas which contains the gas plug. Both parts together form a unit of a flow that is close to periodic. The distribution of oil drops surrounded by water in the pipe is also more or less uniform and, consequently, this flow structure is close to periodic as well. Another example of flows that exhibit periodicity are stratified flows with a wavy interface.

In practice, intermittent flows as observed in experiments are not perfectly periodic; the lengths of all parts deviate in general from their mean value as well as other parameters like the volume fractions of the phases in the stratified part or in the dispersed part as in slug flows. In order to gain insight into the propagation of sound through these flows here they are first assumed to be perfectly periodic. In the next chapter the effects on the propagation of sound waves will be analyzed when the lengths of the parts fluctuate randomly around their mean value.

An inquiry of the acoustics of perfectly periodic flows will be the content of this chapter. In the next section the transfer matrices as discussed in the previous chapter, will be derived for the units (periods) of the periodic flows that consists of two parts whose acoustic properties are constant over the full length of each part. These units may be used to model slug flows or flows of large bubbles of oil in water. Repeated application of the associated transfer matrices provides a means to analyze the sound propagation through these flows.

Transfer matrices for other periodic flows like stratified wavy flows require a different approach since the volume fractions vary more gradually instead of abruptly as

in, for instance, slug flows. One period of these flows will be regarded as a stepwise varying medium consisting of a certain number of parts each one having constant acoustic properties.

How the transmission properties of periodic flows depend on the properties of the transfer matrices, in other words the properties of one unit, will be discussed in section 6.3.

The final section concerns the transmission properties of the waves when one unit is changed as an introduction to more realistic intermittent flows where the units are not all the same but vary around their mean value in a random way.

6.2 Sound transmission through periodic flows

6.2.1 Transfer matrices for periodic flows

Slug units

A gas-liquid slug flow may be decomposed in 'slug units', in which each unit consists of a dispersed or a single phase part and a separated part. Flows of large oil bubbles in water have a similar structure; one part is a single phase flow of water while the other part consists of pure oil or a separated flow of a core annular form. Also, periodic flows of parts of pure water separated by parts containing a dispersion of oil in water have this structure. In the following the units of all periodic flows that consist of two parts are referred to as *slug units*.

Now, let the slug unit consist of a dispersed or single-phase flow of length l_d with sound speed c_d and impedance Z_d, followed downstream by a separated flow of length l_s, sound speed c_s and impedance Z_s, see figure 6.1. Sound transmission through this slug unit is then characterized by applying equation 5.17 twice. The components of the transfer matrix $\boldsymbol{T}$ now read

$$T_{11} = \frac{(Z_s+Z_d)^2}{4Z_sZ_d}\,\mathrm{e}^{\mathrm{i}\omega(\tau_s+\tau_d)} - \frac{(Z_s-Z_d)^2}{4Z_sZ_d}\,\mathrm{e}^{-\mathrm{i}\omega(\tau_s-\tau_d)},$$

$$T_{12} = -\frac{(Z_s+Z_d)(Z_s-Z_d)}{4Z_sZ_d}\,\mathrm{e}^{\mathrm{i}\omega(\tau_s-\tau_d)} + \frac{(Z_s+Z_d)(Z_s-Z_d)}{4Z_sZ_d}\,\mathrm{e}^{-\mathrm{i}\omega(\tau_s+\tau_d)},$$

$$T_{21} = \frac{(Z_s+Z_d)(Z_s-Z_d)}{4Z_sZ_d}\,\mathrm{e}^{\mathrm{i}\omega(\tau_s+\tau_d)} - \frac{(Z_s+Z_d)(Z_s-Z_d)}{4Z_sZ_d}\,\mathrm{e}^{-\mathrm{i}\omega(\tau_s-\tau_d)},$$

$$T_{22} = -\frac{(Z_s-Z_d)^2}{4Z_sZ_d}\,\mathrm{e}^{\mathrm{i}\omega(\tau_s-\tau_d)} + \frac{(Z_s+Z_d)^2}{4Z_sZ_d}\,\mathrm{e}^{-\mathrm{i}\omega(\tau_s+\tau_d)}, \tag{6.1}$$

where the transit times $\tau_s = l_s/c_s$ and $\tau_d = l_d/c_d$ are introduced as the times needed by a wave to travel through the slug part and the dispersed section, respectively. A

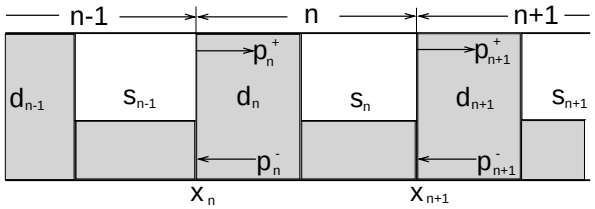

FIGURE 6.1: *Sketch of a series of slug units, $n-1$, n and $n+1$, consisting of a stratified part s and a dispersed part d.*

simplification of the notation by introducing the reflection and transmission coefficients as defined by equation 5.22 results in

$$\begin{aligned}
T_{11} &= \left[\mathrm{e}^{\mathrm{i}\omega(\tau_s+\tau_d)} - \mathcal{R}_{d,s}^2\mathrm{e}^{-\mathrm{i}\omega(\tau_s-\tau_d)}\right]/\mathcal{T}_{d,s}\mathcal{T}_{s,d},\\
T_{12} &= \left[-\mathcal{R}_{d,s}\mathrm{e}^{\mathrm{i}\omega(\tau_s-\tau_d)} + \mathcal{R}_{d,s}\mathrm{e}^{-\mathrm{i}\omega(\tau_s+\tau_d)}\right]/\mathcal{T}_{d,s}\mathcal{T}_{s,d},\\
T_{21} &= \left[\mathcal{R}_{d,s}\mathrm{e}^{\mathrm{i}\omega(\tau_s+\tau_s)} - \mathcal{R}_{d,s}\mathrm{e}^{-\mathrm{i}\omega(\tau_s-\tau_d)}\right]/\mathcal{T}_{d,s}\mathcal{T}_{s,d},\\
T_{22} &= \left[-\mathcal{R}_{d,s}^2\mathrm{e}^{\mathrm{i}\omega(\tau_s-\tau_d)} + \mathrm{e}^{-\mathrm{i}\omega(\tau_s+\tau_d)}\right]/\mathcal{T}_{d,s}\mathcal{T}_{s,d}.
\end{aligned} \tag{6.2}$$

For completeness it is noted that the transfer matrix $\boldsymbol{M}$ for a slug unit has components

$$\begin{aligned}
M_{11} &= \cos(\omega\tau_s)\cos(\omega\tau_d) - Z_s/Z_d\sin(\omega\tau_s)\sin(\omega\tau_d),\\
M_{12} &= (Z_d/\omega)\sin(\omega\tau_d)\cos(\omega\tau_s) + (Z_s/\omega)\cos(\omega\tau_d)\sin(\omega\tau_s),\\
M_{21} &= -(\omega/Z_d)\sin(\omega\tau_d)\cos(\omega\tau_s) - (\omega/Z_s)\cos(\omega\tau_d)\sin(\omega\tau_s),\\
M_{22} &= \cos(\omega\tau_s)\cos(\omega\tau_d) - Z_d/Z_s\sin(\omega\tau_s)\sin(\omega\tau_d).
\end{aligned} \tag{6.3}$$

If the flow is not perfectly periodic the same matrices $\boldsymbol{T}$, $\boldsymbol{M}$ may be derived, but they will, in principle, be different for all units.

Stratified wavy units

Instead of a slug flow whose units consist of two parts, the volume fractions of the phases in stratified wavy configurations vary more gradually. Similarly, a unit may be defined for these periodic flows. Suppose the flow is stratified with fluid 2 flowing on top of fluid 1. The speed of sound and the impedance then follow from equations 3.15, 3.17 as a function of α. Now, let the volume fraction α vary periodically with the axial position along the pipe as

$$\alpha(x) = \alpha_0 + \Delta\alpha\sin(2\pi x/L), \tag{6.4}$$

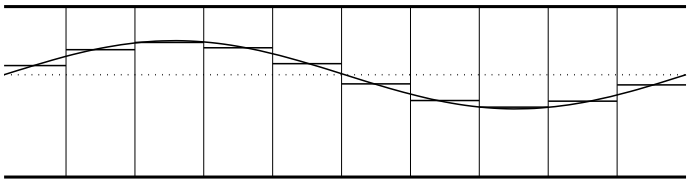

FIGURE 6.2: *Sketch of a unit of a stratified wavy flow including its representation in the stepwise varying medium method with* $M = 10$ *sections.*

where L is the wavelength of the interface waves (the length of the unit), α_0 the mean volume fraction and $\Delta\alpha$ the amplitude of the interface waves.

The corresponding transfer matrix $\boldsymbol{T}$ of one unit may be obtained by regarding the flow as a stepwise varying medium. One unit of length L is divided into M sections separated by $M+1$ interfaces, see figure 6.2. The n^{th} section between x_n and x_{n+1} consists of a separated flow with a constant volume fraction

$$\alpha_n = [\alpha(x_n) + \alpha(x_{n+1})]/2 \tag{6.5}$$

and a transfer matrix $\boldsymbol{T}_n$. The transfer matrix $\boldsymbol{T}$ of one unit is found upon multiplying all matrices $\boldsymbol{T}_n$ according to equation 5.27,

$$\boldsymbol{T} = \boldsymbol{T}_{M-1}\boldsymbol{T}_{M-2}\ldots\boldsymbol{T}_2\boldsymbol{T}_1. \tag{6.6}$$

In practical situations, the amplitude $\Delta\alpha$ is usually small. Yet, if the amplitude is increased to very large values while the volume fraction is limited to the range $[0,1]$; in other words,

$$\alpha(x) = \begin{cases} \min(\alpha_0 + \Delta\alpha\sin(2\pi x/L), 1) & \text{for } x \le L/2 \\ \max(\alpha_0 + \Delta\alpha\sin(2\pi x/L), 0) & \text{for } x > L/2 \end{cases}, \tag{6.7}$$

then the $\boldsymbol{T}$-matrix resembles the transfer matrix of a slug unit whose two parts consist of the phase 2 and the phase 1 as in the stratified flow. The length of each part is equal to $L/2$. This result provides the means to analyze how the properties of the transfer matrix are affected when the abrupt variations in the acoustic properties are slightly moderated as in practical situations.

6.2.2 Finite periodic flows

Having determined two types of transfer matrices let us now consider the idealization of a flow as a chain of identical units of length L (which is $L = l_s + l_d$ for slug units). The description of sound transmission through finite periodic systems becomes particularly simple by repeated application of the $\boldsymbol{T}$-matrix in its diagonalized form.

In order to diagonalize the $\boldsymbol{T}$-matrix first its eigenvalues are to be determined. Since the determinant of $\boldsymbol{T}$ is equal to one, the eigenvalues of the transfer matrix are roots of the characteristic equation

$$\lambda^2 - \mathrm{tr}(\boldsymbol{T})\lambda + 1 = 0, \tag{6.8}$$

and depend only on the trace of the $\boldsymbol{T}$-matrix,

$$\lambda_{1,2} = \tfrac{1}{2}\mathrm{tr}(\boldsymbol{T}) \pm \sqrt{\tfrac{1}{4}\mathrm{tr}(\boldsymbol{T})^2 - 1}. \tag{6.9}$$

In case of slug units the trace is equal to

$$\mathrm{tr}(\boldsymbol{T}) = \frac{2}{\mathcal{T}_{d,s}\mathcal{T}_{s,d}}\left[\cos\omega(\tau_s+\tau_d) - \mathcal{R}_{d,s}^2\cos\omega(\tau_s-\tau_d)\right], \tag{6.10}$$

or, alternatively,

$$\mathrm{tr}(\boldsymbol{T}) = 2\cos(\omega\tau_d)\cos(\omega\tau_s) - \left(\frac{Z_s}{Z_d}+\frac{Z_d}{Z_s}\right)\sin(\omega\tau_d)\sin(\omega\tau_s). \tag{6.11}$$

For the units of stratified wavy flows the trace of the transfer matrix has to be calculated numerically.

The eigenvectors of $\boldsymbol{T}$ may be written as $(1,\xi_1)$ and $(\xi_2,1)$, with

$$\xi_1 = -(T_{11}-\lambda_1)/T_{12}, \quad \xi_2 = -(T_{22}-\lambda_2)/T_{21}, \tag{6.12}$$

and may be used to form the matrices

$$\boldsymbol{P} = \begin{bmatrix} 1 & \xi_2 \\ \xi_1 & 1 \end{bmatrix}, \quad \boldsymbol{P}^{-1} = \frac{1}{1-\xi_1\xi_2}\begin{bmatrix} 1 & -\xi_2 \\ -\xi_1 & 1 \end{bmatrix}. \tag{6.13}$$

The matrix $\boldsymbol{T}$ can now be decomposed as

$$\boldsymbol{T} = \boldsymbol{P}\boldsymbol{D}\boldsymbol{P}^{-1}, \tag{6.14}$$

with $\boldsymbol{D} = \mathrm{diag}(\lambda_1,\lambda_2)$.

The $\boldsymbol{M}$-matrix has the same eigenvalues as the $\boldsymbol{T}$-matrix. Its eigenvectors may be written as $(1,\hat{\xi}_1)$ and $(\hat{\xi}_2,1)$, where now

$$\hat{\xi}_1 = -(M_{11}-\lambda_1)/M_{12}, \quad \hat{\xi}_2 = -(M_{22}-\lambda_2)/M_{21}. \tag{6.15}$$

These may be used to form a $\boldsymbol{Q}$-matrix as follows

$$\boldsymbol{Q} = \begin{bmatrix} 1 & \hat{\xi}_2 \\ \hat{\xi}_1 & 1 \end{bmatrix}, \quad \boldsymbol{Q}^{-1} = \frac{1}{1-\hat{\xi}_1\hat{\xi}_2}\begin{bmatrix} 1 & -\hat{\xi}_2 \\ -\hat{\xi}_1 & 1 \end{bmatrix}, \tag{6.16}$$

and the matrix $\boldsymbol{M}$ can be decomposed as

$$\boldsymbol{M} = \boldsymbol{Q}\boldsymbol{D}\boldsymbol{Q}^{-1}, \tag{6.17}$$

where as before, $\boldsymbol{D} = \mathrm{diag}(\lambda_1, \lambda_2)$.

Now, if the state $\boldsymbol{p}_n$ is known, the state at $x = x_{n+k}$ is given by

$$\boldsymbol{p}_{n+k} = \prod_{m=n}^{n+k} \boldsymbol{T}\boldsymbol{p}_n = \boldsymbol{P}\boldsymbol{D}^k\boldsymbol{P}^{-1}\boldsymbol{p}_n = c_1\lambda_1^k(1, \xi_1) + c_2\lambda_2^k(\xi_2, 1), \tag{6.18}$$

where $(c_1, c_2) = \boldsymbol{P}^{-1}\boldsymbol{p}_n$. For instance, suppose that the flow consists of a finite number, N say, of units. Consider a downstream propagating wave I just to the right of the interface at $x = x_1$. This will result in an upstream propagating reflected wave R, and downstream of $x = x_N$ in a transmitted wave T. The wave motion just to the right of $x = x_N$ then yields the vector $\boldsymbol{c}$ as

$$\begin{bmatrix} c_1 \\ c_2 \end{bmatrix} = \frac{T}{1 - \xi_1\xi_2} \begin{bmatrix} 1 \\ -\xi_1 \end{bmatrix}. \tag{6.19}$$

Alternatively, the state at $x = x_N$ can be written in terms of the eigenvectors of the $\boldsymbol{T}$-matrix as

$$\begin{bmatrix} p^+_{N+1} \\ p^-_{N+1} \end{bmatrix} = \begin{bmatrix} T \\ 0 \end{bmatrix} = \left(\begin{bmatrix} 1 \\ \xi_1 \end{bmatrix} - \xi_1 \begin{bmatrix} \xi_2 \\ 1 \end{bmatrix} \right) \frac{T}{1 - \xi_1\xi_2}. \tag{6.20}$$

This wave structure is now translated k units upstream by repeated application of the transfer matrix $\boldsymbol{T}$. This leads to

$$\begin{bmatrix} p^+_{N+1-k} \\ p^-_{N+1-k} \end{bmatrix} = \left(\lambda_1^{-k} \begin{bmatrix} 1 \\ \xi_1 \end{bmatrix} - \lambda_2^{-k}\xi_1 \begin{bmatrix} \xi_2 \\ 1 \end{bmatrix} \right) \frac{T}{1 - \xi_1\xi_2}. \tag{6.21}$$

Continuing this process up to $k = N$ shows that the transmission and reflection coefficients of N units are given by

$$\frac{T}{I} = \lambda_1^N \frac{1 - \xi_1\xi_2}{1 - (\lambda_1/\lambda_2)^N\xi_1\xi_2}, \quad \frac{R}{I} = \xi_1 \frac{1 - (\lambda_1/\lambda_2)^N}{1 - (\lambda_1/\lambda_2)^N\xi_1\xi_2}, \tag{6.22}$$

two simple relations giving the reflection and transmission coefficients in terms of the eigenvalues and the corresponding eigenvectors of the transfer matrix of one unit.

6.2.3 Examples

As an example, consider the extreme case of a flow in a pipe in which over a length of $10\,\mathrm{m}$ there exists a series of 4 water sections separated by 3 sections of oil. The length of the water sections is taken as $l_w = 1\,\mathrm{m}$ and those of the oil sections

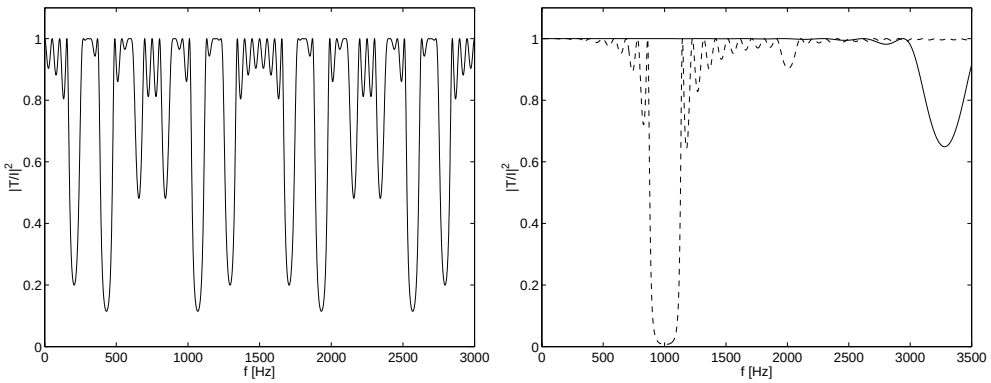

FIGURE 6.3: *Left: energy transmission as a function of frequency for a system consisting of 4 sections with water and 3 sections with oil ($N = 4$), $\nu = 2/7$, $\zeta = 1.1$, $L = 10\mathrm{m}$. Right: for a stratified wavy system ($N = 10$) with $\alpha_0 = 0.5$, $\Delta\alpha = 0.1$, $L = 0.2\mathrm{m}$; oil-water (solid), gas-water (dashed).*

as $l_o = 2\mathrm{m}$. The seven sections are embedded in two half-infinite sections of oil. The densities and the sound speeds of the oil and the water are taken as $\rho_o = 800\mathrm{kgm}^{-3}$, $\rho_w = 1000\mathrm{kgm}^{-3}$, $c_o = 1200\mathrm{ms}^{-1}$, $c_w = 1500\mathrm{ms}^{-1}$. This means that the transit times are $\tau_o = 1/600\mathrm{s}$ and $\tau_w = 1/1500\mathrm{s}$. A sound wave is incident at $x = x_1$ on the first water layer resulting in a transmitted wave T just to the right of the fourth water section. The amplitude I of the incident wave is defined at $x = x_1 - l_o$; in other words, one oil section in front of the first water section. Then the medium consists of $N = 4$ slug units with a total length of $12\mathrm{m}$ consisting of pure oil (the 'dispersed' part) and of pure water (the 'stratified' part). The energy transmission coefficient $|T/I|^2$ is obtained by applying equation 6.22 with $N = 4$ and is presented in figure 6.3 (left) as a function of the frequency. The figure shows a clear band structure of the transmission varying with the frequency.

A second example involves a stratified wavy flow of oil and water. The fluid properties are the same as in the previous example. The volume fraction varies according to equation 6.4 with $\alpha_0 = 0.5$, $\Delta\alpha = 0.1$ and $L = 0.2\mathrm{m}$. The number of units is $N = 10$ which means that the total length becomes $2\mathrm{m}$ The units themselves are divided into $M = 50$ sections which is more than enough to ensure a converged transfer matrix $\boldsymbol{T}$ of the unit. The 10 units are embedded in two half-infinite sections whose compositions are purely stratified with $\alpha = 0.5$. The solid curve in figure 6.3 (right) shows the energy transmission coefficient of this example whereas the dashed line shows the transmission coefficient for an identical system where the oil is replaced by gas ($\rho = 2\mathrm{kgm}^{-3}$, $c = 400\mathrm{ms}^{-1}$). A band structure as appearing in the graph of the previous example cannot be observed in this frequency range for the oil-water flow. Only one (wider) gap is visible at approximately $f = 3275\mathrm{Hz}$. This value is beyond the frequency range of interest and, hence, the gap does not play a role in

the propagation properties of low frequency sound waves of this configuration. The first band in the transmission through the gas-water system is clearly present at about $f = 1000\,\mathrm{Hz}$. The second gap occurring at about $f = 2000\,\mathrm{Hz}$ is much smaller.

The appearance of a band structure in the transmission of waves in periodic media is a well-known phenomenon in many fields of physics as for instance in optics, electronics and solid state physics.

6.3 Bloch waves

6.3.1 Pass bands and stop bands

That the transmission properties of waves travelling through a finite periodic medium exhibit a band structure can be understood from the properties of sound transmission through a periodic system of *infinite* extent for which the propagation structure exhibits a translational symmetry. For such a system Bloch's theorem applies, which states that the wave motion has a spatial dependence

$$\boldsymbol{P}^{-1}\boldsymbol{p}(x_{n+1}) = \boldsymbol{D}\boldsymbol{P}^{-1}\boldsymbol{p}(x_n) \tag{6.23}$$

and so is completely determined by the eigenvalues of the transfer matrix. The eigenvalues may be expressed as $\mathrm{e}^{i\kappa L}$ with L the length of a unit and κ the Bloch propagation constant. The role that κ plays becomes clear (see Harris, 2001) by letting $x \in \langle x_n, x_n + L]$ be the coordinate within a unit and $\boldsymbol{z}(x) = \boldsymbol{P}^{-1}\boldsymbol{p}(x)$ the *global* wave at x. This global wave vector $\boldsymbol{z}(x)$ consists of a downstream and an upstream propagating component, not to be confused with the local waves $p^+(x)$ and $p^-(x)$ which actually form the global wave, see equation 6.23. The downstream running component of the global wave, $z_1 x$, satisfies the functional equation $z_1(x + L) = \mathrm{e}^{i\kappa L} z_1(x)$. The solution equals

$$z_1(x) = \mathrm{e}^{i\kappa x}\phi(x), \quad \text{with,} \quad \phi(x + L) = \phi(x), \tag{6.24}$$

a periodic function that may be expressed in terms of a Fourier series with coefficients c_j, say. Therefore, the time harmonic field $z_1(x)\mathrm{e}^{-\mathrm{i}\omega t}$ may written as

$$z_1(x)\mathrm{e}^{-\mathrm{i}\omega t} = \sum_{j=-\infty}^{\infty} c_j \mathrm{e}^{-\mathrm{i}2\pi j/L}\mathrm{e}^{\mathrm{i}(\kappa x - \omega t)}. \tag{6.25}$$

and it is clear that κ plays the role of the wave number. This wave number κ is related to the structure of the considered unit through the eigenvalues $\lambda_{1,2}$ which satisfy equation 6.8. Since the product $\lambda_1\lambda_2 = \det(\boldsymbol{T}) = 1$ the eigenvalues may be written as $\lambda_1 = \mathrm{e}^{i\kappa L}$, $\lambda_2 = \mathrm{e}^{-i\kappa L}$ and consequently

$$\lambda_1 + \lambda_2 = 2\cos(\kappa L). \tag{6.26}$$

Moreover, equation 6.8 shows that the square of the sum of the eigenvalues is equivalent to

$$(\lambda_1 + \lambda_2)^2 = (\mathrm{tr}(\boldsymbol{T})\lambda_1 - 1) + (\mathrm{tr}(\boldsymbol{T})\lambda_2 - 1) + 2 = (\lambda_1 + \lambda_2)\mathrm{tr}(\boldsymbol{T}) \quad (6.27)$$

and one readily finds from equations 6.26, 6.27 that

$$\cos(\kappa L) = \tfrac{1}{2}\mathrm{tr}(\boldsymbol{T}). \quad (6.28)$$

Three cases may arise:

1. The eigenvalues λ are complex conjugates with modulus 1 corresponding to real values of κ when

$$|\cos(\kappa L)| = |\tfrac{1}{2}\mathrm{tr}(\boldsymbol{T})| < 1. \quad (6.29)$$

   Frequencies for which the eigenvalues are complex belong to *pass bands*.

2. The eigenvalues are real reciprocals, $\lambda_2 = \lambda_1^{-1}$, corresponding to imaginary values of κ when

$$|\cosh(\mathrm{Im}(\kappa L))| = |\tfrac{1}{2}\mathrm{tr}(\boldsymbol{T})| > 1. \quad (6.30)$$

   These represent exponentially growing and decaying solutions due to constructive interference of the reflected waves This phenomenon is referred to as Bragg scattering. Frequencies for which this occurs form the *stop bands*. The corresponding attenuation coefficient per unit length, β, is given by

$$\beta L = |\mathrm{Im}\kappa L|. \quad (6.31)$$

3. The eigenvalues are equal, $\lambda_1 = \lambda_2 = \pm 1$, when

$$|\tfrac{1}{2}\mathrm{tr}(\boldsymbol{T})| = 1. \quad (6.32)$$

   These frequencies signify the boundaries between pass bands and stop bands.

The values of $\cos(\kappa L)$ as a function of the frequency are presented in figure 6.4 for the examples of figure 6.3. It is clearly visible that the frequencies for which $|\cos(\kappa L)|$ exceeds one correspond to the gaps in figure 6.3. Furthermore, the figure suggests that the band structure has a periodic structure, which suggests the need for a deeper analysis.

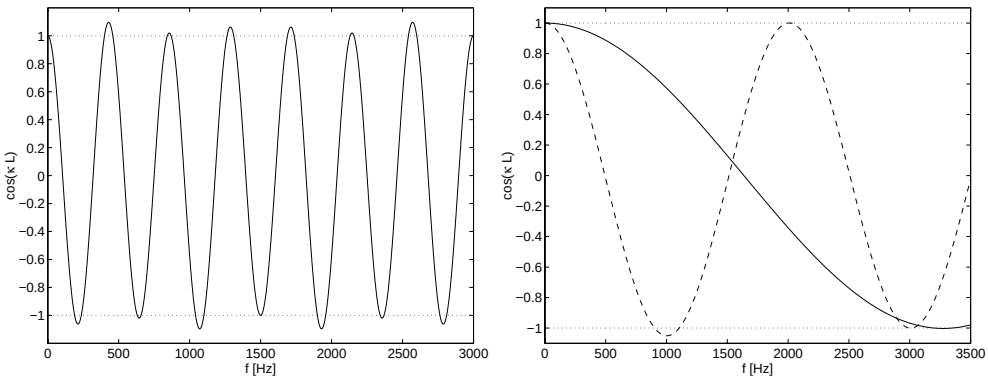

FIGURE 6.4: *Values of* $\cos(\kappa l) = \frac{1}{2}\mathrm{tr}(\boldsymbol{T})$ *varying with the frequency* f*. Left: For the slug flow of figure 6.3 (left). Right: for the stratified wavy flows of figure 6.3 (right); oil-water (solid) and gas-water (dashed).*

6.3.2 Structure of the bands of slug flows

In order to analyze the band structure corresponding to slug flow the following dimensionless parameters are introduced,

$$2\pi f = \omega\tau, \;\; \nu = \tau_d/\tau, \;\; 2\zeta = Z_d/Z_s + Z_s/Z_d, \;\; \text{with } \tau = \tau_d + \tau_s. \tag{6.33}$$

From equation 6.11, we then obtain

$$\cos(\kappa L) = \cos(2\pi f\nu)\cos(2\pi f[1-\nu]) - \zeta\sin(2\pi f\nu)\sin(2\pi f[1-\nu]), \tag{6.34}$$

which expresses the wave number κ in terms of the three parameters f, ν and ζ. The boundaries between stop and pass bands follow from

$$|\cos(2\pi f\nu)\cos(2\pi f[1-\nu]) - \zeta\sin(2\pi f\nu)\sin(2\pi f[1-\nu])| = 1. \tag{6.35}$$

A general solution to equation 6.35 is hard to obtain, but for the special case in which the transit times τ_s and τ_d are equal (i.e. $\nu = 1/2$) progress can be made fairly easily. A layered medium with equal travel times in the layers is known as a Goupillaud medium. Strictly, for a Goupillaud medium periodicity is not required, so here we are dealing with a special case. Equation 6.35 now reduces to

$$|\cos^2(\pi f) - \zeta\sin^2(\pi f)| = 1 \tag{6.36}$$

and, hence, the boundaries of the bands are given by

$$f_b = k, \quad f_b = k \pm \frac{1}{\pi}\tan^{-1}\sqrt{\frac{2}{\zeta-1}}, \;\; k \in \mathbb{N}. \tag{6.37}$$

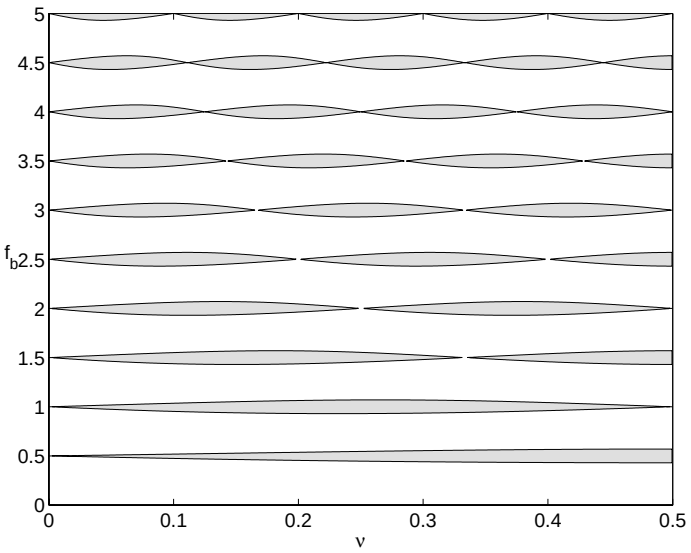

FIGURE 6.5: *Frequency band structure of a periodic slug flow for $\zeta = 1.1$ which is typical for oil-water flows. Stop bands are shaded.*

For other values of ν equation 6.35 has been solved numerically. Figures 6.5 and 6.6 show f_b as a function of ν for the values $\zeta = 1.1$ and $\zeta = 100$, respectively. Because $\mathrm{tr}(\boldsymbol{T})$ is not affected upon exchanging the subscripts s and d of the parameters, the band structure is symmetric with respect to $\nu = 1/2$. So, it is sufficient to restrict attention to values of ν in the range $[0, 1/2]$. Note that in the two figures the value $\nu = 1/2$ corresponds to the Goupillaud medium just mentioned, for which the band structure is described by equation 6.37. Clearly, the values $f_b = k$ are isolated 'stop points' rather than bands. Real stop bands are centered around the frequencies $f = k + 1/2$ and have width

$$1 - (2/\pi)\tan^{-1}(2/(\zeta - 1))^{1/2}. \tag{6.38}$$

The example of figure 6.5, with $\zeta = 1.1$, is for a periodic system of slug units that consist of a part of pure oil and one of pure water. A real oil-water flow would have a value of ζ that is closer to 1, and the stop bands would be even narrower than in the figure. The band structure is in this case close to periodic in ν and is approximately given by

$$f_b = \left[\frac{1}{2} - \frac{1}{\pi}\tan^{-1}\sqrt{\frac{2}{\zeta - 1}}\right]\sin(\pi\nu k) + \frac{k}{2}, \quad k \in \mathbb{N}. \tag{6.39}$$

The example of figure 6.6, with $\zeta = 100$, is more typical for gas-liquid slug flows where the gas volume fraction in the stratified section is 11%. Here, except for rather

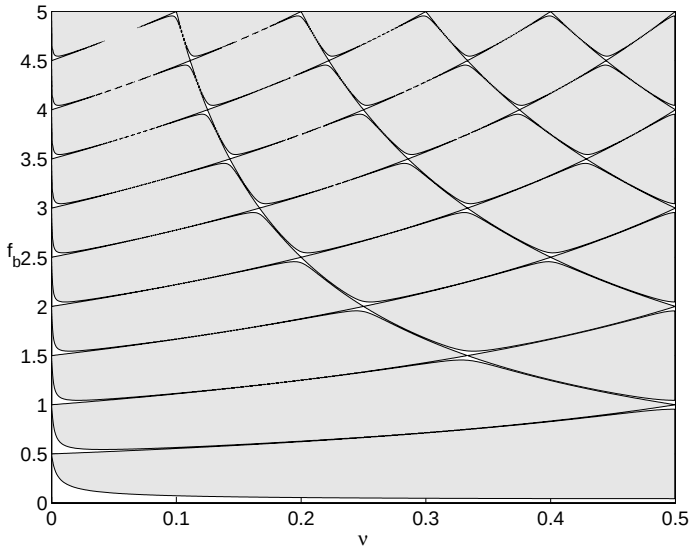

FIGURE 6.6: *Frequency band structure of a periodic slug flow for* $\zeta = 100$ *which is typical for gas-liquid flows. Stop bands are shaded.*

small values of ν, i.e. when the gas plugs are very short, we see that the pass bands are extremely narrow. Due to the large impedance mismatch gas-liquid slug flows do not transmit low frequency sound waves very well. In the limit $\zeta \to \infty$ the band boundaries are given by $\sin^2(2\pi f\nu)\sin^2(2\pi f[1-\nu]) \to 1/\zeta^2$, which means that they can be approximated by the functions

$$f_b = k/(2\nu), \quad f_b = k/(2[1-\nu]), \quad k \in \mathbb{N}. \tag{6.40}$$

Sound wave transmission in a one-dimensional layered waveguide in the form of a "water duct filled with many air blocks" was also recently studied by Luan and Ye (2001a, 2001b). They derive an expression for the band structure which is equal to the one given here, but restrict their numerical examples to systems for which the volume fraction of the gas (i.e. the ratio of the length of the gas blocks to that of the water blocks) is extremely small, typically $10^{-5} - 10^{-4}$. In our notation this would mean excessively small values of ν, and so their work seems not to be of much practical value for gas-liquid flows in pipes. The band structures they present, for example figure 2*b* of their first paper, agree very well with those in our figures 6.5 and 6.6.

The harmonic functions that appear in equation 6.34 suggest that there is a periodicity in the band structure. Such periodicity in f is found when $n_1\nu = n_2(1-\nu)$, for some positive integers n_1 and n_2. This means that $\nu/(1-\nu)$, i.e. the ratio of the travel times in the two sections that form a slug unit, is rational. Let $\nu = k/n$ with k, n the smallest possible positive integers. Then the period in $\mathrm{tr}(\boldsymbol{T})(f)$ (and

thus in the eigenvalues) equals the denominator n. In one period n the cosines and the sines in equation 6.34 with arguments $2\pi f\nu$ and $2\pi f(1-\nu)$ pass through k and $n-k$ periods, respectively. This does not imply that the band structure has exactly that same period. In order to show this, again let $\nu = k/n$, with k, n the smallest possible integers, and note that k and $n-k$ cannot both be even. Then

$$\mathrm{tr}(\boldsymbol{T})(f) = \mathrm{tr}(\boldsymbol{T})(f+n), \tag{6.41}$$

and inspection shows that also

$$\mathrm{tr}(\boldsymbol{T})(f+n/2) = \pm\mathrm{tr}(\boldsymbol{T})(f), \tag{6.42}$$

where the plus sign is for the case in which k and $n-k$ are both odd. Upon taking squares the minus sign is cancelled, so the period in $(\mathrm{tr}(\boldsymbol{T}))^2$ and thus in the band structure is half the period in $\mathrm{tr}(\boldsymbol{T})$. This periodicity in the band structure can be clearly seen in Figures 6.5 and 6.6. For instance, take $\nu = 1/3$. Then the period in $\mathrm{tr}(\boldsymbol{T})$ equals $n = 3$ and the distance between the nodes in the figures takes the expected value $3/2$.

It is noted that in periodic media in which identical homogeneous sections are separated by compact scatterers gaps occur when the length L of the sections is half a wavelength λ. These systems have Goupillaud properties and thus is the first gap given by $f = 1/(2\tau)$. Upon substituting $f = c/\lambda$ and $\tau = L/c$ one readily finds the expected $L = \lambda/2$. These systems are fully transparent to waves when $L = \lambda/4$, which is exactly the center of the first pass band. Yet, these rules of thumb do in general not apply to systems built up of slug units, only when the units have Goupillaud properties or when the impedance contrast is small, like for oil-water slug flows. The gas-liquid systems of figure 6.6 which have a large impedance contrast prove this point.

6.3.3 Examples

Relation to finite periodic flows

Returning now to the system of finite extent, i.e. the example of figure 6.3 (left), where the parameters take the values $\zeta = 1.1$ and $\nu = 2/7 \approx 0.286$. The boundaries between the stop and the pass bands, i.e. the values of f_b as given by equation 6.39, are given (in Hz) in the table below.

1:	190	236	5:	1042	1100
2:	400	458	6:	1264	1310
3:	631	657	7:		1500
4:	843	869			

There is obviously a close agreement with the band structure that was found in figure 6.5 (left). It is noted that for $\nu = 2/7$ the band structure is periodic in f with

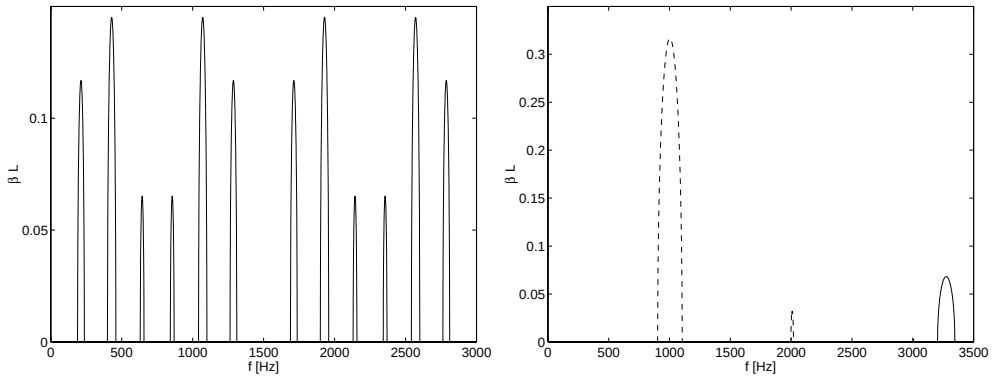

FIGURE 6.7: *Attenuation coefficient per unit. Left: for the system of figure 6.3 (left) where* $\nu = 2/7$*,* $\zeta = 1.1$*. Right: for the stratified wavy configurations of figure 6.3 (right) where* $\alpha_0 = 0.5$*,* $\Delta\alpha = 0.1$*; oil-water (solid), gas-water (dashed).*

period $7/(2\tau) = 1500\,\mathrm{Hz}$, which provides a simple means to determine the band gaps at higher frequencies.

The transit time and the value of ν in stratified wavy flows may be defined as

$$\tau = \int_0^L c(x)^{-1}\mathrm{d}x \;\text{ and }\; \nu = \frac{1}{\tau}\int_0^{L/2} c(x)^{-1}\mathrm{d}x, \tag{6.43}$$

respectively. Then the numerical values of the two for the example of figure 6.3 (right) on the stratified wavy flow of oil and water become $\tau = 1/6549\,\mathrm{s}$ and $\nu = 0.49$. The flow is very close to a Goupillaud medium and, hence, its first band gap is given by $f = 1/2\tau = 3274\,\mathrm{Hz}$, very well approximating the value of $f = 3275$ in the figure. In order to estimate the width of the band one may use equation 6.38. Unfortunately an estimate of ζ for stratified wavy flows has not been found. The parameters of the stratified wavy flow of gas and water become $\tau = 1/2002\,\mathrm{s}$ and $\nu = 0.50$. Here the flow is even closer to a Goupillaud medium. Its band gaps become $f = 1/2\tau = 1001\,\mathrm{Hz}$ and $f = 1/\tau = 2002\,\mathrm{Hz}$, also in very good agreement with the figure. The latter would be a 'stop point' rather than a band in a perfect Goupillaud medium but can clearly be observed as a (small) band in the figure. The expected gap at $f = 3000\,\mathrm{Hz}$ is, however, absent. This will be explained later. Clearly, the locations of the gaps of stratified wavy flows are quite well estimated, at least in these cases, by those of a Goupillaud medium even though these flows are not composed of slug units.

Figure 6.7 shows the attenuation coefficients per unit according to equation 6.31 for the examples above. The graphs agree qualitatively well with the band structure of figure 6.3. Yet, quantitatively the values do not agree with the gaps in the figure. For example the value of the second gap in figure 6.7 (left) is about 0.14. This means

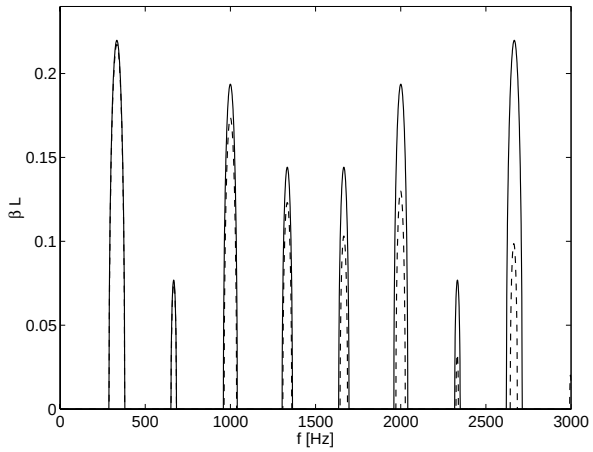

FIGURE 6.8: *Attenuation coefficient per unit for a slug unit (solid) containing a part of pure water and a part of pure oil with $l_d = l_s = 1$ (L=2), and for a stratified wavy unit with $\alpha_0 = 0.5$, $\Delta\alpha = 2$, $L = 2$.*

that the expected value of the energy transmission coefficient is $\exp(-0.14 \cdot 2N) \approx 0.33$. The factor two has to be added because figure 6.3 (left) shows the square of $|T/I|$. The transmission coefficient of the second gap of the oil-water slug flow in figure 6.3 (left) has the value of about 0.11, a factor three lower. The reason for this difference is the finite length of the system in figure 6.3.

When the number of units becomes very large the transmission coefficient as given by equation 6.22 becomes, at least for frequencies in band gaps,

$$\frac{T}{I} = \lambda_1^- N \frac{1 - \xi_1 \alpha_2}{\xi_1 \xi_2}. \tag{6.44}$$

Here the real λ_1 is defined as the largest eigenvalue and $\lambda_2 (= 1/\lambda_1)$ the smallest. It is noted that the modulus $|\xi_1 \xi_2| = 1$ for frequencies in band gaps. Upon substituting $\lambda_1 = \exp(|\mathrm{Im}(\kappa L)|) = \exp(\beta L)$ in equation 6.44 the modulus of the transmission coefficient becomes

$$\left| \frac{T}{I} \right| = \mathrm{e}^{-\beta L N} |1 - \xi_1 \xi_2|. \tag{6.45}$$

Then the waves attenuate with a attenuation coefficient per unit of βL. The factor $|1 - \xi_1 \xi_2|$ is a value in the range $[0, 2]$. For completeness, for large N the modulus of the reflection coefficient R/I tends to one for frequencies in a band gap.

Relation between slug units and stratified wave units

The band structure of transmission coefficient varying with the frequency occurs for slug flows and stratified wavy flows. A major difference, however, is that the bands

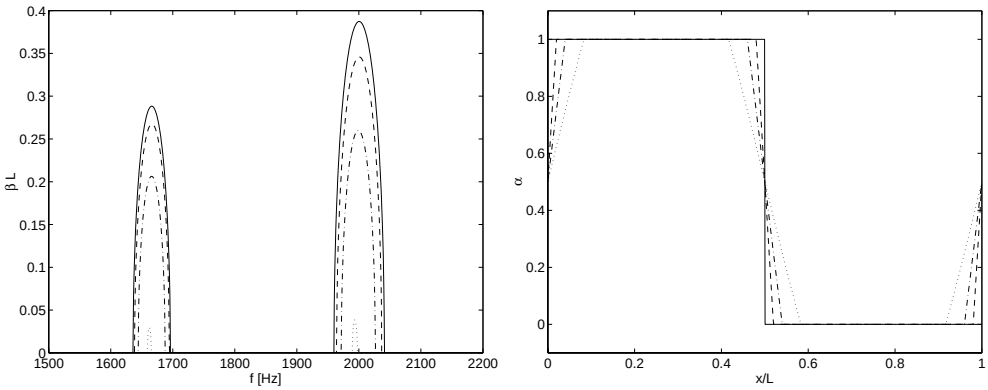

FIGURE 6.9: *Left: attenuation coefficient per unit for the two gaps between* $f = 1500 - 2200\,\mathrm{Hz}$ *for a stratified wavy configuration with* $\alpha_0 = 0.5$*,* $L = 2$ *and with amplitudes* 1 *(dotted),* 2 *(dash-dot),* 4 *(dashed) and for a slug flow (solid) with* $l_d = l_s = 1$*. Right: corresponding volume fraction of the water* α*.*

of slug flows remain present as the frequency increases while the expected bands of stratified wavy flows are absent at higher frequencies; see for example the expected but missing band at $f = 2002\,\mathrm{Hz}$ of the gas-water flow of figure 6.7 (right). The reason for this is that in stratified wavy systems the wavelengths corresponding to higher frequencies become smaller than the length scale in which the impedance varies. The consequence is that reflections become weaker; the medium tends to a more gradually varying medium where the WKB-method as described in section 5.3 applies. In slug flow this does not occur, simply because here the impedance varies discontinuously and the variation of the impedance remains abrupt regardless of the frequency.

In order to estimate how the band structure is affected when the discontinuous variation of the impedance of slug flows is slightly moderated, the case is considered where the two parts of a slug unit both have a length of $1\,\mathrm{m}$; so $l_d = l_s = 1\,\mathrm{m}$ ($L = 2\,\mathrm{m}$). The two parts consist of just water and of just oil. This system is resembled by a stratified wavy flow of oil flowing on top of water that has a volume fraction α according to equation 6.7 with $\alpha = 0.5$, say, and with a large amplitude $\Delta\alpha$. In figure 6.8 the band structure is presented in the form of the attenuation coefficient per unit βL for $\Delta\alpha = 2$. As the first gap is approximately the same for the two systems, the gaps of the stratified wavy flows decrease relatively to the ones of the slug flow when the frequency goes up. Moreover, a small gap of the stratified wavy flow may be recognized at $f = 3000\,\mathrm{Hz}$ whereas the corresponding one of the slug flow is absent. This is due to the fact that $f = 3000\,\mathrm{Hz}$ is a 'stop point' instead of a gap for the slug flow, but a band for the stratified wavy flow which has a slightly different value of ν. Figure 6.9 (left) shows the gaps between $f = 1500\,\mathrm{Hz}$ and $f = 2200\,\mathrm{Hz}$

in more detail for $\Delta\alpha = 1$, $\Delta\alpha = 2$ and $\Delta\alpha = 4$. Figure 6.9 (right) visualizes the corresponding values of α. It is clear that the attenuation coefficients corresponding to the gaps drop when the amplitude $\Delta\alpha$ decreases. Furthermore, the changing value of ν affects the location of the gaps. It shifts to a slightly lower frequency when the amplitude $\Delta\alpha$ decreases.

It is noted that for a pipe with a diameter of $0.1\,\mathrm{m}$ the slope of the interface ranges from about 0.3 for $\Delta\alpha = 1$ to infinity for the slug flow. A slope of 3.4 corresponding to an amplitude of $\Delta\alpha = 4$ seems a more realistic value for real intermittent flows. The band structure as for idealized slug flow is not much affected in this case, at least not for frequencies up to $2000\,\mathrm{Hz}$.

6.4 Defect modes

Although wave propagation in periodic waveguides has been a subject of intensive research for mechanical, optical and electronic systems, publications that are concerned explicitly with acoustic wave propagation in fluid dynamical systems are rare. Examples are the papers by Bradley (1994*a*, 1994*b*) and, more recently, of Robertson, Ash and McGaugh (2002) and Munday et al. (2002). These last authors study sound propagation in straight pipes, that are given periodic waveguide properties. In the first reference this is achieved by attaching a dangling side branch system to the pipe and in the second reference by varying the cross-section of the pipe. Munday et al. (2002) look at what happens when there is a defect in the periodicity of the wave guide, in their case when one of the pipe sections is given a different length. It is instructive to repeat their analysis, extend it a little bit, and then show what it implies for sound transmission in an oil-water slug flow. For instance how the band structure is affected when the flow is not perfectly periodic.

The waveguide of Munday et al. (2002) is a PVC pipe of length $157.9\,\mathrm{cm}$, the diameter of which varies periodically from $1.9\,\mathrm{cm}$ to $3.2\,\mathrm{cm}$. The $1.9\,\mathrm{cm}$ diameter sections have a length of $17.7\,\mathrm{cm}$, and the length of the $3.2\,\mathrm{cm}$ diameter sections is $17.4\,\mathrm{cm}$, which means that the waveguide has almost the properties of a Goupillaud medium. The authors do not mention the physical properties of the fluid medium inside the pipe, but if we assume that it is air with density $1.3\,\mathrm{kg\,m^{-3}}$ and sound speed $340\,\mathrm{m\,s^{-1}}$ ($\nu = 0.50$, $\zeta = 1.6$) the transmission coefficient for the system would be that shown in figure 6.10. There are band gaps between $330 - 640\,\mathrm{Hz}$ and $1300 - 1610\,\mathrm{Hz}$.

Now, suppose that the middle section is given a different length, e.g. that is changed in the first case by a factor 1.97 and in the second case by a factor 0.76. Figure 6.11 (which is equivalent to figure 5(*b*) in Munday et al. (2002)) shows what happens. The whole band structure is modified, with the most prominent feature that a defect mode appears in a stop band. The waveguide becomes 'transparent' for a

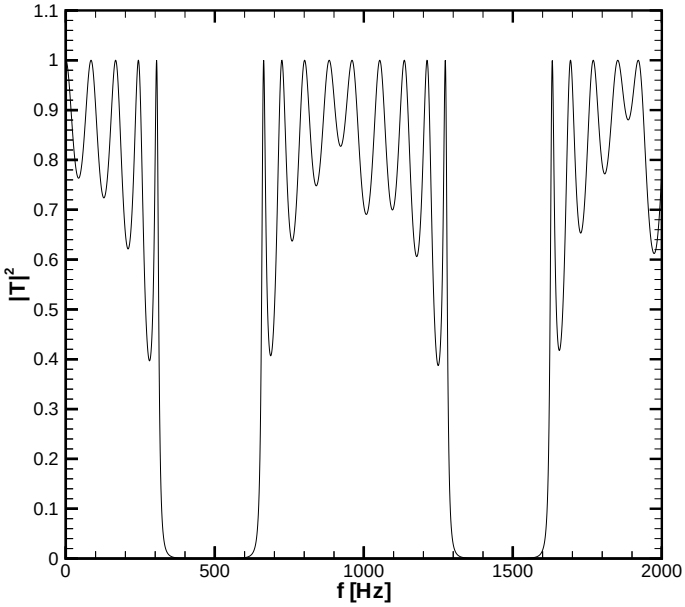

FIGURE 6.10: *Energy transmission as a function of frequency in the periodic waveguide studied by Munday et al. (2002).*

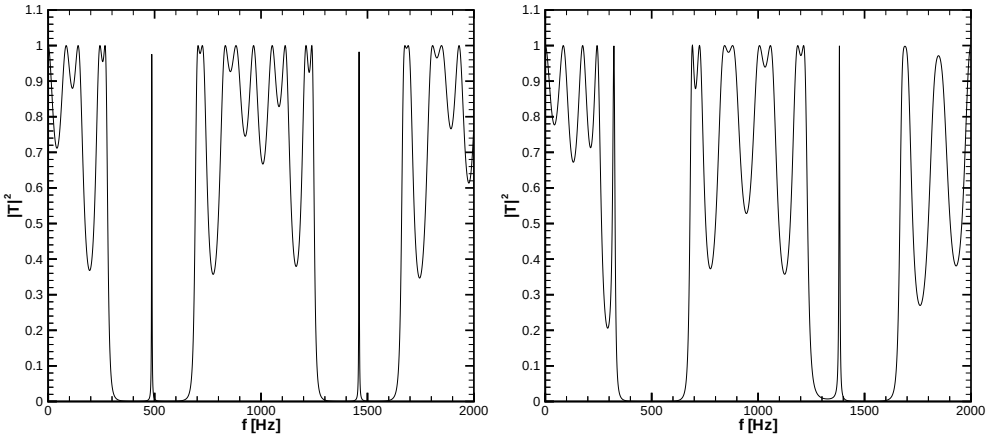

FIGURE 6.11: *As in figure 6.10 but with the length of the middle section increased by a factor* 1.97 *(left) and a factor* 0.76 *(right).*

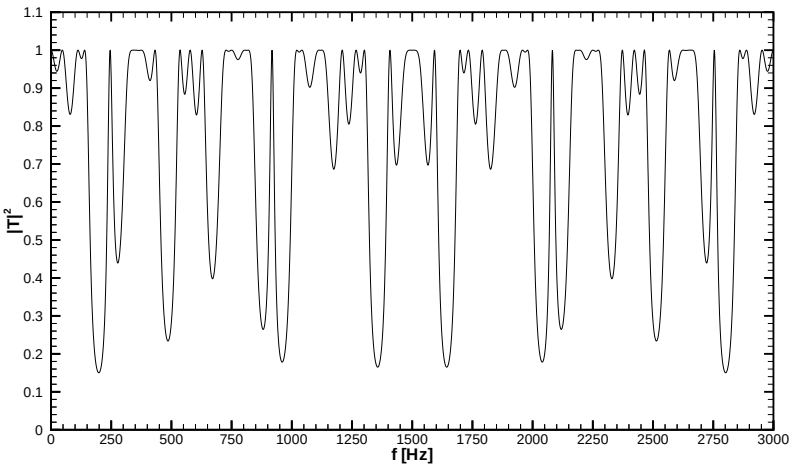

FIGURE 6.12: *Energy transmission as a function of frequency for a system consisting of 4 sections with water and 3 sections with oil, but with the length of middle section (with oil) doubled. ($\nu = 2/7$, $\zeta = 1.1$, $L = 10$ m).*

very narrow range of frequencies within the stop bands, around $491\,\mathrm{Hz}$ and $1474\,\mathrm{Hz}$ in the first case and around $326\,\mathrm{Hz}$ and $1395\,\mathrm{Hz}$ in the second case.

The phenomenon of defect modes is fruitfully used in optics (e.g. Fowles, 1968) where a stack of dielectric films with alternating indices of refraction is used. The layer in the middle is doubled in length. The result is a multilayer Fabry-Perot interference filter that is only transparent for a very narrow frequency band while the light waves of other frequencies are reflected. These filters are superior compared to other filters because of the lower absorbtion and the higher reflectance.

What Munday et al. (2002)) do not show is that the breakup of the band structure also depends on the choice of the section that is given a different length. This is illustrated in figure 6.13 for a Goupillaud medium consisting of 9 sections of which the length of one of the sections is doubled, a different section in each of the graphs.

It should be pointed out that the appearance of a well-defined, narrow band gap within the stop bands as found by Munday et al. (2002) is due to the fact that their waveguide had Goupillaud properties. In the oil-water slug flows found in practice, of course, this will usually not be the case. The consequence is that it is much harder to obtain information from the observed breakup of the band structure. To illustrate this the calculations of the example of figure 6.3 (left) (which is not close to a Goupillaud medium) is repeated, but now with the middle section doubled in length. The result is shown in figure 6.12, and a comparison with figure 6.3 makes this point clear. Moreover, in oil-water flows defects will not appear at one location in the pipe. In fact the lengths of, basically, all sections deviate from their values in a perfectly periodic composition. This complicates considerably the extension of the transmission properties of periodic systems to those of systems that are close to periodic.

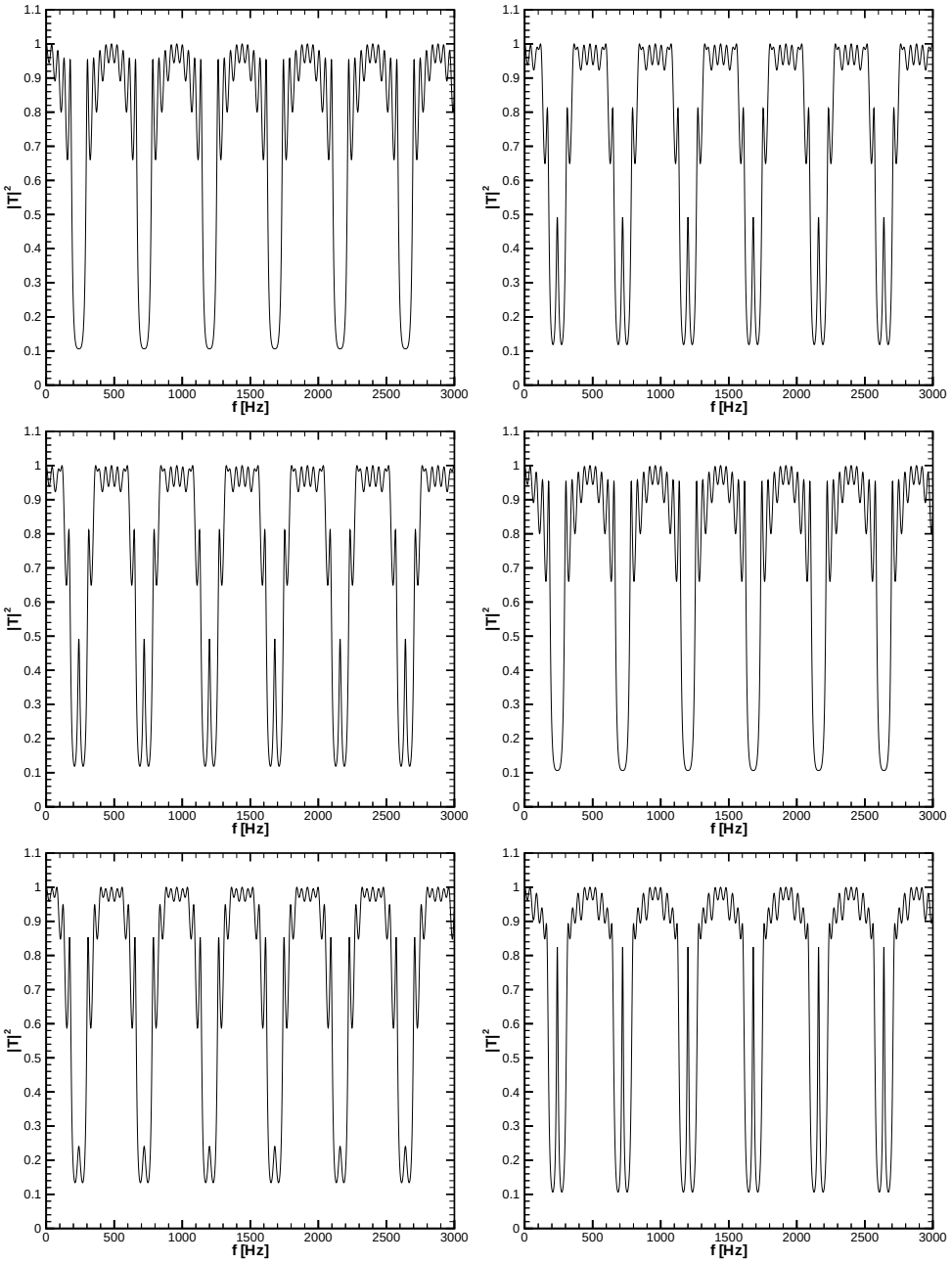

FIGURE 6.13: *Energy transmission as a function of frequency in a Goupillaud medium with* 9 *sections of which one section has a length that is twice as large. In the upper graphs this is the* 1^{st} *section (left) and the* 3^{rd} *section (right), in the graphs in the middle row the* 7^{th} *(left) and the* 9^{th} *section (right), and in the graphs in the bottom row the* 2^{nd} *(left) and the* 4^{th} *section (right).*

6.5 Discussion

Flows of large oil bubbles in water, gas-liquid slug flows or flows of water with clouds of dispersed small oil bubbles are examples of intermittent flows. The composition of these flows varies abruptly with position along the pipe. In the idealized situation intermittent flows have a perfectly periodic structure. Also stratified flows with a wavy interface are examples of periodic flows, but here the acoustic properties vary more gradually. One period of the two classes of these periodic flows was represented by a slug unit and a stratified wavy unit. The corresponding transfer matrices were derived by means of the transfer-matrix method, which provided an analytical relation to the transfer matrices for slug units. The transfer matrices associated with the stratified wavy units were calculated numerically.

Upon diagonalizing the transfer matrices expressions were found that relate the transmission and the reflection coefficients of a chain of units to the eigenvalues and eigenvectors of the transfer matrix. The transmission coefficient as a function of the frequency for sound waves propagating through finite periodic flows has a band structure. For certain frequency bands (the stop bands) waves attenuate and do not propagate through the pipe unlike the waves of frequencies corresponding to the pass bands.

This band structure of the transmission coefficient can be understood by considering an infinite pipe where Bloch's theorem applies. The properties of the resulting Bloch wavenumber are directly related to the eigenvalues of the transfer matrix of a slug unit. Asymptotic solutions to the band structure were found for flows with a very low and a very high impedance contrast, in terms of the transit time of a unit τ and two parameters ν and ζ that are related to the ratio of the transit times through the two section of a slug unit and the impedance contrast, respectively. When the impedance contrast is low the stop bands are narrow, in contrast to those of gas-water flows. In the latter case the stop bands are very wide which indicates that actually sound waves of almost the full frequency range do not propagate through gas-water slug flows at all.

Upon generalizing the definition of ν the locations of the stop band centers for stratified wavy flows are approximately given by the same relations as those for slug flow. Yet, a generalized form of ζ and consequently relations for the width and the attenuation coefficient of the band gaps have not been found. Numerical simulations demonstrate that the first stop band for stratified wavy oil-water flows exceeds the frequency range of interest. The gas-water analogue, however, showed a very clear stop band. Except for frequencies in this stop band sound propagates well through stratified wavy gas-water flows unlike sound waves in gas-liquid slug flows. The high value of the attenuation coefficient for frequencies of the first band gap may provide a means to estimate the interface wavelength of stratified wavy gas-liquid flows.

When the frequency increases the composition of the stratified wavy flows varies

more gradually on the scale of the corresponding wave length of the sound waves. The result is that the attenuation coefficients of the band gaps decrease. This is not the case for slug units where the composition varies abruptly. Even when the abrupt variations in composition are somewhat moderated the band structure is not significantly affected. For stratified wavy flows, however, only a few gaps at low frequencies were observed in the examples. For high frequencies the waves propagate without being reflected significantly.

When the length of a single section of a finite periodic flow is doubled defect modes occur. In the stop bands narrow bands arise where the attenuation coefficient is much smaller than in the remaining part of the gaps. The medium may even become fully transparent at these frequencies. This remarkable phenomenon is an example of what may happen when the periodicity of the medium is locally disarranged. In the next chapter all sections will be (randomly) altered to model more realistic intermittent flows.

ACOUSTICS OF RANDOM PERIODIC FLOWS

CHAPTER 7

7.1 Introduction

In the previous chapter the acoustics of perfectly periodic flows were discussed. Such flows are idealizations of stratified wavy flows and intermittent flows like gas-liquid slug flows or flows of large bubbles of oil in water, see figure 2.1 (q,r) and figure 2.2 (3,4,7,8). In practice, these flows are not fully periodic. In gas-liquid slug flows, for instance, the volume fractions of the gas in the stratified part (the plug) and that in the dispersed part (the slug) differ with each slug unit. The lengths of the parts may also vary appreciably. Furthermore, in flows of large oil bubbles in water the sizes of the bubbles and the distances between them all differ in an apparently random way.

This chapter involves the effects upon the band structure of the transmission coefficient of periodic flows when the lengths of the sections are varied at random. It will be shown that these random variations in length give the sound transmission remarkable statistical properties. By studying these statistics it may be possible to find ways to extract information about the medium by measuring (stochastic) sound propagation.

In order to illustrate some of the effects, first some examples will be given of a system where an upstream propagating wave I is incident upon a randomly varied periodic flow of length L resulting in a transmitted wave T. For simplicity the flow is assumed to consist of alternating sections of just oil and just water, following the main example in the previous chapter. Some of the statistical properties of the sound transmission will be discussed on the basis of the extensive literature on waves in random media and it will be demonstrated that the prominent quantity of interest for these systems is the Lyapunov exponent and its reciprocal, the localization length. The Lyapunov exponent associated with a pipe of finite length is a stochastic variable. Section 7.3 discusses the conditions for which a remarkable property of the probability distribution of the Lyapunov exponent, the single parameter scaling, applies. In section 7.4 more remarkable statistical properties will be presented with respect to the distribution of energy in the pipe. In addition, it will be shown that the

phenomenon of Anderson localization occurs in these systems.

Waves in random media are studied in many fields of physics. A famous paper is that of Anderson (1958) in which the phenomenon of localization was introduced. As Maynard (2001) explains, Anderson localization means that for certain conditions the amplitudes of waves in a one-dimensional random medium may grow at certain locations in the waveguide. At the two sides of the resulting peaks the wave amplitudes decrease exponentially. Anderson localization was used to explain the metal-to-insulator transition in disordered metals. The occurrence of the phenomenon in oil-water slug flows will be presented in section 7.4.

Another field of physics where waves in random media are of interest is geophysics. Here it is attempted to obtain information on the randomly layered earth's crust by generating acoustic pulses at the surface and analyzing the reflected sound waves (e.g. Shapiro, 1999; Papanicolaou, 1998). Waves in random media are also studied in mechanics (e.g. Langley, 1995; Sobnack and Crighton, 1994) and in fluid dynamics, for example in studies of gravity waves propagating in channels with an irregular bottom (e.g. Ardhuin and Herbers, 2002; Devillard et al., 1988).

7.2 Break-up of the band structure

The oil-water slug flow that will be considered in the examples below is the periodic system of figure 6.3 (left). However, the lengths of the two parts of each period*, l_o and l_w, and thus the transit times τ_o and τ_w vary in a uniformly random manner. This means that each section i has length

$$l_i = \langle l_i \rangle \ (1 + \tilde{\delta}), \tag{7.1}$$

where the mean lengths $\langle l_i \rangle$ are those of the periodic system; i.e. the oil sections have a mean length $\langle l_o \rangle$ and the water sections a mean length $\langle l_w \rangle$. The random variations $\tilde{\delta}$ denote numbers that are chosen randomly from the interval $[-\delta, \delta]$ with a uniform probability distribution. δ signifies the degree of randomness and will be called 'randomness' in what follows. All randomly chosen numbers are statistically independent of the others. It is recalled that the number that characterizes the ratio of the impedances of the flow sections has the (constant) value $\zeta = 1.1$ in this example. Again, the mean lengths are $\langle l_w \rangle = 1\,\mathrm{m}$, $\langle l_o \rangle = 2\,\mathrm{m}$. The value of ν, the number that characterizes the ratio of the transit times, basically differs per period but based on the mean flow,

$$\nu = \frac{\langle l_w \rangle / c_w}{\langle l_w \rangle / c_w + \langle l_o \rangle / c_o}, \tag{7.2}$$

it has the value of $\nu = 2/7$.

*Since the flow is no longer perfectly periodic the term period is, perhaps, somewhat unsuitable in this context; it is based on the mean flow.

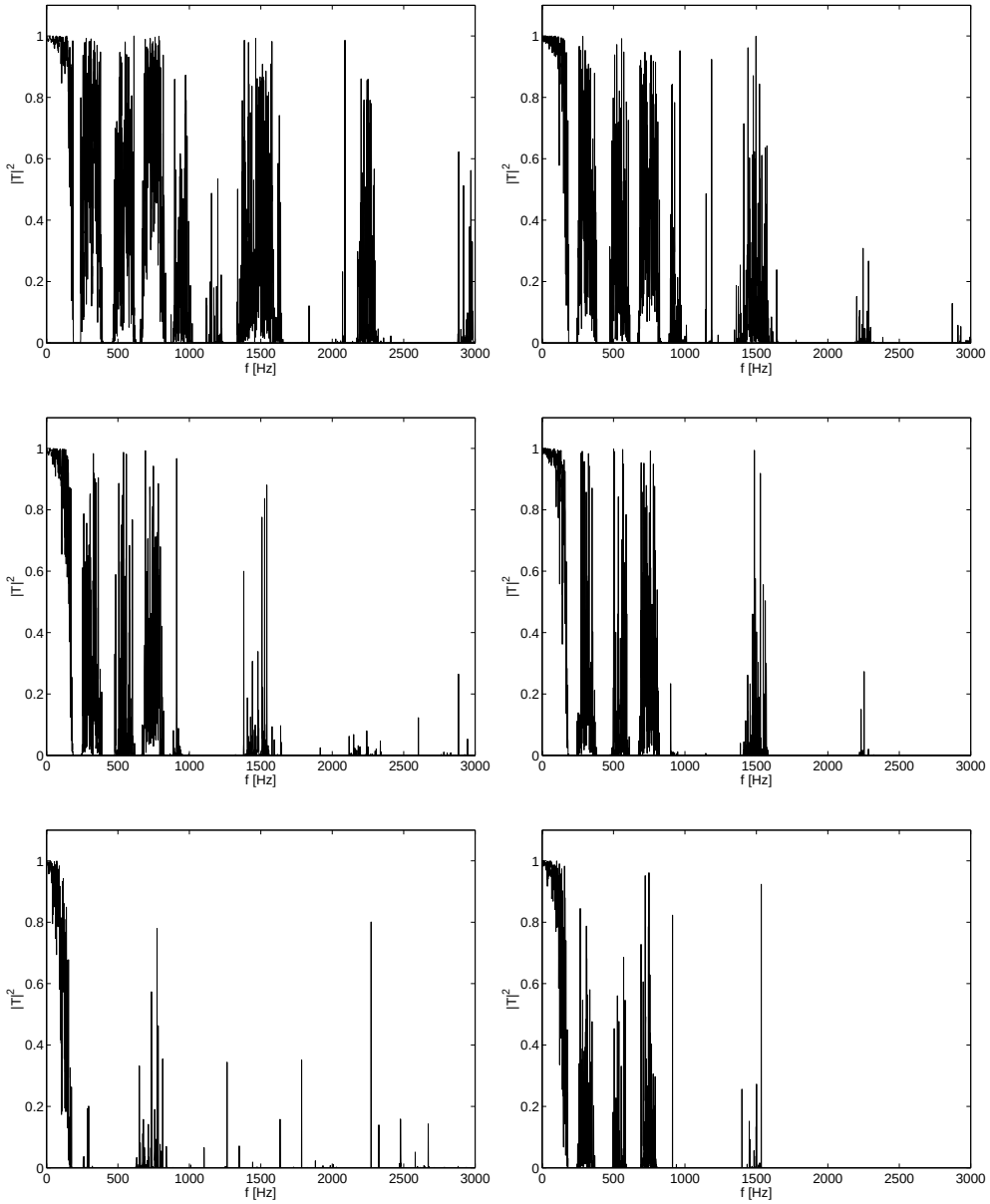

FIGURE 7.1: *Energy transmission as a function of frequency for a system consisting of $N/2$ water and $N/2$ oil sections of randomly chosen lengths with $\langle l_1 \rangle = 1$, $\langle l_2 \rangle = 2$, $\nu = 2/7$, $\zeta = 1.1$. Left: varying randomness with $N = 400$ and $\delta = 0.05$ (top), $\delta = 0.1$ (middle), $\delta = 0.25$ (bottom). Right: varying number of sections with $\delta = 0.05$ and $N = 800$ (top), $N = 1600$ (middle), $N = 3200$ (bottom).*

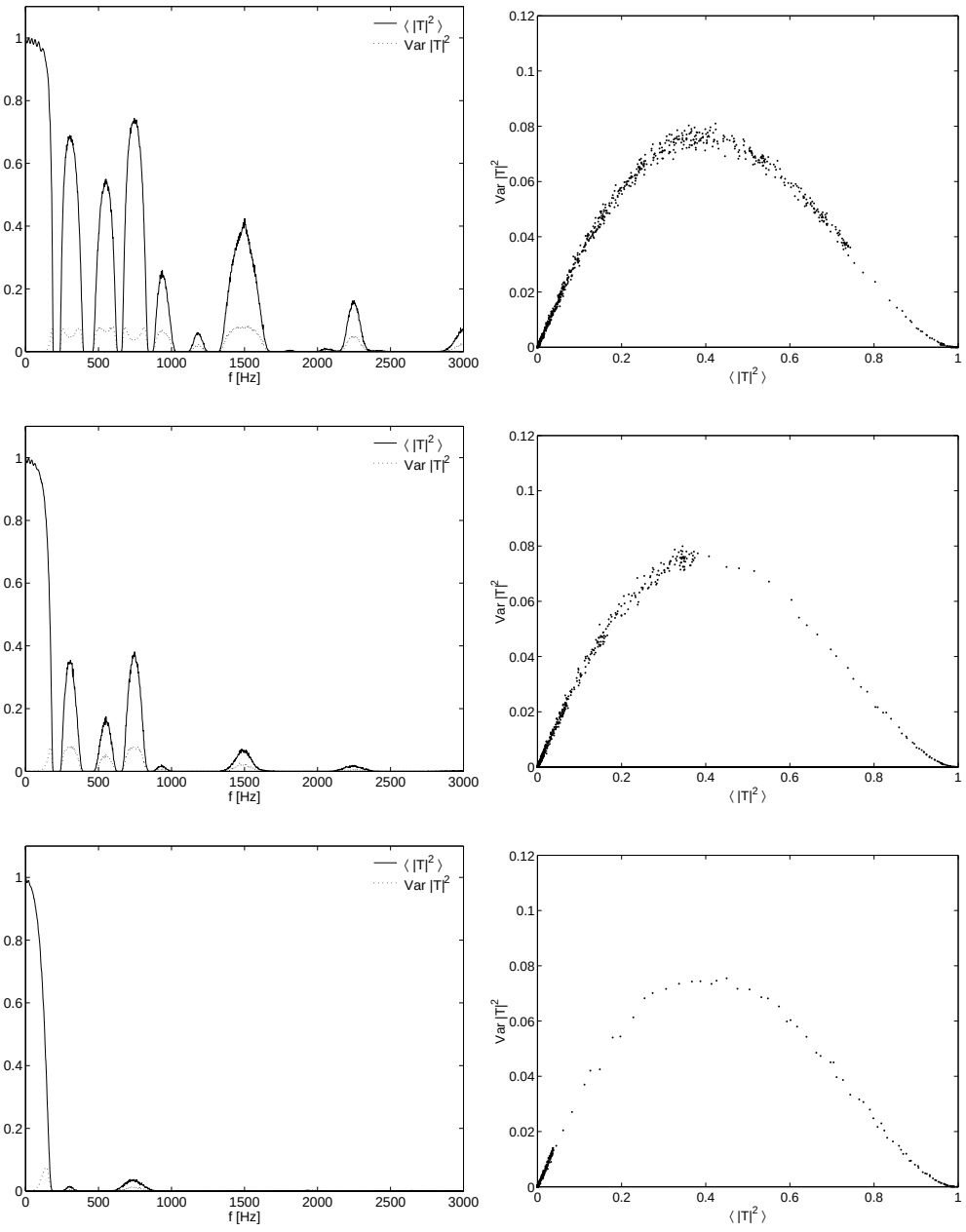

FIGURE 7.2: *Ensemble average over* 1500 *realizations of the energy transmission as in figure 7.1 with* $N = 400$*. Left: the mean energy transmission and its variance varying with the frequency;* $\delta = 0.05$ *(top),* $\delta = 0.1$ *(middle),* $\delta = 0.25$ *(bottom). Right: the variance plotted against the mean;* $\delta = 0.05$ *(top),* $\delta = 0.1$ *(middle),* $\delta = 0.25$ *(bottom).*

The system of figure 6.3 (left) contains 4 periods, thus 4 sections of oil and 4 sections of water (N=8 sections), and has a length of $12\mathrm{m}$. Figure 7.1 (left) shows what happens to the energy transmission $|T/I|^2$ when the system is much longer, $600\mathrm{m}$ in the mean (N=400 sections), and the randomness δ is increased from 0.05 to 0.1 and 0.25. For each graph of figure 7.1 a single realization was generated at random and the energy transmission for that realization was calculated as a function of frequency. The left graphs illustrate that the randomness breaks up the band structure (as given by the table in section 6.3) and that as the randomness increases the system becomes less and less transparent, in particular for the higher frequencies.

The graphs in figure 7.1 (right) are for another realization of the system in the upper graph of figure 7.1 (left), but with a length that is doubled to $1200\mathrm{m}$ (N=800). The other two graphs illustrate what happens if for the same value of the randomness $\delta = 0.05$ the length of the system is increased from $1200\mathrm{m}$ to $2400\mathrm{m}$ and $4800\mathrm{m}$. As before, the system becomes less transparent, especially at the higher frequencies. The graph suggests that each frequency has a 'penetration depth'; a depth that is shorter as the frequency is higher and also becomes shorter as the randomness increases. The latter seems more effective in decreasing this penetration depth.

The energy transmission $\mathcal{T}_L = |T/I|^2$ for a certain length L can be considered as a stochastic variable. Rather than looking at values of this variable for individual realizations of the system, it is more useful to study its statistical properties. Figure 7.2 (left) shows how for a mean length of $L = 600\mathrm{m}$ its average value $\langle \mathcal{T}_L \rangle$ and its variance

$$\mathrm{Var}\,\mathcal{T}_L = \left\langle \mathcal{T}_L^2 \right\rangle - \langle \mathcal{T}_L \rangle^2 \,, \tag{7.3}$$

estimated by the mean and the variance of an ensemble of 1500 realizations, depend on wave frequency f and randomness δ. The band structure of the original periodic system is still clearly visible in the upper two graphs of figure 7.2 (left). The pass bands, however, disappear as the randomness increases. The rate at which this happens is different for each pass band. Note that in the upper graph the variance in the first few pass bands has a doubly peaked structure, a feature that is not present in the fifth and higher pass bands. When the randomness is increased these peaks coalesce, and the variance in the low frequency pass bands behaves as that of the high frequencies pass bands at lower values of the randomness. Moreover, the graphs of figure 7.2 (left) and Figure 7.1 (left) show that the waveguide is not fully transparent for *any* frequency; i.e. the randomness limits the penetration depth of *all* frequencies.

Something remarkable is found when for a large number of frequencies, from both pass bands and stop bands of the original periodic waveguide, $\mathrm{Var}\,\mathcal{T}_L$ is plotted against $\langle \mathcal{T}_L \rangle$. Figure 7.2 (right) suggests that there is a universal relation between the two. Of course, as the randomness increases both the mean and the variance of $\mathcal{T}_L$ decrease, so all data points contract towards the origin, but nevertheless the gross universal structure remains apparent.

7.3 Statistical properties of transmitted waves

7.3.1 Lyapunov exponents

A very extensive literature exists on the propagation of classical waves in *homogeneous* random media† (e.g. Sheng, 1995; van Rossum and Nieuwenhuizen, 1999). Rather than those of $\mathcal{T}_L$, it is common to study the statistics of the random variable

$$\gamma_L = -(1/2L) \ln \mathcal{T}_L, \tag{7.4}$$

i.e. the logarithmic decrement of the transmission coefficient $|T/I| = \sqrt{\mathcal{T}_L}$. The limiting value for $L \to \infty$ of γ_L is known as the Lyapunov exponent,

$$\gamma = \lim_{L\to\infty} \gamma_L, \tag{7.5}$$

and therefore the stochastic variable γ_L may be defined as the Lyapunov exponent associated with a system of length L. Also the limiting value for $L \to \infty$ of the ensemble average $\langle \gamma_L \rangle$ is equal to the Lyapunov exponent,

$$\gamma = \lim_{L\to\infty} \langle \gamma_L \rangle \,. \tag{7.6}$$

For sufficiently large L (much larger than the localization length defined below) the Lyapunov exponent γ can be estimated from γ_L and even more accurately from $\langle \gamma_L \rangle$. The variable γ_L can be viewed as the spatially averaged attenuation coefficient for waves propagating in a pipe of a finite length L. Note that γ_L is a spatially averaged attenuation coefficient; the true attenuation of the waves in a typical realization of the medium is not necessarily constant; i.e. when a wave propagates through the pipe its amplitude may fluctuate and thus even grow in certain regions. Only on average the wave attenuates with an attenuation coefficient γ_L. This implies that the reciprocal of γ_L should not be considered as a penetration depth; due to the growth of the wave amplitudes in certain regions the wave energy may penetrate much deeper into the medium than one would expect based on the value of $1/\gamma_L$. Moreover, γ_L is a stochastic variable which means that all realizations of the medium yield a different value of γ_L. However, its variance reduces with increasing length of the pipe L, so for a pipe of infinite length the variance tends to zero and, hence, the spatially averaged attenuation coefficient has the same value for all realizations. The ensemble averaged Lyapunov exponent $\langle \gamma_L \rangle$ may be regarded as the spatially averaged attenuation coefficient of the ensemble averaged waves. For a clear example of a random system where the statistics of the amplitude fluctuations are calculated analytically, the reader is referred to Scott (1985).

† In these systems the medium is homogeneous but contains randomly located scatterers.

An appropriate length scale of the amplitude fluctuations is the localization length of the system which is defined as the reciprocal of the limiting value of γ_L, the Lyapunov exponent γ,

$$L_{\mathrm{loc}} = 1/\gamma. \tag{7.7}$$

The localization length of the wave energy is half this value.

For a perfectly ordered periodic system of infinite length the Lyapunov exponent γ is given by the imaginary part of the Bloch wavenumber, $\gamma = |\mathrm{Im}\kappa|$ (see equation 6.31), which is constant. This means that waves of frequencies in the stop bands truly attenuate exponentially and that here the localization length may be regarded as the penetration depth. In random systems all frequencies attenuate, but one can consider a system of length L only as truly opaque for these waves when $L_{\mathrm{loc}} \ll L$.

7.3.2 Single parameter scaling

A great discovery (Anderson, Thouless, Abrahams and Fisher, 1980) is that in homogeneous random media for certain conditions, the probability distribution of γ_L is Gaussian, and that its moments all depend on one single parameter only, namely the Lyapunov exponent γ. In particular one has

$$\mathrm{Var}\,\gamma_L = \langle\gamma_L\rangle / L. \tag{7.8}$$

This relation is known as the single parameter scaling (SPS) (Deych, Yamilov and Lisyanski, 2001).

The propagation of classical waves in one-dimensional disordered waveguides that are *periodic on average* has also attracted considerable attention (e.g. McGurn, Christensen, Mueller and Maradudin, 1993; Nishiguchi, Tamura and Nori, 1993a; Freilikher, Lianski, Yurkevich, Maradudin and McGurn, 1995; Langley, 1995; Deych, Zaslavsky and Lisyanski, 1997; Luan and Ye, 2001a) One of the interests is to what extent the statistical properties of the waves resemble those of classical waves in one-dimensional random homogeneous systems; in particular, for which conditions single parameter scaling, as expressed by equation 7.8, also applies here (Deych, Lisyanski and Altshuler, 2000).

Let us proceed by interpreting the data of figure 7.1 in terms of the Lyapunov exponent γ_L as defined above and discuss the statistical properties of sound transmission in random oil-water slug flows following the illuminating paper of Deych, Zaslavsky and Lisyanski (1998). This paper is concerned with scalar waves in a superlattice with properties such that, in our notation, $\zeta = 1.004$ and $\nu = 0.477$, so very close to those of a Goupillaud medium where $\nu = 1/2$.

Figure 7.3 (left) exemplifies again the break-up of the band structure of the periodic system as given by the table in section 6.3. The ‘peaks’ of the Lyapunov exponent correspond to the band gaps of the periodic system, whereas the valleys correspond

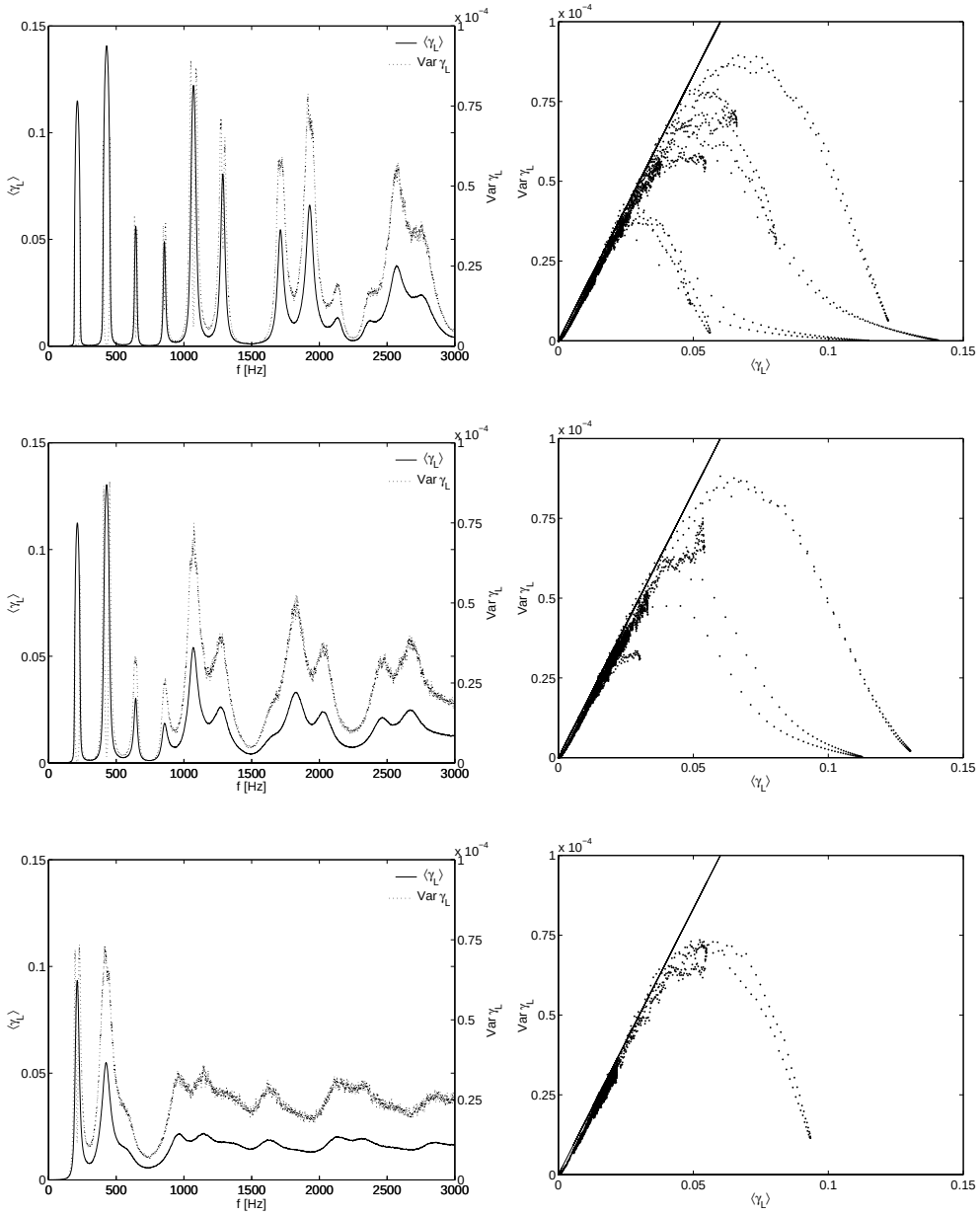

FIGURE 7.3: *Ensemble average over* 1500 *realizations of the Lyapunov exponent for the system of figure 7.1 with* $N = 400$*. Left: the Lyapunov exponent and its variance varying with the frequency;* $\delta = 0.05$ *(top),* $\delta = 0.1$ *(middle),* $\delta = 0.25$ *(bottom). Right: the variance plotted against the mean (dots) and the variance as given by the single parameter scaling (solid);* $\delta = 0.05$ *(top),* $\delta = 0.1$ *(middle),* $\delta = 0.25$ *(bottom).*

to the pass bands. As the randomness increases it destroys more and more the interference pattern of the perfectly ordered periodic system. The result is that the height of the peaks diminishes, which implies that the localization lengths of frequencies in the stop bands increase, or in other words, the system becomes less opaque for these frequencies. The valleys on the other hand are found at greater heights, so that the localization length for frequencies in the pass bands becomes less, for these frequencies the system becomes less transparent. As the randomness increases there is a growing range of frequencies, expanding towards the lower frequencies, for which there is no clear distinction between pass bands and stop bands anymore. For these frequencies the medium has no 'underlying' periodicity; i.e. the medium can be considered as fully random. That implies that the value of the Lyapunov exponent for this range of frequencies is determined only by the 'microstructure' of the system; i.e. the values of ζ (here 1.1) and ν (here 2/7). Moreover, figure 7.3 (left) shows that this value of $\langle\gamma_L\rangle$, which is nearly independent of the frequency, is approximately $0.02\,\mathrm{m}^{-1}$, so that the localization length of the wave energy is $L_{\mathrm{loc}} \approx 25\,\mathrm{m}$; much less than the length of the system ($600\,\mathrm{m}$).

Figure 7.3 (left) also shows graphs of the variance of the Lyapunov exponent as a function of frequency for the same systems. Upon comparing the two figures it appears that already at low values of the randomness for most frequencies single parameter scaling applies, i.e. the Lyapunov exponent and its variance are related by equation 7.8. This is confirmed by figure 7.3 (right) where for the entire frequency range the variance of the Lyapunov exponent is plotted against the Lyapunov exponent itself. Most of the points coincide with the straight line as given by equation 7.8. The graphs in figure 7.3 (right) also show multi-branched structures which imply a violation of single parameter scaling for certain frequencies. Inspection shows that the different branches originate from frequencies belonging to different band gaps of the original periodic system. In these band gaps the variance exhibits a doubly peaked structure. The double lines which form each of the branches correspond to different halves of the same band gap, precisely as was found by Deych et al. (1998). As the randomness increases the band structure is broken up, especially at the higher frequencies. Figure 7.3 shows that the double peaks and the corresponding multi-branches disappear and that for an increasing range of frequencies single parameter scaling is applicable.

7.3.3 Transition from periodic to fully random

In order to answer the question for which precise conditions single parameter scaling applies, it is illuminating (Deych et al., 1998) to look at the behavior of the Lyapunov exponent for frequencies within a band gap as the randomness is increased. For this the band gap at $1071\,\mathrm{Hz}$ between $1042\,\mathrm{Hz}$ and $1100\,\mathrm{Hz}$ is considered. The upper two graphs in figure 7.4 (left) show the dependence of the Lyapunov exponent upon the randomness δ for frequencies that belong to a pass band; here the band between

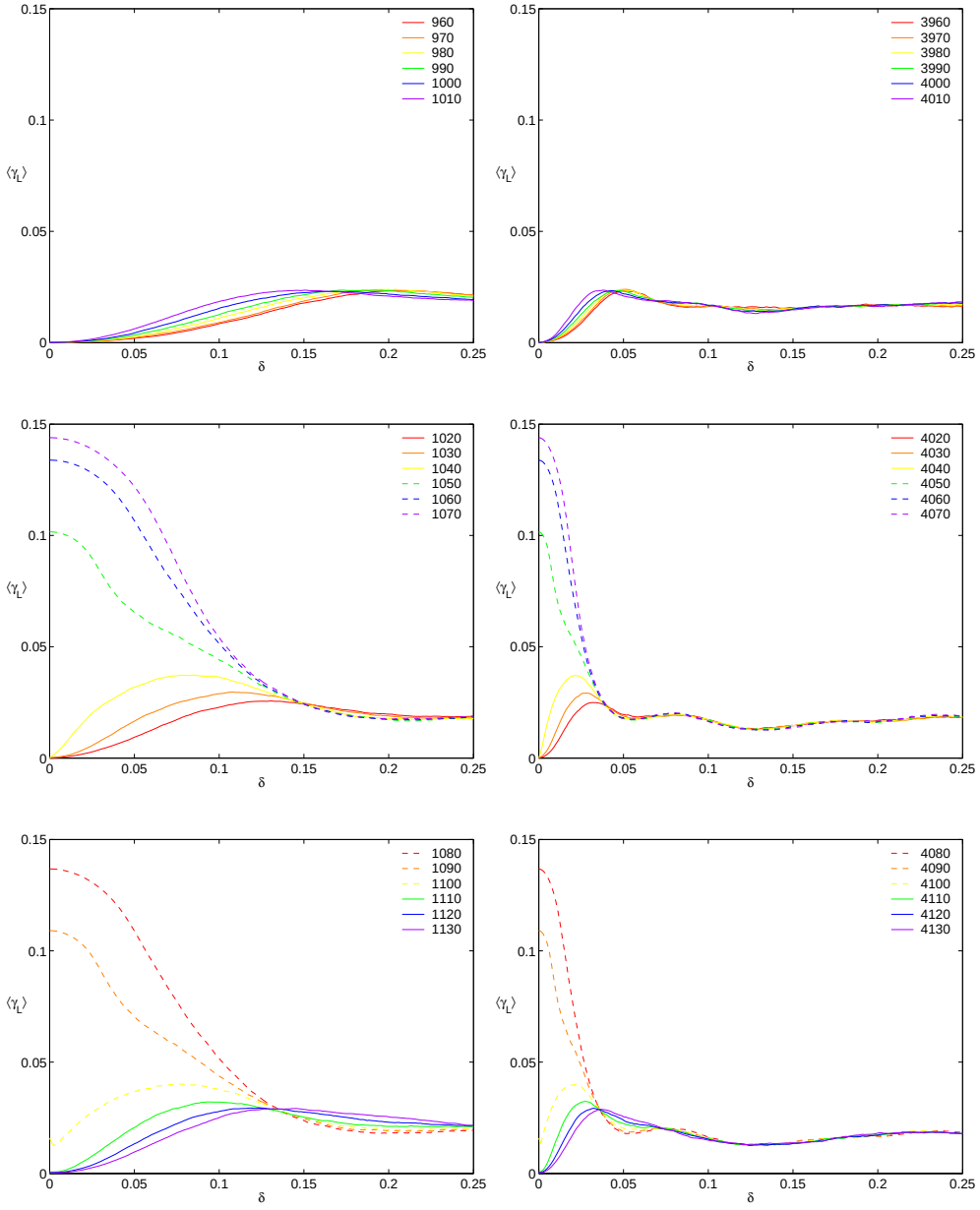

FIGURE 7.4: *Lyapunov exponent plotted as a function of the randomness δ for the system of figure 7.1 with $N = 400$, ensemble average over 400 realizations. Left: for frequencies near the gap at $f = 1071\,\mathrm{Hz}$. Right: for frequencies near the gap at $f = 4071\,\mathrm{Hz}$. The dashed lines indicate that the particular frequencies belong to the stop band.*

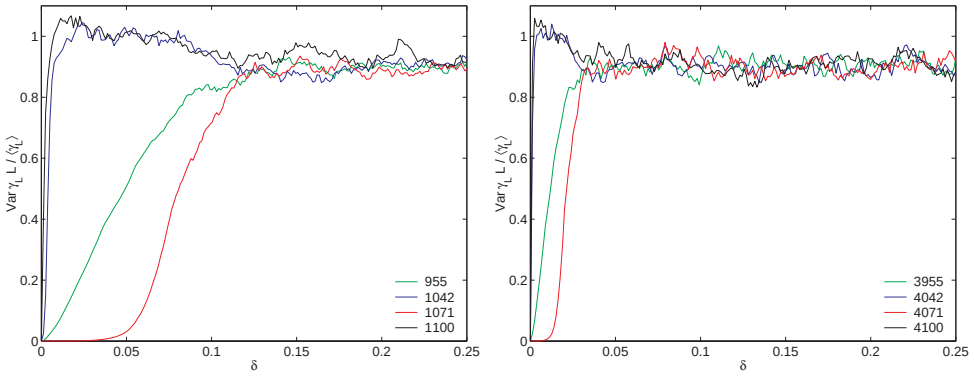

FIGURE 7.5: *The value of* $\mathrm{Var}\,\gamma_L L/\langle\gamma_L\rangle$ *plotted as a function of the randomness* δ *for the system of figure 7.1 with* $N = 400$*, ensemble average over 3000 realizations. The four frequencies in each graph correspond to the center of a pass band, the first gap boundary, the center of the gap and the second gap boundary. Left: for frequencies around and in the gap at* $f = 1071\,\mathrm{Hz}$*. Right: for frequencies around and in the gap at* $f = 4071\,\mathrm{Hz}$*.*

$869\,\mathrm{Hz}$ and $1042\,\mathrm{Hz}$. The Lyapunov exponent has a universal behavior, which for $\delta \to 0$ is given by $\langle\gamma_L\rangle \propto \delta^2$. The middle graph of figure 7.4 (left) shows that significant changes in the shape of the function $\langle\gamma_L(\delta)\rangle$ occur when the frequency is increased from the pass band to the center frequency of the stop band ($1071\,\mathrm{Hz}$). For frequencies at the edges of the pass band ($1042\,\mathrm{Hz}$ and $1100\,\mathrm{Hz}$) $\langle\gamma_L\rangle \propto \delta^{2/3}$, as $\delta \to 0$, but for frequencies in the band gap the Lyapunov exponent approaches a nonzero value as $\delta \to 0$. The localization length decreases towards the center of the band gap. The bottom graph in figure 7.4 (left) shows a similar behavior of the Lyapunov exponent as the frequency increases through the right half of the band gap.

Universal behavior for all frequencies around and in the gap is lost for low values of the randomness, indicating violation of the single parameter scaling, but is restored above a critical value which is estimated as $\delta_{\mathrm{crit.}} \approx 0.14$. For comparison the behavior of the function $\langle\gamma_L(\delta)\rangle$ in the band gap between $4042\,\mathrm{Hz}$ and $4100\,\mathrm{Hz}$ is shown in figure 7.4 (right). A similar qualitative change occurs, but here the universality is restored at a much lower critical value of the randomness, $\delta_{\mathrm{crit.}} \approx 0.04$. The validity of the single parameter scaling is presented in figure 7.5 for the two cases. In the figure the function $\mathrm{Var}\,\gamma_L L/\langle\gamma_L\rangle$ is plotted against δ. A value of one indicates full single parameter scaling according to equation 7.8. The graphs show that all curves tend to a constant value of about 0.9, thus smaller than the expected value of one. The reason for this difference is not clear, but has probably a numerical origin. The two frequencies in each graph that correspond to the band edges (blue and black) exhibit single parameter scaling, even for very low values of δ. The center of the gap (red) and the center of the pass band (green) demonstrate single parameter scaling when the randomness is larger than the critical randomness.

The critical randomness may be explained by the randomization of the phases of the waves. Within a section i the amplitude of the upstream and the downstream running waves remains constant while their phases change with $\pm\omega\tau_i$. This leads to an interference pattern like the band structure as observed for perfectly periodic flows. Varying the length of a section with $\tilde{\delta}\langle l_i\rangle$ leads to a relative phase shift between the two waves of $2\omega\tilde{\delta}\langle\tau_i\rangle$. Upon recalling that the random variations $\tilde{\delta}$ are randomly chosen numbers from the interval $[-\delta,\delta]$ with a uniform probability distribution, the relative phase shift covers the *full* range $[0,2\pi]$ if $2\omega 2\delta\langle\tau_i\rangle = 2\pi$ and becomes thus completely random. The relation expresses the 'full randomization randomness' in terms of the frequency and the mean transit time $\langle\tau_i\rangle$.

Since the system contains water and oil sections one may define the 'full randomization randomness' δ_{rnd} as

$$\delta_{\mathrm{rnd}} = \frac{1}{4f}\min\left[\langle\tau_o\rangle^{-1},\langle\tau_w\rangle^{-1}\right]. \tag{7.9}$$

For the example above for $f = 1071\,\mathrm{Hz}$ and $f = 4071\,\mathrm{Hz}$ δ_{rnd} takes the values $\delta_{\mathrm{rnd}} = 0.14$ and $\delta_{\mathrm{rnd}} = 0.037$, respectively. These values agree well with the critical randomness as found in figures 7.4 and 7.5 which suggests that $\delta_{\mathrm{crit.}}$ and δ_{rnd} yield the same values, at least for this system. It is noted that these values correspond to the oil sections. Since the centers of the pass bands and the stop bands are the result of the extremes of constructive and destructive interference the randomness has to be larger than δ_{rnd} to overcome the underlying periodicity of the medium. At the band edges small values of δ are already sufficient. This can clearly be observed in figure 7.5.

Instead of relating δ_{rnd} to a certain given frequency, equation 7.9 also provides the lowest frequency for which the phases of the waves can be fully randomized. The limiting value of δ is 1 since larger values would yield negative section lengths. Then according to equation 7.9 the associated frequency for the system above then becomes $f = 150\,\mathrm{Hz}$, which is located in the first pass band and is thus smaller than the frequencies of the first band gap. Therefore the band gaps will be absent at this maximum randomness. In this first pass band the system does not necessarily exhibit single parameter scaling.

Moreover, when for some given randomness the phases of the waves are fully random then for even higher frequencies the probability distribution of the phases becomes uniform irrespective of the probability distribution of the section length variations $\tilde{\delta}$ (as long as the distribution is reasonably smooth). A further increase of the frequency does not affect the statistics of the interference anymore. Hence, the Lyapunov exponent tends to a constant in the high frequency limit.

It is perhaps worth mentioning that Luan and Ye (2001a),(2001b) have studied whether single parameter scaling applies in their 'water duct filled with many air blocks'. For their system ν and ζ have the extreme values of $\nu = 4.4\,10^{-4}$ and

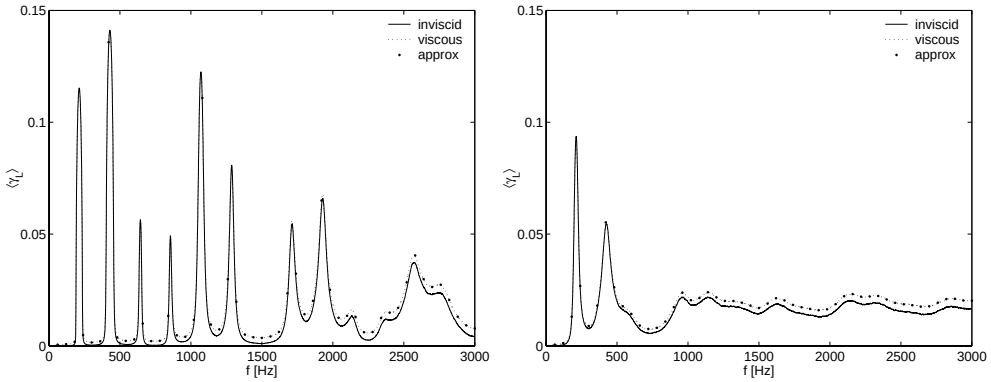

FIGURE 7.6: *Ensemble average over 1500 realizations of the Lyapunov exponents varying with the frequency for the system of figure 7.2. The solid and the dotted lines denote the inviscid and the viscous Lyapunov exponents, respectively, and the larger dots the approximation equation 7.11;* $\delta = 0.05$ *(left),* $\delta = 0.25$ *(right).*

$\zeta = 1697$. They keep the length of the air blocks constant, but vary the length of the water sections up to a randomness of $\delta = 1.0$. They observe large deviations from single parameter scaling as expressed by equation 7.8. Also, they observe that for high values of the randomness ($\delta > 0.3$) the variance of the Lyapunov exponent is approximately constant above a certain frequency (as our simulations showed as well), but that the Lyapunov exponent itself is not, or perhaps above a much higher frequency.

7.3.4 Effects of dissipation

In the above analysis the effects of dissipation have been ignored. There is no question that the scattering process is affected by dissipative attenuation (see e.g. Deych et al., 2001).

As explained in section 3.3 dissipation can be included by modifying the effective density of the medium, see equation 3.34. In the case of single phase sections as for the system above, the dominant contribution comes from frictional attenuation at the pipe wall, which can be incorporated easily by replacing the two different wave speeds c_i and the impedances Z_i by

$$c_i \left[1 - \frac{4}{D}\sqrt{\frac{\mathrm{i}\nu_i}{\omega}}\right]^{\frac{1}{2}} \quad \text{and} \quad Z_i \left[1 - \frac{4}{D}\sqrt{\frac{\mathrm{i}\nu_i}{\omega}}\right]^{-\frac{1}{2}}, \tag{7.10}$$

respectively, where D is the diameter of the pipe and ν_i the kinematic viscosity of phase i.

In order to find a simple relation that includes the effects of dissipation one can follow the often employed line of reasoning which considers wave attenuation due to

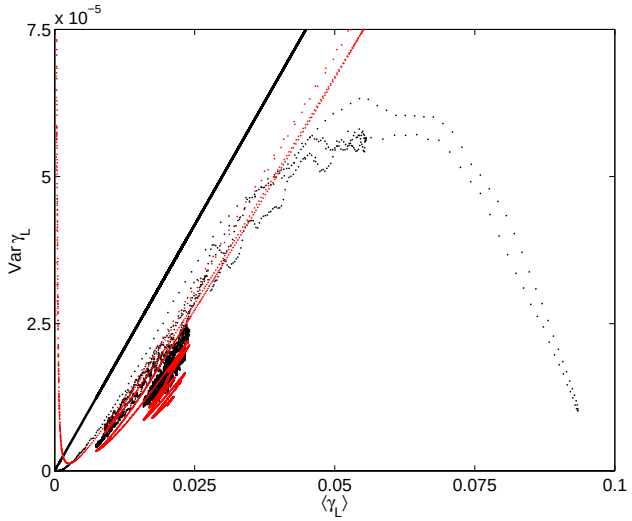

FIGURE 7.7: *Variance of the Lyapunov exponent varying with the mean value (black dots) for the system of figure 7.6 (right). The black line and the red dots denotes the variance as given by regular and the modified single parameter scaling.*

multiple scattering and due to dissipation as independent processes. This implies that the Lyapunov exponent for the dissipative system may be approximated by adding the Lyapunov exponent of the inviscid system and the attenuation coefficient resulting from wall friction, γ_{wf},

$$\gamma_{L,\mathrm{vis}} = \gamma_L + \gamma_{\mathrm{wf}}. \tag{7.11}$$

The attenuation coefficient due to wall friction in section i can be taken as, see equation 3.46,

$$\gamma_{\mathrm{wf},i} = \frac{\sqrt{2\nu_i\omega}}{Dc_i}, \tag{7.12}$$

and for the entire system as

$$\gamma_{\mathrm{wf}} = \frac{l_1\gamma_{\mathrm{wf},1} + l_2\gamma_{\mathrm{wf},2}}{l_1 + l_2}. \tag{7.13}$$

For the example of figure 7.2 the kinematic viscosities of water and of oil are taken as $\nu_{\mathrm{w}} = 1\cdot10^{-6}\mathrm{m}^2\mathrm{s}^{-1}$ and $\nu_{\mathrm{o}} = 9\cdot10^{-6}\mathrm{m}^2\mathrm{s}^{-1}$, respectively. The diameter of the pipe is $D = 0.1\mathrm{m}$. Figure 7.6 presents the Lyapunov exponent for the inviscid and the viscous system including the approximation given by equation 7.11. It is clearly visible that the approximation agrees very well with the full calculation. The major effect of dissipation occurs in the pass bands of the system with the small randomness, see figure 7.6 (left). Here the dissipation dominates the effects of multiple

scattering while multiple scattering dominates the acoustics in the band gaps and at higher degrees of randomness, see figure 7.6 (right).

In figure 7.7 the variance of the Lyapunov exponent (black dots) is plotted against the mean value for the system of figure 7.6 (right). It is clear that the variance is smaller than the value that the single parameter scaling yields as given by the black line. Still, Deych et al. (2001) mention a correction to the regular single parameter scaling of the form

$$\Gamma = \mathrm{Var}\,\gamma_L L / \langle \gamma_L \rangle \,, \tag{7.14}$$

which reduces to the regular single parameter scaling if $\Gamma = 1$. When the attenuation coefficient due the wall friction (or another cause of dissipation) is much smaller than the Lyapunov exponent, $\eta = \gamma_{\mathrm{wf}}/\gamma_L \ll 1$, then the correction is given by

$$\Gamma = 1 - 2\eta \log(1/\eta). \tag{7.15}$$

The red dots in the figure denote the values of the variance as given by the modified single parameter scaling. The figure shows that it agrees reasonably well with the results of the full calculation given by the black dots.

7.4 Energy distribution in the pipe

Instead of analyzing the statistics of the transmitted waves and the Lyapunov exponent as a characteristic exponent of the decay and growth of the waves in the waveguide we will proceed by describing some remarkable results concerning the sound intensity $|p|^2/Z$ in the system, in particular the occurrence of Anderson localization. Anderson localization means that the amplitudes of the waves do not decay exponentially with the Lyapunov exponent as decay rate, but also grow at certain locations.

For the same system as above the energy distribution in the pipe will be presented for three different frequencies, one is the center of a pass band, $955\,\mathrm{Hz}$, one is the center of a stop band, $f = 1071\,\mathrm{Hz}$, and the third one is the band edge at $f = 1042\,\mathrm{Hz}$. It is recalled that the localization length of the energy, $L_{\mathrm{loc,en}}$ is half the value of the localization length as given by equation 7.7, thus $L_{\mathrm{loc,en}} = 1/(2\gamma)$.

Figure 7.8 (left) presents the energy distribution for the band edge. When the randomness is small, $\delta = 0.05$, (top) Anderson localization is clearly present in the form of three peaks. The lengths in which the peaks grow and decay is, indeed, roughly the same as the localization length of $L_{\mathrm{loc,en}} = 13.5\,\mathrm{m}$. When the randomness increases to $\delta = 0.1$ only one main peak remains close to the source. Also here the length scale in which the peak grows and decays is roughly the localization length of $L_{\mathrm{loc,en}} = 12.4\,\mathrm{m}$, close to the value given above.

As mentioned earlier, the localization length should not be confused with the penetration depth, as the figure clearly shows. Although the localization lengths of the two systems are about the same, in the upper graph the energy penetrates roughly $150\,\mathrm{m}$ into the medium in contrast to the penetration depth of $50\,\mathrm{m}$ in the bottom graph.

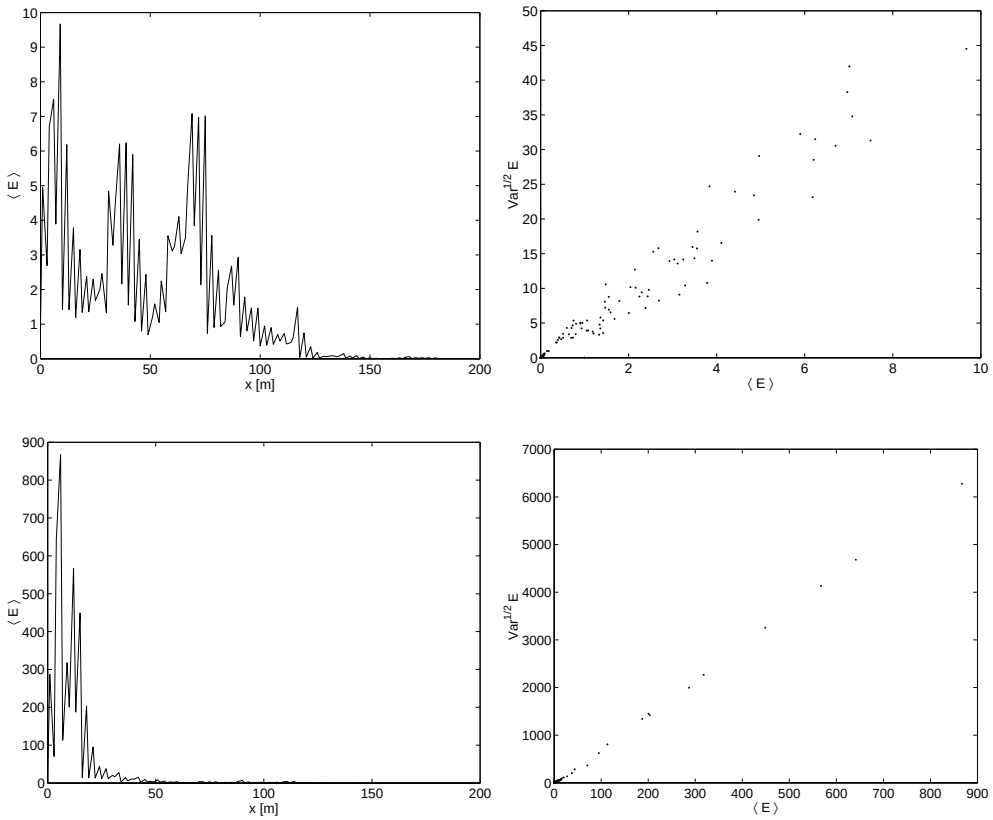

FIGURE 7.8: *Ensemble average over* 10^5 *realizations of the distribution of the sound intensity versus the distance from the source (left). In the graphs at the right the standard deviation is plotted against the mean. The frequency is* $f = 1042\,\mathrm{Hz}$ *which corresponds to a band edge. Top:* $\delta = 0.05$*,* $L_{\mathrm{loc,en}} = 13.5\,\mathrm{m}$*,* $C = 4.680$*; Bottom:* $\delta = 0.1$*,* $L_{\mathrm{loc,en}} = 12.4\,\mathrm{m}$*,* $C = 7.221$*.*

In the graphs at the right-hand side of the figure the standard deviation, being the square root of the variance, is plotted against the mean. In the top graph where the randomness is small, a linear relationship between the standard deviation and the mean is apparent, although the scatter is somewhat large. This changes as the randomness is increased to $\delta = 0.1$, as in the bottom graph where a very clear linear relationship between the two can be observed. This remarkable universality can be expressed as

$$\mathrm{Var}\,\tfrac{1}{2}|p|^2/Z] = C\ \left\langle |p|^2/Z \right\rangle \tag{7.16}$$

where C is a constant which is estimated as $C = 7.221$ by means of the linear least squares method.

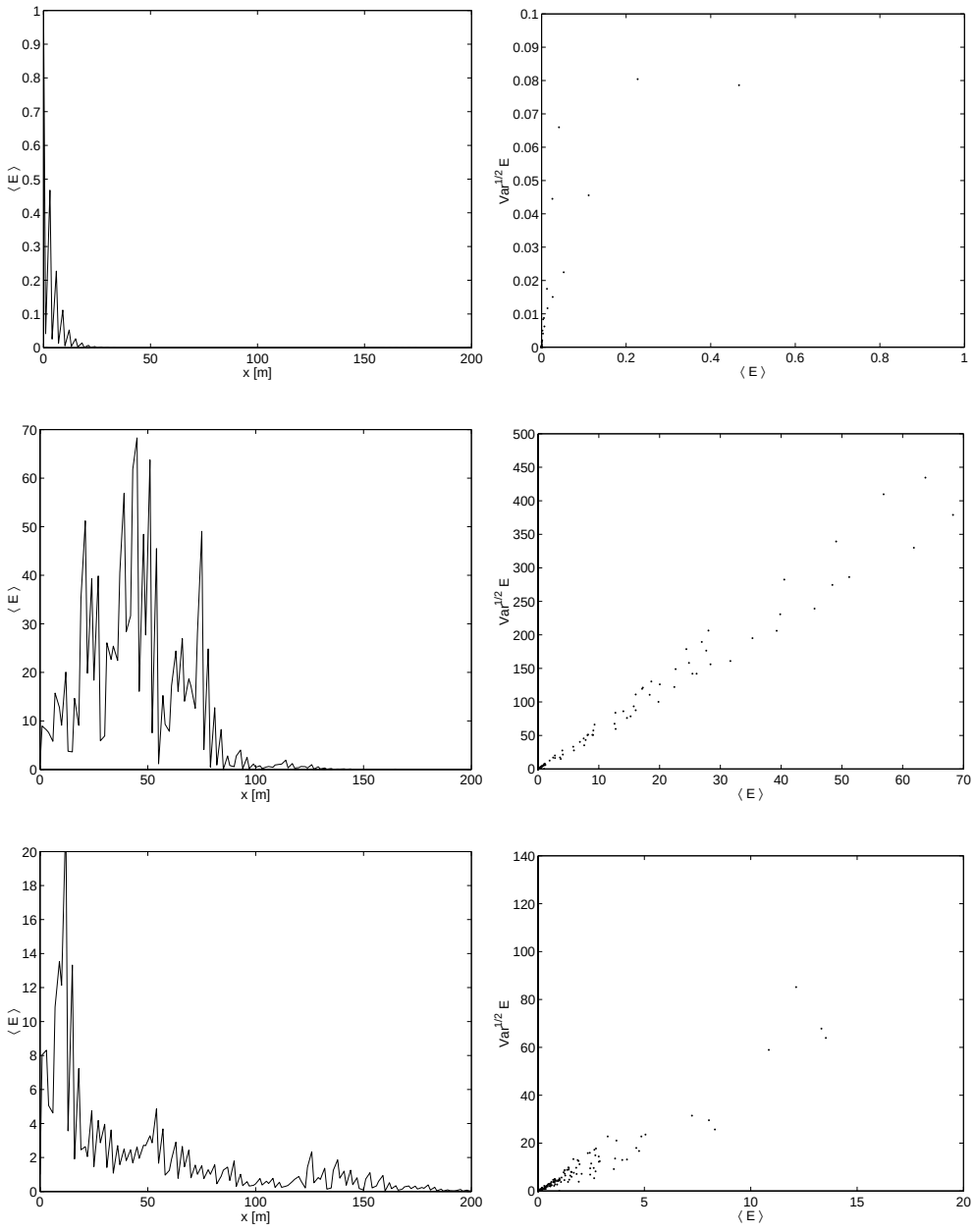

FIGURE 7.9: *Ensemble average over* 10^5 *realizations of the distribution of the sound intensity versus the distance from the source (left). In the graphs at the right the standard deviation is plotted against the mean. The frequency is* $f = 1071\,\mathrm{Hz}$ *which is the center of a stop band. Top:* $\delta = 0.05$*,* $L_{\mathrm{loc,en}} = 4.08\,\mathrm{m}$*,* $C = 0.076$*; Middle:* $\delta = 0.1$*,* $L_{\mathrm{loc,en}} = 9.12\,\mathrm{m}$*,* $C = 6.050$*; Bottom:* $\delta = 0.25$*,* $L_{\mathrm{loc,en}} = 26.7\,\mathrm{m}$*,* $C = 5.51$*.*

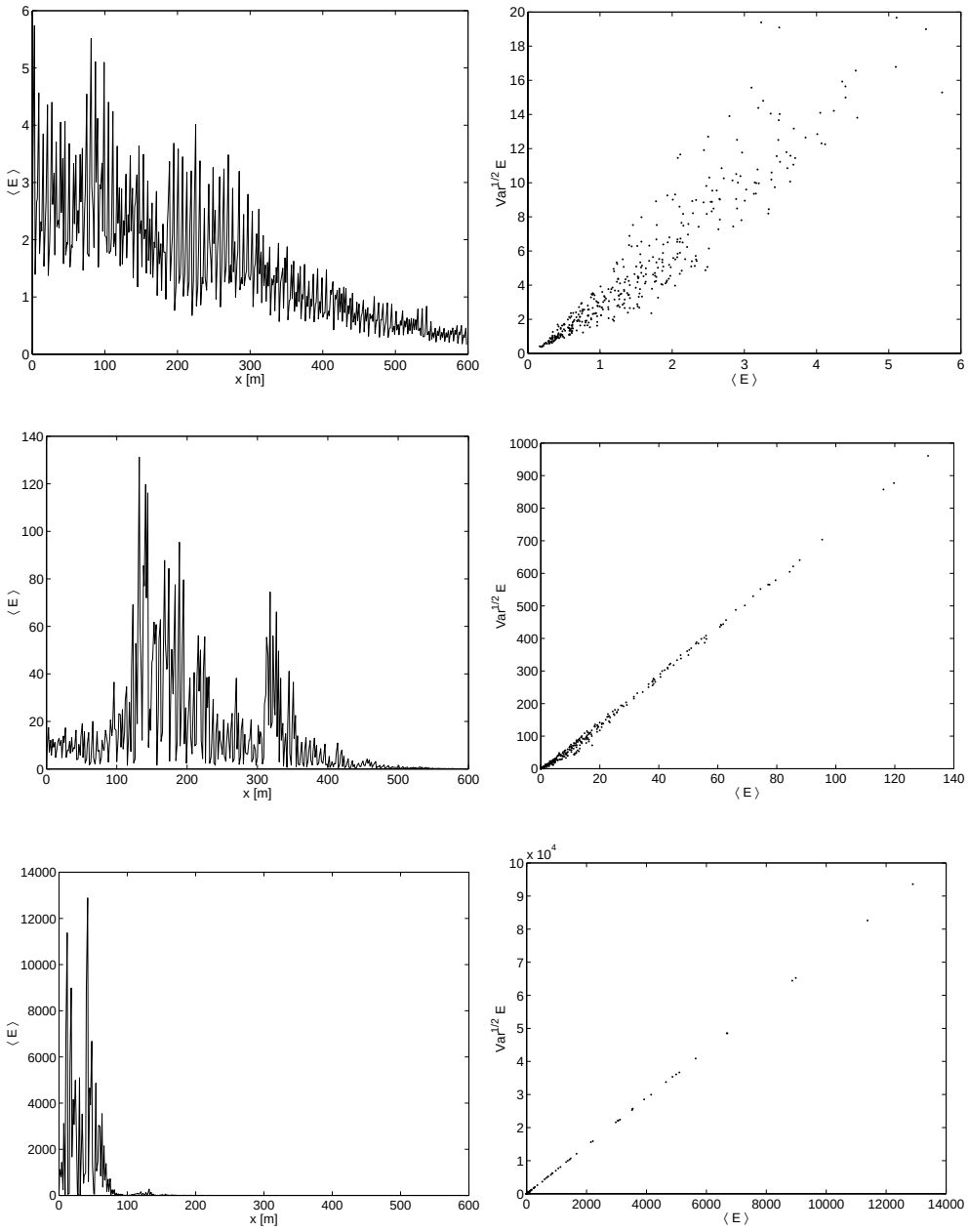

FIGURE 7.10: *Ensemble average over* 10^5 *realizations of the distribution of the sound intensity versus the distance from the source (left). In the graphs at the right the standard deviation is plotted against the mean. The frequency is* $f = 955\,\mathrm{Hz}$ *which is the center of a pass band. Top:* $\delta = 0.05$, $L_{\mathrm{loc,en}} = 219.2\,\mathrm{m}$, $C = 3.257$*; Middle:* $\delta = 0.1$, $L_{\mathrm{loc,en}} = 60.2\,\mathrm{m}$, $C = 7.132$*; Bottom:* $\delta = 0.25$, $L_{\mathrm{loc,en}} = 24.2\,\mathrm{m}$, $C = 7.25$.

For the upper graph the value of C is estimated in the same way as $C = 4.680$. As far as we are aware, discussions on this phenomenon have not been given in literature. Moreover, these values of C demonstrate that the standard deviation is larger than the mean value, which implies that many realizations of the medium result in sound fields that are far from the mean field, or, that the sound fields of few realizations extremely differ from the mean field.

Figure 7.9 shows the same graphs but now for $f = 1071\,\mathrm{Hz}$, a frequency from a stop band. The upper graph of figure 7.9 (left) gives an example of the strong decay of the sound intensity with distance for small values of the randomness $\delta = 0.05$ ($L_{\mathrm{loc,en}} = 4.08\,\mathrm{m}$), while the middle graph of the figure again shows that at a higher value of the randomness, $\delta = 0.1$, more sound energy is found deeper into the medium. The larger randomness increases the localization length up to $L_{\mathrm{loc,en}} = 9.12\,\mathrm{m}$, and again much of the sound energy is found at larger distances from the source. The bottom graph where $\delta = 0.25$ and $L_{\mathrm{loc,en}} = 26.7\,\mathrm{m}$ shows that also here the energy is confined in a region more close to the source. The required randomness is, however, larger than at the band edge. This is in agreement with the break-up of the band structure which is established at a much lower randomness at the band edges than in the gaps or the pass bands.

The middle and the bottom graphs in figure 7.9 (right) suggest that the linear relation between the standard deviation and the mean may be established as the randomness becomes larger. In these graphs there is still considerable scatter, but the mean squares method gives the values $C = 6.050$ and $C = 5.51$, respectively.

Figure 7.10 presents the same graphs but now for a frequency of $f = 955\,\mathrm{Hz}$. The upper left graph demonstrates weak localization, which occurs when the pipe is longer than the localization length of $L_{\mathrm{loc,en}} = 219.2\,\mathrm{m}$ but too short to allow for a sufficient attenuation of the waves. In the middle plot where $\delta = 0.1$ and $L_{\mathrm{loc,en}} = 60.2\,\mathrm{m}$ the strong form of Anderson localization is restored. In the graph at the bottom the energy is again more confined to the left of the pipe whereas the localization length, $L_{\mathrm{loc,en}} = 24.2\,\mathrm{m}$, is close to its value for the stop band with $\delta = 0.25$. The linear relation between the standard deviation and the mean is, as at the band edge, established from $\delta = 0.1$. The corresponding values of C are for $\delta = 0.1$ and $\delta = 0.25$ equal to $C = 7.132$ and $C = 7.25$, respectively.

7.5 Discussion

The band structure of the transmission coefficient of periodic flows is broken up when the lengths of the sections are varied at random. In particular at high frequencies the flow becomes less transparent when the degree of randomness or the length of the pipe increases. Because of the randomness of the medium also the corresponding transmission coefficient is a stochastic quantity. Graphs of the variance of its proba-

bility distribution plotted against the mean exhibit a universal structure.

A prominent quantity of interest in the statistics of the sound transmission is the logarithmic decrement of the transmission coefficient, the Lyapunov exponent γ_L associated with a system of finite length. When the length of the pipe tends to infinity its value converges to the true Lyapunov exponent. The fact that the Lyapunov exponent is the logarithmic decrement of the transmission coefficient suggests that its reciprocal, the localization length, is a measure for the penetration depth of the medium. This is not the case. Only on spatial average the waves attenuate with an attenuation coefficient γ_L. Locally in the pipe the wave amplitudes may increase and decrease and as a result the waves may penetrate much deeper into the medium than one would expect based on the value of γ_L.

For certain conditions the statistics of the Lyapunov exponent γ_L show a remarkable relation; the probability distribution is Gaussian while the associated variance and thus all the higher moments are related to the mean value. This relation is called the single parameter scaling.

The single parameter scaling was found to apply to certain homogeneous systems containing randomly located scatterers. However, for certain conditions it also applies to random media that are periodic on average. The considered example suggests a sufficient condition. That is the difference between the phases of the upstream and downstream propagating waves must be fully random. This leads to a simple relation that expresses the 'randomization randomness' δ_{rnd} in terms of the frequency and the mean transit times. When the randomness δ is larger than δ_{rnd} the medium overcomes its periodicity and becomes completely random, then the single parameter scaling applies. This condition is too restrictive for most frequencies; at the band edges a randomness that is much smaller than δ_{rnd} already yields single parameter scaling.

Graphs of the energy distribution in the pipe make clear that the localization length should not be confused with the penetration depth. The energy indeed remains confined to the source, but does not attenuate exponentially with respect to the distance to the source. Instead, the energy alternately grows and decreases at certain locations in the pipe and as a result, peaks are formed. This phenomenon is called Anderson localization.

Moreover, also the energy distribution shows remarkable statistics. For a sufficiently large randomness the standard deviation is proportional to the mean. The standard deviation is found to be much larger than the mean value. This implies that it is questionable whether extracting information about these flows from recordings of the sound waves is possible.

DISCUSSION

CHAPTER 8

8.1 Summarizing conclusion

Acoustic signals that are recorded in oil pipelines contain information about the flow and the well. In order to extract this information from the pressure recordings, detailed knowledge about the transmission properties of sound waves in the pipes is required.

The flows in the pipelines of interest basically consist of oil and water, but sometimes also small gas bubbles or even sand may be present. The flows appear in a rich variety of flow patterns such as dispersions of the one phase into the other, stratified configurations where oil flows on top of a layer of water, possibly with a wavy interface, or flows of large oil bubbles in water. In addition, combinations of these patterns occur. These flow configurations have different acoustic properties.

The signals that have been recorded so far suggest the presence of sound waves in the frequency range $200-2000\,\mathrm{Hz}$, which warrants to restrict attention to longitudinal waves (i.e. the fundamental mode) only, as long as the frequencies in this range are below the smallest cutoff frequency.

The cutoff frequency for a single phase flow of pure oil in a pipe with a diameter of $0.1\,\mathrm{m}$ is about $7000\,\mathrm{Hz}$, which indicates that indeed the condition is satisfied. The smallest cutoff frequency as that of a single phase flow is hardly affected by medium inhomogeneities when the flow consists of oil and water, two fluids with similar acoustic properties. This is not the case for gas-water flows, where the smallest cutoff frequencies are often higher than what one would expect based on the values for single phase flows. In gas-water flows it is the gas that actually forms the waveguide, unless the volume fraction of the gas is small. In addition, the fundamental mode is hardly dispersive for oil-water systems and for gas-liquid systems as long as the frequency is smaller than, roughly, a few times the smallest cutoff frequency; i.e. the speed of sound is almost independent of the frequency.

The propagation properties of longitudinal sound waves in well-separated and in dispersed two-phase flows in pipes were considered in Chapter 3. Expressions were derived for the speed of sound and the impedance of these two-phase flows whose

composition does not vary with axial position along the pipe. The derived relations suggest that the acoustic properties of oil-water flows for the two considered configurations are almost the same. This is not the case for gas-water systems; the speed of sound in gas-liquid dispersions drops to values even below the sound speed of the pure fluids, whereas in stratified flows the sound speed is very close to that of the gas, except for very large volume fractions of water.

Non-equilibrium effects due to viscous friction near the wall and relaxation mechanisms in dispersions result mainly in the dissipation of sound; the speed of sound and the impedance as in the equilibrium situation are hardly affected. The attenuation length due to wall friction is for the analyzed systems at $1000\,\mathrm{Hz}$ about $700 - 1400\,\mathrm{m}$ in oil-water flows while the theory provides values in the range $10 - 1000\,\mathrm{m}$ for gas-water systems. It is noted that friction at the interfaces between the phases was neglected. This is justified for oil-water systems but not for gas-liquid flows where the induced velocities in the two phases differ considerably. In order to calculate the attenuation in dispersions the theory of Epstein and Carhart (1953) and Allegra and Hawley (1972) was employed. At $1000\,\mathrm{Hz}$ the attenuation length was found to be in the range $500 - 1000\,\mathrm{m}$ for dispersions of 10% kerosene in water and only slightly smaller for dispersions of 10% water in kerosene for drop sizes of $0.2 - 2\,\mathrm{mm}$.

In Chapter 5 two methods were presented that describe the acoustics of longitudinal acoustic waves in pipe flows whose composition varies with axial position in the pipe. In the first method reflections of waves are neglected and the energy flux is assumed to remain constant. This method fails when the impedance fluctuations are substantial within a wavelength of the sound waves. Moreover, many negligibly small impedance fluctuations may add up to substantial reflections when the pipe is long enough. In these two cases reflections cannot be ignored.

The second method presented is the transfer-matrix method, which may be employed to calculate the acoustics of basically all phase distributions. In this method the medium is regarded as stepwise varying. The medium in each section may be single phase, well-separated or dispersed. The required effective properties, the speed of sound and the impedance, of these sections are given in Chapter 3. In addition, the transfer-matrix method is generic so also other compositions of the sections may be employed as long as they do not vary appreciably with axial position in the pipe and, obviously, the speed of sound and the impedance are known. The resulting transfer matrices express the wave amplitudes in one section to those in neighboring sections. The complete field may be computed by first determining the effective reflection coefficients of all layers and then the effective transmission coefficients through a recurrence relation. Furthermore, the Green function for this stepwise varying medium was derived. This revealed that the medium upstream, say, is fully characterized by the effective reflection coefficient at the first interface upstream and only affects the (complex) amplitude of the sound field downstream.

The transfer-matrix method has been employed to calculate periodic flows as idealized flows of large oil bubbles in water, gas-liquid slug flows and stratified flows with a wavy interface. One period of these periodic flows was represented by a slug unit or a stratified wavy unit. The corresponding transfer matrices for the units were derived by means of the transfer-matrix method, which provided an analytical relation of the transfer matrices for slug units. The transfer matrices associated with the stratified wavy units were calculated numerically. Expressions were found that relate the transmission and the reflection coefficients of a chain of units to the eigenvalues and eigenvectors of the transfer matrix.

The transmission coefficient as a function of the frequency has a band structure. For certain frequency bands (the stop bands or band gaps) waves attenuate and do not propagate through the pipe unlike the waves of frequencies corresponding to the pass bands. This band structure of the transmission coefficient can be understood by considering an infinite pipe where Bloch's theorem applies. The properties of the resulting Bloch wavenumber are directly related to the eigenvalues of the transfer matrix of a slug unit. Asymptotic solutions of the band structure were found for flows with a very low and a very high impedance contrast, in terms of the transit time of a unit τ and two parameters ν and ζ that are related to the ratio of the transit times through the two section of a slug unit and the impedance contrast, respectively.

When the impedance contrast is low the stop bands are narrow, in contrast to those of gas-water flows. In the latter case the stop bands are very wide which indicates that actually sound waves of almost the full frequency range do not propagate through gas-water slug flows at all.

Upon generalizing the definition of ν the locations of the centers of the stop band for stratified wavy flows are approximately given by the same relations as those for slug flow. Yet, a generalized form of ζ and consequently relations for the width and the attenuation coefficient of the band gaps have not been found. Numerical simulations demonstrate that the first stop band for stratified wavy oil-water flows exceeds the frequency range of interest. The gas-water analogue, however, showed a very clear stop band. Except for frequencies in this stop band sound propagates well through stratified wavy gas-water flows unlike sound waves in gas-liquid slug flows. The high value of the attenuation coefficient for frequencies of the first band gap may provide a means to estimate the interface wavelength of stratified wavy gas-liquid flows.

In Chapter 7 it was shown that the band structure of the transmission coefficient of periodic flows is broken up when the lengths of the sections are varied at random. In particular at high frequencies the flow becomes less transparent when the degree of randomness or the length of the pipe increases. Because of the randomness of the medium also the corresponding transmission coefficient is a stochastic quantity. Graphs of the variance of its probability distribution plotted against the mean exhibit

a universal structure.

A prominent quantity of interest to study the statistics of the sound transmission is the logarithmic decrement of the transmission coefficient, the Lyapunov exponent γ_L associated with a system of finite length. When the length of the pipe tends to infinity its value converges to the true Lyapunov exponent. The fact that the Lyapunov exponent is the logarithmic decrement of the transmission coefficient suggests that its reciprocal, the localization length, is a measure for the penetration depth of the medium. This is not the case. Only on spatial average the waves attenuate with an attenuation coefficient γ_L. Locally in the pipe the wave amplitudes may increase and decrease and as a result the waves may penetrate much deeper into the medium than one would expect based on the value of γ_L.

For certain conditions the statistics of the Lyapunov exponent γ_L show a remarkable relation; the probability distribution is Gaussian while the associated variance and thus all the higher moments are related to the mean value. This relation is called the single parameter scaling, which was found to apply to certain homogeneous systems containing randomly located scatterers. However, for certain conditions it also applies to random media that are periodic on average. The considered example suggests a sufficient condition. That is the difference between the phases of the upstream and downstream propagating waves must be fully random. This leads to a simple relation that expresses the 'randomization randomness' δ_{rnd} in terms of the frequency and the mean transit times. When the randomness δ is larger than δ_{rnd} the medium overcomes its periodicity and becomes completely random, then the single parameter scaling applies. This condition is too restrictive for most frequencies; at the band edges a randomness that is much smaller than δ_{rnd} already yields single parameter scaling.

Graphs of the energy distribution in the pipe illuminate that the localization length should not be confused with the penetration depth. The energy indeed remains confined to the source, but does not attenuate exponentially with respect to the distance to the source. Instead, the energy alternately grows and decreases at certain locations in the pipe and as a result, peaks are formed. This phenomenon is called Anderson localization. Moreover, also the energy distribution shows remarkable statistics. For a sufficiently large randomness the standard deviation is proportional to the mean.

8.2 Applications to flow identification

At present, information on the volume fractions of homogeneous mixtures of oil and water is obtained by measuring the transit time of the acoustic waves as they propagate along different sensors in the pipe through cross-correlating their recordings (Gysling et al., 2000). The ratio of the known distances between the sensors and the corresponding transit times yield estimates of the sound speed of the flow. Given the

acoustic properties of the individual phases the volume fractions of the oil and of the water are estimated by Wood's relation (Wood, 1941) with an expected accuracy of $5 - 10\%$.

This study has pointed out that other configurations hardly affect the speed of sound as given by Wood's relation as long as the medium does not vary significantly with axial position in the pipe. The attenuation of sound waves is, however, different in each configuration and may yield ways to distinguish different configurations.

Instead of recording sound that is induced naturally by the flow, one could also think of generating sound actively. Then a way to extract information from the sound recordings may be based on the resonance frequencies as presented in Chapter 4. The different two-phase configurations exhibit certain characteristic distributions of resonance frequencies. A sweep of sound containing a wide range of frequencies, generated somewhere in the pipe yields an acoustic response where these resonances may be recognized. Perhaps, then certain parameters of the flow configuration could be extracted from these measured resonances.

When the flow is periodic or periodic on average with a low degree of randomness, the band gaps may be recognized in the signals. The location of the gaps is related to the transit time of one period, while the width contains information on the impedance ratio between the sections. However, it is demonstrated that the first stop band for stratified wavy oil-water flows exceeds the frequency range of interest, this in contrast to the gas-water analogue that showed a very clear stop band. Except for frequencies in this stop band sound propagates well through stratified wavy gas-water flows unlike sound waves in gas-liquid slug flows. The high value of the attenuation coefficient for frequencies of the first band gap indicates that it is likely that the interface wavelength of stratified wavy gas-liquid flows can be estimated by measuring the location of the gap center.

Extracting information from the random flows as discussed in Chapter 7 is much more complicated. The standard deviation of the energy distribution in the pipe is found to be much larger than the mean value. This implies that it is questionable whether extracting information about the flow is possible at all. However, upon noting that the energy is positive, the fact that the standard deviation is larger than the mean indicates that the probability distribution at a distance x from the source cannot be symmetric. Therefore values of the energy that are larger than two times the mean value may have a significant probability. It is also very well possible that realizations having a low probability yield extreme energy distributions, which contribute appreciably to the mean and the variance; i.e. the probability distribution of the 90% of the realizations that yield the smallest amplitudes may have a smaller mean value and a much smaller variance. Furthermore, also the conditional probability distribution of the energy distribution as the probability distribution of the energy distribution *given* the energy at a certain number of locations, may have a much smaller variance. These

smaller values of the variance may yield ways to extract information about the flow. The statistical relations such as single parameter scaling may be useful in the study of the conditional probabilities.

In many studies on waves in random media the principle of time-reversal is employed (e.g. Fink, Cassereau, Derode, Prada, Roux, Tanter, Thomas and Wu, 2000). That the medium is in rest, however, is a necessary condition to apply this principle. This condition is, of course, not satisfied when dealing with the flowing oil-water distributions in pipes but, perhaps, the *lack* of time-reversal may be used to obtain information about the flow, in particular about the flow velocity.

8.3 Recommendations

So far the acoustics of oil-water flows has been studied analytically. In order to verify whether the obtained results are in agreement with the acoustics in real pipelines, experiments are required.

In the experiments it is important to realize that the attenuation lengths are in the order of at least several hundreds of meters so that long pipes are presumably required to measure the attenuation of the sound waves.

One of the aspects that may play a role in the experiments is the influence of the wall elasticity on sound propagation. In order to estimate the effect, the pipe of the experimental setup could be immersed in water.

Furthermore, small amounts of gas bubbles may be present in the liquids. This would reduce the sound speed considerably and dominate the acoustics of liquid-liquid flows. In that case the experiment does not represent the acoustics of liquid-liquid flows in the downhole network where gas bubbles are usually not present. A way to avoid the presence of gas is necessary to obtain meaningful results of the experiments concerning the acoustics of oil-water flows.

The attenuation in dense dispersions is also a point of interest, as well as a better understanding of the stochastic propagation and attenuation properties of sound waves in random media.

REFERENCES

Abramowitz, M. and Stegun, I. A.: 1965, *Handbook of Mathematical Functions*, Dover Publications, Inc., New York.

Allegra, J. R. and Hawley, S. A.: 1972, Attenuation of sound in suspensions and emulsions: theory and experiments, *J. Acoust. Soc. Am.* **51**(5), 1545–1564.

Anderson, P. W.: 1958, Absence of diffusion in certain random lattices, *Phys. Rev.* **109**, 1492–1505.

Anderson, P. W., Thouless, D. J., Abrahams, E. and Fisher, D. S.: 1980, New method for a scaling theory of localization, *Phys. Rev.* B **22**, 3519–3526.

Angeli, P. and Hewitt, G. F.: 2000a, Drop size distributions in horizontal oil-water dispersed flows, *Chem. Eng. Sc.* **55**, 3133–3143.

Angeli, P. and Hewitt, G. F.: 2000b, Flow structure in horizontal oil-water flow, *Intl J. Multiphase Flow* **26**.

Ardhuin, F. and Herbers, T. H. C.: 2002, Bragg scattering of random surface gravity waves by irregular seabed topography, *J. Fluid Mech.* **451**, 1–33.

Aspelund, A. and Midttveit, O.: 1996, Challenges in downhole multiphase measurements, SPE 35559, European Production Operations Conference and Exhibition, Stavanger, Norway.

Azzopardi, B. J.: 2002, Similarities and differences between gas/liquid and liquid/liquid flows, Internal Report, School of Chemical, Environmental and Mining Engineering, University of Nottingham.

Bai, R., Chen, K. and Joseph, D. D.: 1992, Lubricated pipelining: stability of core-annular flow. part 5. experiments and comparison with theory., *J. Fluid Mech.* **240**, 97–132.

Bradley, C. E.: 1994, Time harmonic acoustic bloch wave propagation in periodic waveguides. part i. theory, *J. Acoust. Soc. Am.* **96**, 1844–1853.

Brauner, N.: 2001, The prediction of dispersed flows boundaries in liquid-liquid and gas-liquid systems, *Intl J. Multiphase Flow* **27**.

Brauner, N. and Moalem Maron, D.: 1999, Classification of liquid-liquid flow systems and the prediction of flow pattern maps, Two-phase Flow Modelling and Experimentation, Edizioni ETS, Pisa.

Charles, M. E., Govier, G. W. and Hodgson, G. W.: 1961, The horizontal pipeline flow of equal density oil-water mixtures, *Can. J. Chem. Eng.* **39**, 27–36.

Collins, S. B. and Knudsen, J. G.: 1970, Drop-size distributions produced by turbulent pipe flow, *Can. J. Chem. Eng.* **16**(6), 1072–1080.

Crighton, D. G., Dowling, A. P., Ffows Williams, M., Heckle, M. and Leppington, F. G.: 1992, *Modern Methods in Analytical Acoustics*, Springer-Verlag.

Devillard, P., Dunlop, F. and Souillard, B.: 1988, Localization of gravity waves on a channel with a random bottom, *J. Fluid Mech.* **186**, 521–538.

Deych, L. I., Lisyanski, A. A. and Altshuler, B. L.: 2000, Single parameter scaling in one-dimensional localization revisited, *Phys. Rev. Lett.* **84**, 2678–2681.

Deych, L. I., Yamilov, A. and Lisyanski, A. A.: 2001, Scaling in one-dimensional localized absorbing systems, *Phys. Rev.* B **64**, 024201.

Deych, L. I., Zaslavsky, D. and Lisyanski, A. A.: 1997, Wave localization in generalized thue-morse superlattices with disorder, *Phys. Rev.* E **56**(4), 4780–4790.

Deych, L. I., Zaslavsky, D. and Lisyanski, A. A.: 1998, Statistics of the lyapunov exponent in 1d random periodic-on-average systems., *Phys. Rev. Lett.* **81**, 5390–5393.

Elseth, G.: 2001, *An experimental study of oil-water flow in horizontal pipes*, PhD thesis, Telemark University College, Norway.

Epstein, P. S. and Carhart, R. R.: 1953, The absorbtion of sound in suspensions and emulsions. i. water fog in air, *J. Acoust. Soc. Am.* **25**(3), 553–565.

Evans, J. M. and Linton, C. M.: 1994, On step approximations for water-wave problems, *J. Fluid Mech.* **278**, 229–249.

Fink, M., Cassereau, D., Derode, A., Prada, C., Roux, P., Tanter, M., Thomas, J. L. and Wu, F.: 2000, Time-reversed acoustics, *Rep. Prog. Phys.* **63**, 1933–1995.

Fowles, G. R.: 1968, *Introduction to Modern Optics*, Dover Publications Inc., New York.

Freilikher, V. D., Lianski, B. A., Yurkevich, I. V., Maradudin, A. A. and McGurn, A. R.: 1995, Enhanced transmission due to disorder, *Phys. Rev.* E **51**, 6301–6304.

Garvin, J.: 2002, Use the correct constant-volume specific heat, *CEP Magazine* **98**(7), 64–65.

Gysling, D., Vandeweijer, T. and van der Spek, A.: 2000, Development of a permanent downhole two-phase flow meter, SRI Multiphase Metering and Pumping Conference, Houston.

Harris, J. G.: 2001, *Linear Elastic Waves*, Cambridge University Press.

Hinze, J.: 1955, Fundamentals of the hydrodynamic mechanism of splitting in dispersion processes, *AIChE J.* **1**(3), 289–295.

Hinze, J.: 1959, *Turbulence*, McGraw-Hill, New York.

Ho, W. S. and Li, N. N.: 1994, Core-annular flow of liquid membrane emulsion, *AIChE J.* **40**(12), 1961–68.

Isakovich, M. A.: 1948, *Zh. Eksp. i Teor. Fiz.* **18**, 907.

Joseph, D. D., Bai, R., Chen, K. P. and Renardy, Y. Y.: 1997, Core-annular flows, *Ann. Rev. Fluid Mech.* **29**, 65–90.

Kapteijn, P.: 2003, De slimme olieput, *De Ingenieur* **115**(14), 44–46. interview in Dutch.

Karabelas, A.: 1978, Droplet size spectra generated in turbulent pipe flow of dilute liquid/liquid dispersions, *AIChE J.* **24**(2), 170–180.

Karplus, H. B.: 1961, The velocity of sound in liquids containing gas bubbles, *Res. Develop/Rep ARF-4132-12*, Atomic Energy Commission.

Kersey, A. D., Gysling, D. L. and Bostick, F. X.: 1999, Fiber-optic systems for reservoir monitoring, *World Oil* **10**.

Kirchhoff, G.: 1868, Ueber den einfluss der wärmtegeleitung in einem gase auf die schallbewegung, *Poggendorfer Annalen* **134**, 177–193.

Kolmogorov, A. N.: 1949, On the breaking of drops in turbulent flow, *Doklady Akad. Nauk.* **66**, 825–828.

Lafleur, L. D. and Shields, F. D.: 1995, Low-frequency model in a liquid-filled elastic tube waveguide, *J. Acoust. Soc. Am.* **97**(2).

Langley, R. S.: 1995, Wave transmission through one-dimensional near periodic structures: optimum and random disorder, *J. Sound Vibr.* **188**, 717–743.

Langley, R. S.: 1996a, The frequency band-averaged wave transmission coefficient of a periodic structure, *J. Acoust. Soc. Am.* **100**, 304–311.

Langley, R. S.: 1996b, The statistics of wave transmission through disordered periodic waveguides, *J. Sound Vibr.* **189**, 421–441.

Langley, R. S.: 1996c, A transfer matrix analysis of the energetics of structural wave motion and harmonic vibration, *Proc. R. Soc. Lond.* A **452**, 1631–1648.

Lasheras, J., Eastwood, C., Martínez-Bazán, C. and Montañés, J. L.: 2002, A review of statistical models for the break-up of an immiscible fluid immersed into a fully developed turbulent flow, *Intl J. Multiphase Flow* **28**, 247–278.

Lee, S. J., Chang, K. S. and Kyungdoo, K.: 1998, Pressure wave speeds from the characteristics of two fluids, two-phase hyperbolic equation system, *Intl J. Multiphase Flow* **24**, 855–866.

Lighthill, M. J.: 1978, *Waves in Fluids*, Cambridge University Press.

Lord Rayleigh: 1896, *Theory of Sound*, Vol. II, 2nd edn, The Macmillan Company, London.

Luan, P. G. and Ye, Z.: 2001a, Acoustic wave propagation in a one-dimensional layered system, *Phys. Rev.* E **63**, 066611.

Luan, P. G. and Ye, Z.: 2001b, Statistics of the lyapunov exponent in one-dimensional layered systems, *Phys. Rev.* E **64**, 066609.

Maynard, J. D.: 2001, Colloquium, acoustical analogs of condensed-matter problems, *Rev. Mod. Phys.* **73**.

McGurn, A. R., Christensen, K. T., Mueller, F. M. and Maradudin, A. A.: 1993, Anderson localization in one-dimensional randomly disordered optical systems that are periodic on average, *Phys. Rev.* B **47**, 13 120–13 125.

Morioka, S. and Matsui, G.: 1975, Pressure wave propagation through a separated gas-liquid layer in a duct, *J. Fluid Mech.* **70**, 721–731.

Morse, P. M. and Ingard, K. U.: 1968, *Theoretical Acoustics*, McGraw-Hill Book Company.

Munday, J. N., Brad Bennett, C. and Robertson, W. M.: 2002, Band gaps and defect modes in periodically structured waveguides, *J. Acoust. Soc. Am.* **112**, 1353–1358.

Nishiguchi, N., Tamura, S. and Nori, F.: 1993a, Phonon-transmission rate, fluctuations, and localization in random semiconductor superlattices: Green's-function approach, *Phys. Rev.* B **48**(4), 2515–2528.

Nishiguchi, N., Tamura, S. and Nori, F.: 1993b, Phonon universal-transmission fluctuations and localization in semiconductor superlattices with a controlled degree of order, *Phys. Rev.* B **48**(19), 14426–14435.

Ooms, G., Segal, A., Meerhof, A. J. and Oliemans, R. V. A.: 1984, A theoretical model for core-annular flow of a very viscous core and a water annulus through a horizontal pipe, *Intl J. Multiphase Flow* **10**, 41.

Papanicolaou, G.: 1998, Mathematical problems in geophysical wave propagation, *Doc. Math. J. DMV* pp. 403–427.

Pierce, A. D.: 1981, *Acoustics*, Acoustical Society of America, New York.

Risso, F. and Fabre, J.: 1998, Oscillations and breakup of a bubble immersed in a turbulent field, *J. Fluid Mech.* **372**, 323–355.

Robertson, W. M., Ash, J. and McGaugh, J. M.: 2002, Breaking the sound barrier: Tunneling of acoustic waves through the forbidden transmission region of a one-dimensional acoustic band gap array, *Am. J. Phys.* **70**, 689–693.

Russel, T. W. F., Hodgson, G. W. and Govier, G. W.: 1959, Horizontal pipeline flow of mixtures of oil and water, *Can. J. Chem. Eng.* **37**, 9–17.

Scott, J. F. M.: 1985, The statistics of waves propagating in a one-dimensional random medium, *Proc. R. Soc. Lond.* A **398**, 341–363.

Sevik, M. and Park, S. H.: 1973, The splitting of drops and bubbles in turbulent fluid flow, *J. Fluid Eng. Trans. ASME 95* **54-59**.

Shapiro, S. A.: 1999, *Elastic Waves in Random Media*, number 80 in *Lecture Notes in Earth Sciences*, Springer-Verlag.

Sheng, P.: 1995, *Introduction to Wave Scattering Localization, and Mesoscopic Phenomena*, Academic Press.

Simmons, M. J. H. and Azzopardi, B. J.: 2001, Drop size distributions in dispersed liquid-liquid pipe flow, *Intl J. Multiphase Flow* **27**.

Sinai, Y. L.: 1984, Acoustic speeds for stratified two-phase fluids in rectangular ducts, *Intl J. Multiphase Flow* **10**, 415–423.

Sobnack, M. B. and Crighton, D. G.: 1994, Anderson localization effects in the transmission of energy down an irregularly ribbed fluid-loaded structure, *Proc. R. Soc. Lond.* A **444**, 185–200.

Temkin, S.: 1992, Sound speeds in suspensions in thermodynamic equilibrium, *Phys. Fluids A* **4**(11), 2399–2409.

Temkin, S.: 2000, Attenuation and dispersion of sound in dilute dispersions of spherical particles, *J. Acoust. Soc. Am.* **108**(1), 126–146.

Tijdeman, H.: 1975, On the propagation of sound waves in cylindrical tubes, *J. Sound Vibr.* **39**(1), 1–33.

Trallero, J.: 1995, *Oil-water flow patterns in horizontal pipes*, PhD thesis, University of Tulsa, Oklahoma.

Trallero, J., Sarica, C. and Brill, J.: 1997, A study of oil-water flow patterns in horizontal pipes, Vol. SPE production and facilities, Soc. of Petroleum Eng., Richardson.

van Rossum, M. C. W. and Nieuwenhuizen, T. M.: 1999, Multiple scattering of classical waves: microscopy, mesoscopy and diffusion, *Rev. Mod. Phys.* **71**, 313–371.

van Wijngaarden, L.: 1976, Some problems in the formulation of the equations for gas/liquid flows, *in* W. T. Koiter (ed.), *Theoretical and Applied Mechanics*, North-Holland, pp. 249–260.

von Helmholtz, H.: 1863, *Verhandlungen der Naturhistorisch-Medizinischen Vereins zu Heidelberg*, Bd III, 16.

Wood, A. B.: 1941, *A Textbook of Sound*, G. Bell and Sons.

SUMMARY

Acoustic signals that are recorded in oil pipelines contain information about the flow. In order to extract this information from the pressure recordings, detailed knowledge about the transmission properties of sound waves in the pipes is required.

The flows in the pipelines of interest basically consist of oil and water and appear in a rich variety of flow patterns. Examples of these patterns are dispersions, stratified configurations in which oil flows on top of a layer of water, possibly with a wavy interface, or flows of large oil bubbles in water. In addition, combinations of these patterns occur. These flow configurations have different acoustic properties.

It has been suggested that the recordings show the presence of sound waves in the frequency range $200 - 2000\,\mathrm{Hz}$, which warrants to restrict attention to longitudinal waves, as long as the frequencies in this range are below the smallest cutoff frequency. The cutoff frequency for a single phase flow of pure oil in pipes of interest suggests that this condition is satisfied. Further analysis shows that the cutoff frequency is hardly affected by medium inhomogeneities when the flow consists of oil and water, two fluids with similar acoustic properties. In addition, the cutoff frequencies for certain gas-liquid configurations are investigated analytically and numerically, as well as effects of dispersion of the fundamental mode.

The propagation speed and the acoustic impedance of longitudinal sound waves in well-separated and in dispersed two-phase flows in pipes are discussed. Non-equilibrium effects due to viscous friction near the wall and relaxation mechanisms in dispersions are analyzed for oil-water flows and compared to results for gas-liquid flows obtained with the same method. Here it is assumed that the flows do not vary with axial position in the pipe and, hence, reflections do not occur.

Two methods are presented that describe the properties of longitudinal acoustic waves in flows whose composition does vary with axial position in the pipe. In the first method reflections of waves are neglected and the energy flux is assumed to remain constant. This method is not generally applicable. The second method is the transfer-matrix method, which may be employed to calculate the acoustics of basically all configurations. In this method the medium is regarded as stepwise varying. The medium in each section may be single phase, well-separated or dispersed. For

each section a transfer matrix is calculated which expresses the wave amplitudes in the section in terms of those in the next section.

The transfer-matrix method is employed to calculate periodic flows as idealized flows of large oil bubbles in water, gas-liquid slug flows and stratified flows with a wavy interface. One period of these periodic flows is represented by a slug unit or a stratified wavy unit. The transfer matrices corresponding to these units are derived and, by employing Bloch's theorem, their eigenvalues are related to the transmission properties of the periodic flows. It is shown that the transmission coefficient as a function of the frequency has a band structure. For certain frequency bands (the stop bands or band gaps) waves attenuate and do not propagate through the pipe, unlike the waves of frequencies corresponding to the pass bands. The asymptotic behavior of the band structure is analyzed for flows with a very low and for flows with a very high impedance contrast.

In practice, two-phase pipe flows are not fully periodic. It is shown how the band structure is affected when the lengths of the sections are varied at random. Because of the randomness of the medium also the corresponding transmission coefficient becomes a stochastic quantity, which exhibits remarkable statistics.

A prominent quantity of interest to study the statistics of the sound transmission is the logarithmic decrement of the transmission coefficient, the Lyapunov exponent; its reciprocal is called the localization length. For certain conditions the statistics of the Lyapunov exponent show a particular relation, the single parameter scaling. Originally, the single parameter scaling was found to apply to certain systems containing random scatterers. A sufficient condition for which it also applies to random media that are periodic on average is suggested.

Finally, the energy distribution in the pipe is calculated for three different degrees of randomness. It is shown that also the energy distribution shows remarkable statistics. The likely occurrence of Anderson localization in acoustic wave propagation in two-phase pipe flows is demonstrated.

SAMENVATTING

Akoestische signalen die worden gemeten in oliepijpleidingen bevatten informatie over de stroming. Om deze informatie te extraheren uit de gemeten druksignalen is gedetailleerde kennis nodig over de transmissie-eigenschappen van geluidsgolven in buizen.

De stromingen in de betreffende oliepijpleidingen bestaan in het algemeen principe uit olie en water en vertonen een rijke verscheidenheid aan stromingspatronen. Voorbeelden van deze patronen zijn dispersies, gelaagde configuraties waarin olie boven een laag water stroomt, mogelijk met een golvend contactoppervlak, of stromingen van grote oliebellen die omgeven zijn met water. Bovendien komen ook combinaties van deze patronen voor. Deze stromingspatronen hebben verschillende akoestische eigenschappen.

De signalen die men dusver heeft gemeten suggereren de aanwezigheid van geluidsgolven in het frequentiegebied van $200 - 2000\,\mathrm{Hz}$. Dit betekent dat de aandacht mag worden beperkt tot longitudinale golven indien de frequenties lager zijn dan de laagste afsnijfrequentie. De afsnijfrequentie voor een stroming die bestaat uit een enkele fase van olie in een buis met een diameter die kenmerkend is voor de betreffende oliepijpleidingen, suggereert dat aan deze voorwaarde wordt voldaan. Een verdere analyse toont aan dat de afsnijfrequentie nauwelijks verandert wanneer het medium niet homogeen is vanwege de aanwezigheid van olie én water, twee vloeistoffen met soortgelijke akoestische eigenschappen. Daarnaast worden de afsnijfrequenties voor gas-vloeistof configuraties zowel analytisch als numeriek onderzocht, net als de dispersie-effecten van de fundamentele mode.

De voortplantingssnelheid en de akoestische impedantie van longitudinale geluidsgolven in buizen met daarin volledig gescheiden fluïda of dispersies van fluïda worden behandeld. Niet-evenwichtseffecten die veroorzaakt worden door viskeuze wrijving bij de wand en door relaxatiemechanismen in dispersies worden geanalyseerd voor olie-water stromingen en vergeleken met het resultaat voor gas-vloeistof stromingen. Hierbij wordt aangenomen dat de stromingen niet veranderen in de axiale richting in de buis en dat reflecties dus niet voorkomen.

Twee methoden worden behandeld die het gedrag van longitudinale akoestische

golven beschrijven in stromingen waarvan de samenstelling wel verandert in de axiale positie in de buis. Bij de eerste methode worden de reflecties van de golven verwaarloosd terwijl de energiestroom constant wordt verondersteld. Deze methode is niet algemeen toepasbaar. De tweede methode is de overgangsmatrix-methode die kan worden gebruikt om in principe alle stromingsconfiguraties door te rekenen. Bij deze methode wordt het medium als stapsgewijs veranderend beschouwd. In elke sectie kan het medium bestaan uit een enkele fase, uit een volledig gescheiden stroming of uit een dispersie. Voor elke sectie wordt vervolgens een overgangsmatrix berekend die de amplitude van de golven in de elke sectie relateert aan die in de volgende sectie.

De overgangsmatrix-methode wordt gebruikt om periodieke stromingen uit te rekenen die geïdealiseerde stromingen zijn van grote oliebellen in water, van gas-vloeistof propstromingen en van gelaagde stromingen met een golvend contactoppervlak. Eén periode van deze stromingen wordt voorgesteld door een propeenheid of een golvendgelaagde eenheid. De bij deze eenheden behorende overgangsmatrices worden afgeleid en hun eigenwaarden gerelateerd aan de transmissie-eigenschappen van de periodieke stromingen door het theorema van Bloch toe te passen. Het wordt aangetoond dat de transmissiecoëfficiënt als functie van de frequentie een bandstructuur heeft. Voor zekere frequentiebanden (de stopbanden) dempen de golven uit en planten zich niet voort door de buis, in tegenstelling tot de golven met frequenties die behoren tot de doorlaatbanden. Het asymptotische gedrag van de bandstructuur wordt onderzocht voor stromingen met een zeer laag en met een zeer hoog contrast in impedantie.

In werkelijkheid zijn twee-fase stromingen in buizen niet volledig periodiek. Het wordt onderzocht hoe de bandstructuur verandert wanneer de lengtes van de secties willekeurig worden gevarieerd. Vanwege het willekeurige karakter van het medium is ook de bijbehorende transmissiecoëfficiënt een stochastische variabele die opmerkelijke statistiek laat zien.

Een belangrijke en relevante grootheid is het logaritmisch decrement van de transmissiecoëfficiënt, de Lyapunov exponent met als reciproque de lokalisatielengte. Onder bepaalde voorwaarden bestaat er een zekere relatie in de statistiek van de Lyapunov exponent, de enkele parameter schaling. Oorspronkelijk was de enkele parameter schaling van toepassing op bepaalde systemen die willekeurig vestrooiende objecten bevatten. Een voldoende voorwaarde wordt gesuggereerd waarvoor de schaling ook van toepassing is op willekeurige media die gemiddeld gezien periodiek zijn.

Tenslotte wordt de energieverdeling in de buis uitgerekend voor drie verschillende niveau's van willekeur. Het wordt aangetoond dat ook de energieverdeling opmerkelijke statistiek vertoont en dat Anderson-lokalisatie van geluidsgolven zou kunnen optreden in twee-fase stromingen in buizen.

ACKNOWLEDGMENT

This dissertation is written to conclude the research of the past four years which was conducted under supervision of dr. A. Biesheuvel and prof. dr. A. Prosperetti. First, I would like to express my gratitude to them. Dear Arie, thank you very much for all your advices and significant contributions to the project. Your help in uncomfortable moments is very well appreciated. Dear Andrea, thank you very much for being my promotor. I am very grateful for the opportunity to study in Baltimore and for the many interesting discussions in Enschede. Usually it took me some time to fully comprehend that you were right, so the γ for liquids was quite a relief.

I would like to thank the staff, my fellow PhD-students, the supporting staff and all students of the Engineering Fluid Dynamics group for their support, in particular prof. dr. ir. H.W.M. Hoeijmakers. Dear Harry, thank you very much for being my promotor and for all the opportunities you have provided, not only during this project but also before. I am also very grateful to Rob Hagmeijer for all the fruitful discussions about fluid dynamics and the many other topics.

Furthermore, I would like to express my gratitude to dr. ir. M.H.P. Zuidgeest. Dear Mark, thank you very much for your motivating spirit and for showing the pitfalls during your PhD-project, two weeks before I would face them.

The project could not have been conducted without the financial support of Shell International Exploration an Production B.V., Technology & EP. This support is gratefully acknowledged.

Bart en Eline, ik waardeer het zeer dat jullie mijn paranimfen willen zijn.

Tenslotte wil ik mijn familie en in het bijzonder mijn ouders bedanken voor alle steun en liefde, niet alleen tijdens mijn studie maar ook daarvoor.

ABOUT THE AUTHOR

Peter J. van Dijk was born in Arnhem on 30 October 1974. As secondary education he attended 'Het Stedelijk Gymnasium Arnhem'. After graduation in 1993 he started his academic studies in Physics at the University of Nijmegen where he graduated for the propaedeutic exam. In 1995 Peter moved to Enschede to study Mechanical Engineering at the University of Twente. This included the study tour 'INCA' in Brazil and Argentina and a traineeship at the 'Shell Research and Technology Centre' in Amsterdam on gas-liquid slug flows. In January 2001 he graduated on condensing gas-vapor flows, with distinction.

From April 2001 to May 2005 he conducted his Ph.D. research at the University of Twente under guidance of dr. Arie Biesheuvel and prof. dr. Andrea Prosperetti. In this period he also studied one semester at The Johns Hopkins University in Baltimore (MD, USA) and followed several courses in Udine (Italy), Cargèse (France), Leiden (The Netherlands), and Enschede (The Netherlands).

Parts of his work were presented at the 3^{rd} Japanese-European Two-Phase Flow Group Meeting 2003 in Certosa di Pontignano (Italy), at the 5^{th} Euromech Fluid Mechanics Conference 2003 in Toulouse (France), and at the 5^{th} International Conference on Multiphase Flow 2004 in Yokohama (Japan).